

# **Investigation of transformation reactions of phenolic compounds by oxidative processes in aqueous systems**

## **Dissertation**

zur Erlangung des akademischen Grades eines  
Doktors der Naturwissenschaften  
– Dr. rer. nat. –

vorgelegt von

**Jens Terhalle**

geboren in Ahaus

Lehrstuhl für Instrumentelle Analytische Chemie  
der  
Universität Duisburg-Essen

**2022**

Die vorliegende Arbeit wurde im Zeitraum von Juni 2017 bis September 2020 im Arbeitskreis von Prof. Dr. Torsten C. Schmidt in der Fakultät für Chemie im Bereich Instrumentelle Analytische Chemie der Universität Duisburg-Essen durchgeführt.

Tag der Disputation: 15.06.2022

Gutachter: Prof. Dr. Torsten C. Schmidt  
Prof. Dr. Holger V. Lutze

Vorsitzender: Prof. Dr. Maik Walpuski

# DuEPublico

Duisburg-Essen Publications online

UNIVERSITÄT  
DUISBURG  
ESSEN

*Offen im Denken*

ub | universitäts  
bibliothek

Diese Dissertation wird via DuEPublico, dem Dokumenten- und Publikationsserver der Universität Duisburg-Essen, zur Verfügung gestellt und liegt auch als Print-Version vor.

**DOI:** 10.17185/duepublico/76136

**URN:** urn:nbn:de:hbz:465-20220711-100450-5

Alle Rechte vorbehalten.

---

## Summary

Ozone (O<sub>3</sub>) and chlorine dioxide (ClO<sub>2</sub>) have been used as disinfectant for a long time and its use in trace organic compound abatement in water treatment has recently been suggested. Phenolic moieties in trace organic compounds (TrOCs) and dissolved organic matter are the main reaction sites for both oxidative agents. The mechanistic understanding of phenolic compound transformation may help to predict oxidant depletion, secondary oxidant and transformation products (TPs) formation. Therefore, the reaction of phenolic compounds with ClO<sub>2</sub> and O<sub>3</sub> were investigated. A new concept for the indirect determination of hypochlorous acid (HOCl) in the reaction of phenol with ClO<sub>2</sub> by 2- and 4-bromophenol was developed. The reaction formed 62 ± 4 % chlorite and 42 ± 3 % HOCl per ClO<sub>2</sub> consumed. The addition of ClO<sub>2</sub> to real wastewater (5 × 10<sup>-5</sup> M ClO<sub>2</sub>) resulted in transformation of 40 % atenolol and 47 % metoprolol (TrOCs) while the presence of the selective HOCl scavenger, glycine, largely diminished their transformation. This indicates that both compounds were transformed by the reaction with HOCl (e.g.,  $k(\text{atenolol} + \text{HOCl}) = 3.5 \times 10^4 \text{ M}^{-1} \text{ s}^{-1}$ ), which is formed in reactions of ClO<sub>2</sub> with the wastewater matrix. During the investigation of the ozonation of phenolic compounds, the amount of O<sub>3</sub> to degrade one mole of compound (stoichiometric ratio) increased with increasing pH for phenol, 4-methylphenol and 4-methoxyphenol. In the case of 4-chlorophenol, stoichiometric ratio of O<sub>3</sub> decreased with increasing pH, which was explained by the formation of organic TPs. However, the increase of stoichiometric ratio of O<sub>3</sub> in the case of phenol and activated phenols could be explained by the formation of highly reactive superoxide, which strongly contributes to O<sub>3</sub> depletion. The results of the reverse order dosage experiments contradict previous studies suggesting that formed organic products are responsible for enhanced O<sub>3</sub> amount. In the additional investigation by compound-specific stable isotope analysis (CSIA), a dependence of the reaction rate constant to carbon isotope fractionation was observed. The fractionation strongly depends on the phenol speciation. With decreasing pH values and reaction rates <math> < 10^5 \text{ M}^{-1} \text{ s}^{-1}</math>, the isotope enrichment factor  $\epsilon$  increases ( $\epsilon$  is between -5.2 and -1.0 ‰). For faster reactions ( $> 10^5 \text{ M}^{-1} \text{ s}^{-1}$ ), the carbon isotope enrichment was not significant anymore ( $\epsilon$  is between -1.0 and 0 ‰). Based on these data we propose a concept to correlate isotope enrichment factors with kinetic data for aromatic compounds. In conclusion, this work confirmed the postulated mechanism of ClO<sub>2</sub> with phenol and found an influence of HOCl on compound transformation. Additionally, the high stoichiometry of O<sub>3</sub> in the reaction with phenol could not be explained. However, prior assumptions could be refuted and new starting points (e.g. investigation of superoxide) could be found. Finally, the

## Summary

---

correlation of isotope enrichment factors with reaction rate constants supported the use of CSIA in the investigation of oxidative reactions. This thesis shows fundamental aspects for further studies of compounds with other functional groups in ClO<sub>2</sub> application and for the use of CSIA in oxidation reactions.

### Zusammenfassung

Ozon ( $O_3$ ) und Chlordioxid ( $ClO_2$ ) werden bereits seit langem als Desinfektionsmittel eingesetzt. In den letzten Jahren wurde ihr Einsatz zur Verringerung organischer Spurenstoffe (TrOCs) in der Wasseraufbereitung eingeführt. Phenolverbindungen in organischen Spurenstoffen und gelösten organischen Material (DOM) sind die wichtigsten Reaktionspartner für diese beiden Oxidationsmittel in der Wasseraufbereitung. Das fundamentale Verständnis des Abbaus dieser Phenolderivate kann dazu beitragen, den Verbrauch der Oxidationsmittel, die Bildung sekundärer Oxidationsmittel und die Entstehung sogenannter Transformationsprodukte (TPs) vorherzusagen. Aus diesem Grund wurde die Reaktion von Phenolverbindungen mit  $ClO_2$  und  $O_3$  untersucht. Es wurde ein neues Konzept für die indirekte Bestimmung von hypochloriger Säure (HOCl) bei der Reaktion von Phenol mit  $ClO_2$  durch 2- und 4-Bromphenol entwickelt. Bei der Reaktion wurden  $62 \pm 4$  % Chlorit und  $42 \pm 3$  % HOCl pro verbrauchtem  $ClO_2$  gebildet. Die Zugabe von  $ClO_2$  zu echtem Abwasser ( $5 \times 10^5$  M  $ClO_2$ ) führte zu einem Abbau von 40 % Atenolol und 47 % Metoprolol (TrOCs), während in Anwesenheit des selektiven HOCl-Fängers Glycin, der Abbau weitgehend verringert wurde. Dies deutet darauf hin, dass beide Verbindungen durch die Reaktion mit HOCl abgebaut wurden (z. B.  $k(\text{Atenolol} + \text{HOCl}) = 3,5 \times 10^4 \text{ M}^{-1} \text{ s}^{-1}$ ). Die Untersuchung der Ozonierung von folgenden Phenolverbindungen: Phenol, 4-Methylphenol und 4-Methoxyphenol zeigte, dass die Menge  $O_3$ , welche benötigt wird, um ein Mol der Verbindung abzubauen (stöchiometrische Verhältnis), mit dem pH-Wert ansteigt. Bei 4-Chlorphenol nahm das stöchiometrische Verhältnis mit steigendem pH-Wert ab, was durch die Bildung von hochreaktiven organischen TPs erklärt wurde. Der Anstieg des stöchiometrischen Verhältnisses des  $O_3$  im Fall von Phenol und den aktivierten Phenolen (4-Methylphenol und 4-Methoxyphenol) könnte jedoch durch die Bildung von hochreaktivem Superoxid erklärt werden, welches stark zum  $O_3$ -Verbrauch beiträgt. Die Ergebnisse der Umgekehrten-Dosierungs-Experimente stehen im Widerspruch zu früherer Studien, die darauf hindeuten, dass die gebildeten organischen Produkte zu einem erhöhten  $O_3$ -Verbrauch beitragen. Bei der zusätzlichen Untersuchung mittels verbindungsspezifischer stabiler Isotopenanalyse (CSIA) wurde eine reaktionsratenabhängige Kohlenstoffisotopenfraktionierung beobachtet. Die Fraktionierung hing stark von der Phenolspeziation ab. Mit sinkenden pH-Werten und Reaktionsgeschwindigkeiten  $<10^5 \text{ M}^{-1} \text{ s}^{-1}$  nimmt der Isotopenanreicherungsfaktor  $\epsilon$  zu ( $\epsilon$  liegt zwischen -5,2 und -1,0 ‰). Bei schnelleren Reaktionen ( $>10^5 \text{ M}^{-1} \text{ s}^{-1}$ ) war die Kohlenstoffisotopenanreicherung nicht mehr signifikant messbar ( $\epsilon$  liegt zwischen -1,0 und 0 ‰). Auf Grundlage dieser Daten wurde ein Konzept zur

Korrelation von Isotopenanreicherungsfaktoren mit kinetischen Daten für aromatische Verbindungen vorgeschlagen. Alles in Allem bestätigt diese Arbeit den postulierten Mechanismus von  $\text{ClO}_2$  mit Phenol und zeigt einen bisher unbekanntem Einfluss von  $\text{HOCl}$  auf den Abbau von organischen Verbindungen. Das hohe stöchiometrische Verhältnis des  $\text{O}_3$  in der Reaktion mit Phenol konnte in dieser Arbeit nicht geklärt werden, dennoch konnten neue Ansätze, wie z.B. die Untersuchungen zur Superoxidbildung gezeigt werden. Für die Untersuchung oxidativer Reaktionen durch CSIA wird die Korrelation des isotopischen Anreicherungsfaktors mit der Reaktionsgeschwindigkeit zukünftig helfen. Unter anderem dadurch schafft diese Arbeit grundlegende Aspekte für den Einsatz von CSIA in Oxidationsreaktionen und für aufbauende Untersuchungen von organischen Verbindungen mit anderen funktionellen Gruppen in der  $\text{ClO}_2$ -Forschung.

**Table of contents**

<b>Summary .....</b>	<b>iii</b>
<b>Zusammenfassung.....</b>	<b>v</b>
<b>Table of contents.....</b>	<b>vii</b>
<b>1. Chapter: Introduction.....</b>	<b>1</b>
1.1 Oxidative water treatment .....	2
1.1.1 Ozone as oxidant .....	4
1.1.2 Chlorine dioxide as oxidant.....	6
1.2 Stoichiometric ratio and kinetics of the oxidation of compounds .....	9
1.3 Investigation of reaction mechanism .....	11
<b>2. Chapter: Scope &amp; Aims .....</b>	<b>15</b>
<b>3. Chapter: Chlorine dioxide – Pollutant transformation and hypochlorous acid formation as a secondary oxidant.....</b>	<b>18</b>
3.1 Introduction .....	19
3.2 Material and methods .....	21
3.2.1 Chemicals .....	21
3.2.2 Equipment .....	21
3.2.3 Generation of ozone and chlorine dioxide stock solutions .....	21
3.2.4 Detection of hypochlorous acid in the reaction of chlorine dioxide with phenol	21
3.2.5 Experiments in wastewater.....	23
3.3 Results and discussion .....	25
3.3.1 Validation of the HOCl detection.....	25
3.3.2 Detection of hypochlorous acid from reactions of chlorine dioxide with phenol	28

## Table of contents

---

3.3.3	Pollutant transformation in ClO <sub>2</sub> based wastewater treatment.....	29
3.4	Supporting Information .....	35
3.4.1	Reaction mechanism of phenol with chlorine dioxide .....	35
3.4.2	Chlorine dioxide production and handling.....	39
3.4.3	Detection of hypochlorous acid in the reaction of chlorine dioxide with phenol 42	
3.4.4	HPLC- and IC-methods.....	43
3.4.5	Dissolved Organic Carbon analysis .....	44
3.4.6	Experiments for determining oxidant depletion.....	46
3.4.7	Chloride concentration .....	48
3.4.8	Bromophenol formation .....	48
3.4.9	Determination of oxidant exposure .....	51
<b>4.</b>	<b>Chapter: Ozone consumption in the reaction with phenolic compounds: Effects of pH, radical scavengers and products.....</b>	<b>56</b>
4.1	Introduction .....	57
4.2	Material and methods .....	61
4.2.1	Chemicals .....	61
4.2.2	Equipment .....	61
4.2.3	Generation of ozone stock solution.....	61
4.2.4	Experimental part .....	61
4.3	Results and discussion.....	64
4.4	Conclusion.....	70
4.5	Supporting information.....	70
4.5.1	Measurement of methansulfonic acid and methansulfinic acid .....	75
4.5.2	Species diagram of the substituted phenol: .....	76
4.5.3	OH radical formation in the reaction of phenol .....	77



## Table of contents

---

4.5.4	Text S2: Formation of superoxide.....	79
<b>5.</b>	<b>Chapter: Reaction rate-dependent carbon isotope fractionation during ozonation of phenols.....</b>	<b>80</b>
5.1	Introduction .....	81
5.2	Material and methods .....	83
5.2.1	Chemicals .....	83
5.2.2	Sample preparation for batch experiments.....	83
5.2.3	Determination of the second-order reaction rate constant of phenol- <sup>13</sup> C <sub>6</sub> with ozone	84
5.2.4	Analytical instrumentation and methods.....	85
5.2.5	Calculation of the enrichment factor .....	86
5.3	Results and discussion .....	87
5.4	Conclusions .....	92
5.5	Supporting Information .....	93
5.5.1	Reaction pathways of phenol with ozone.....	93
5.5.2	Generation of ozone stock solutions .....	103
<b>6.</b>	<b>Chapter: General conclusions &amp; Outlook.....</b>	<b>109</b>
<b>7.</b>	<b>Chapter: References.....</b>	<b>113</b>
<b>8.</b>	<b>Chapter: Appendix.....</b>	<b>124</b>
8.1	List of Figures.....	125
8.2	List of Tables .....	132
8.3	List of Abbreviations .....	134
8.4	List of Publications .....	138
8.4.1	Publications in peer-reviewed journals .....	138
8.4.2	Oral presentations.....	139

## Table of contents

---

8.4.3	Poster presentations .....	139
8.5	Declaration of scientific contributions .....	140
8.6	Curriculum Vitae .....	141
8.7	Erklärung .....	142
8.8	Danksagung .....	143

# 1. Chapter: Introduction

### 1.1 Oxidative water treatment

Safe drinking water is essential for public health. Therefore, the highest possible quality standards in drinking water production as well as the protection of their resources must be ensured (WHO, 2017). In this regard, discharging of contaminated wastewater into drinking water resources should be avoided, which can be ensured by a well-performed wastewater treatment. Additionally, contaminated drinking water resources should remain useable by drinking water treatment (Huber et al., 2005). The following methods are applied for the water treatment: physical treatment (e.g. sorption with activated carbon or membrane filtration), biological treatment (e.g. biological filtration) and chemical treatment (e.g., oxidation processes). Removal of contaminants by physical treatment is based on physical separation of pollutants from the water by e.g., adsorption at activated carbon (AC) (Reungoat et al., 2012). AC treatment is limited by the AC sorption capacities, which thus has to be renewed regularly (Reungoat et al., 2010). For biological treatment, the biodegradation of the pollutants is a prerequisite. In addition, biological purification takes time because of the adaption of biological community to current conditions before it can be biodegraded. Hence, it is not possible to cope with suddenly increase of contaminants. Oxidative treatment is another, yet more flexible tool, which can be used for pollutant degradation and disinfection (Joss et al., 2008).

Originally, oxidative water treatment was used for disinfection in order to supply consumers with microbiologically safe drinking water, e.g. to decrease the threat of waterborne lethal diseases like typhus or cholera. In the further development, oxidants such as ozone (O<sub>3</sub>) or chlorine dioxide (ClO<sub>2</sub>) have also been used for oxidation of iron (II), manganese (II) or arsenic (Gates, 1998, von Sonntag and von Gunten, 2012, Knocke et al., 1991). Additional important fields of application are color removal, as well as taste and odor control (Wenk et al., 2013). Nowadays, oxidative treatment is also implemented for removal of trace organic compounds (TrOCs). TrOCs comprise diverse chemical classes such as pesticides, biocides, human and veterinary pharmaceuticals, consumer products, and industrial chemicals. The concentration and the number of TrOCs varies due to the use of new pharmaceuticals and new personal care products in the population. Additionally, the agriculture industry use a high amount of pesticides and fertilizer to ensure the increased demand of foodstuffs (von Gunten, 2018). Moreover, due to the increasing sensitivity and lower detection limits of recent analytical methods, which allow quantification of chemicals at low nanogram per liter levels, an increasing number of xenobiotic chemicals have been detected in surface waters during the last years. Many of these TrOCs reach the water cycle and endanger the quality of drinking water

(von Gunten, 2018). Although TrOCs are typically only present at low microgram per liter or even nanogram per liter levels, some of these chemicals raise toxicological concerns, in particular when present in mixtures (Schwarzenbach et al., 2006). Therefore, in the best case, TrOCs are completely degraded with the oxidant to carbon dioxide (CO<sub>2</sub>) and water (H<sub>2</sub>O). However, a complete mineralization does not happen in real applications. In most cases, the use of oxidants forms undesired by-products, i.e., disinfection by-products (DBPs) or transformation products (TPs), and handling of partially toxic chemicals, remains another drawback of oxidative processes (von Sonntag and von Gunten, 2012). DBPs are formed from the reactions of chemical oxidants with matrix components such as dissolved organic matter (DOM), bromide or iodide. TPs are formed from the partial oxidation of TrOCs (Figure 1.1) (von Gunten, 2018).

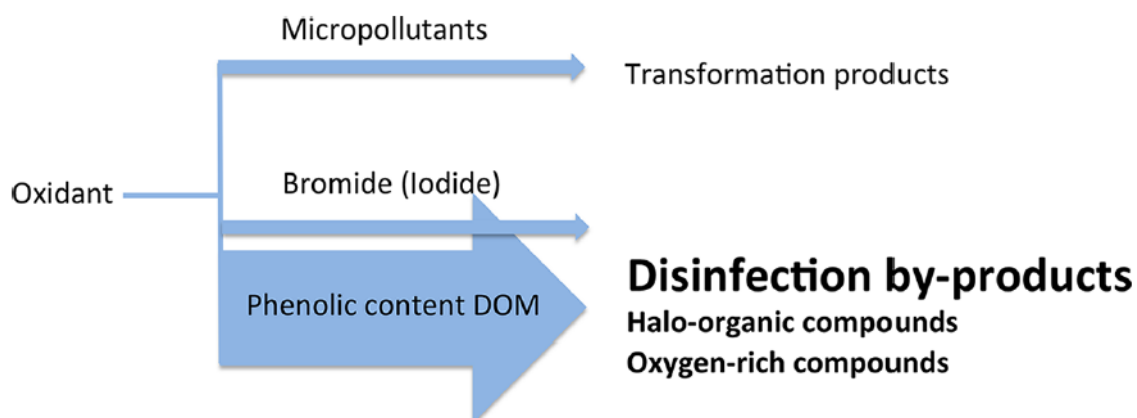


**Figure 1.1: Relative contribution of the various water solutes to the consumption of oxidants. Micropollutants is another word for TrOCs (von Gunten, 2018).**

DOM is a complex mixture of aromatic and aliphatic hydrocarbon structures and consumes the largest fraction of chemical oxidants. The main parts of DOM are humic acid, fulvic acid and hydrophilic fractions (Figure 1.2). For example, wastewater effluent DOM may contain ~45% fulvic acid. Fulvic acid comprises ~2.5 mM oxidizable phenolic structures per mol carbon (Tentscher et al., 2018). DOM concentrations on nature vary among waters of different origin. For example, in wastewaters, DOM ranges between 5 and 20 mg/L, while in drinking water it is typically below 4 mg/L (von Sonntag and von Gunten, 2012). At a DOM concentration of 10 mg/L this would result in a phenol concentration of ~10-13 µM, which is significantly higher than the concentration of phenolic moieties in TrOCs (Tentscher et al., 2018). Nevertheless,

phenolic structures are also common moieties in many TrOCs. A list of 563 surface water TrOCs (Götz et al., 2010), contains 35 substances with phenolic moieties, and more can be formed as primary products from oxidation reaction of nonphenolic aromatics (von Sonntag and von Gunten, 2012, von Sonntag et al., 1997b, Tentscher et al., 2018). The combined pool of phenolic compounds is structurally diverse, with different substituents on the phenolic ring in all positions. The abundant presence of phenolic structures in DOM and TrOCs makes phenols to the main reaction partner of the oxidants and to a perfect model compound for this thesis.

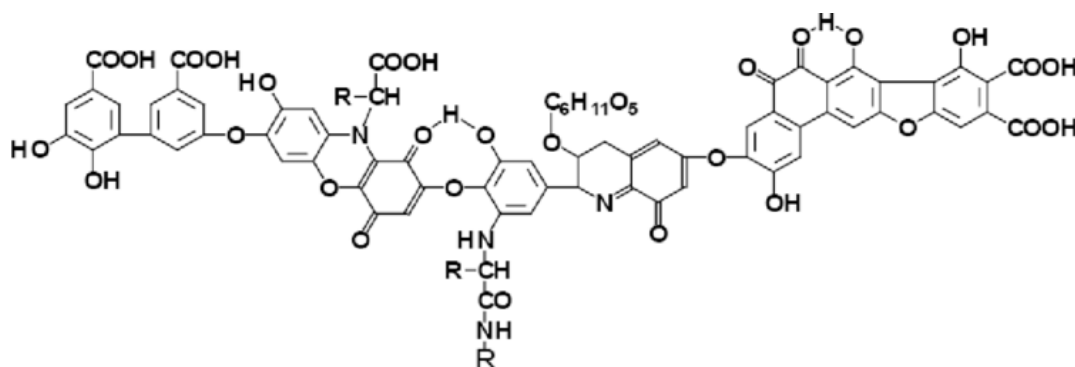


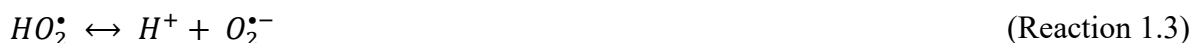
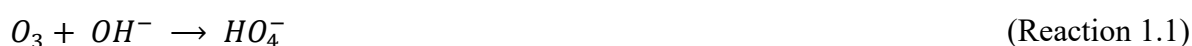
**Figure 1.2: Hypothetic structure of a part of dissolved organic matter (Stevenson and Schnitzer, 1982)**

### 1.1.1 Ozone as oxidant

Nowadays, ozonation is one of the most important steps in drinking water treatment in France and Switzerland, whereas it plays only a minor role in the USA or Japan, for example (von Sonntag and von Gunten, 2012). Already at the beginning of the 20th century, the first ozonation plants were built in Europe, which, however, were closed again after a few years due to the lower costs of chlorination for disinfection. Even today, both types of disinfection compete in water treatment and the prevalence of ozonation as a drinking water treatment step is still very different in the industrialized countries. However, the generation of  $O_3$  for water treatment purposes is rather simple compared to e.g. chlorine or chlorine dioxide applications because no hazardous or toxic chemicals need to be stored on site.  $O_3$  may be generated by electrolysis (McKenzie et al., 1997) or in the plasma of microdischarge columns in a silent discharge process (Eliasson et al., 1987, Okazaki et al., 1988) using dry oxygen ( $O_2$ ) or air as feed gas. The latter generation process is most common for commercial ozone generators (von Sonntag and von Gunten, 2012).

O<sub>3</sub> is a highly selective oxidative agent. Preferred reaction sites of organic compounds are double bonds of olefins, reduced sulfur moieties, deprotonated amines and activated aromatic systems (von Sonntag and von Gunten, 2012, von Gunten, 2003a). There are several possible primary reactions of O<sub>3</sub> with such compounds. A detailed and comprehensive description of regularly observed pathways can be found in von Sonntag and von Gunten (2012). Phenols are composed of an activated aromatic system and therefore, O<sub>3</sub> reacts moderately fast with phenol ( $k = 1.3 \times 10^3 \text{ M}^{-1}\text{s}^{-1}$ ). However, the reaction of the deprotonated phenol (phenolate) is close to diffusion controlled ( $k = 1.4 \times 10^9 \text{ M}^{-1}\text{s}^{-1}$ ) (Mvula and von Sonntag, 2003). With a pK<sub>a</sub> of 9.9, the rate of reaction observed at pH 7 is hence determined by the reaction of phenolate. The reaction mechanism of phenolate with O<sub>3</sub> is described in many studies (Mvula and von Sonntag, 2003, Ramseier and von Gunten, 2009, Tentscher et al., 2018).

In the research of O<sub>3</sub> chemistry, in defined aqueous solutions, free radicals could be formed in a side reaction of O<sub>3</sub> with electron rich moieties of several compounds, i.e. free amines and activated aromatic compounds yielding hydroxyl radicals (OH radicals). However, the resulting OH radical quantity depends on the given conditions of the water such as the pH or content of DOM (von Gunten, 2003a). The OH radicals are extremely reactive with any organic and some inorganic matter present in water (Buxton et al., 1988). Hence, compounds, which are refractory in O<sub>3</sub> chemistry, may be degraded in ozone-based processes due to the formation of OH radicals (von Gunten, 2003b). One possibility for OH radical formation is the reaction of O<sub>3</sub> with the hydroxyl ion (OH<sup>-</sup>) (Reaction 1.1).



According to kinetic and quantum chemical calculations, it is most likely that O<sub>3</sub> and OH<sup>-</sup> form an adduct prior the decay to a perhydroxyl radical (HO<sub>2</sub><sup>•</sup>) and superoxide (O<sub>2</sub><sup>•-</sup>) (Reaction 1.2) (Merényi et al., 2010b). The HO<sub>2</sub><sup>•</sup> (pK<sub>a</sub>(HO<sub>2</sub><sup>•</sup>) = 4.8) is in equilibrium with O<sub>2</sub><sup>•-</sup> (Reaction 1.3) (Bielski et al., 1985). In reaction 1.4, an ozonide radical anion (O<sub>3</sub><sup>•-</sup>) is formed, which is the OH

radical precursor (Sehested et al., 1983). The  $O_3^{\cdot-}$  is in equilibrium with  $O_2$  and  $O^{\cdot-}$  in which the forward reaction rate constant is significantly slower than the backward reaction (Reaction 1.5) (Elliot and McCracken, 1989). The resulting  $O^{\cdot-}$  is in equilibrium with its conjugated acid, the OH radical ( $pK_a$  (OH radical) = 11.8) (Reaction 1.6) (von Sonntag and von Gunten, 2012, Merényi et al., 2010a). The finale products of  $O_3^{\cdot-}$  are  $O_2$  and OH radical (von Sonntag and von Gunten, 2012).

The indirect ozonation processes, which involve the OH radicals in sufficient quantity to affect water purification, are called advanced oxidative processes (AOPs) (Glaze et al., 1987). Therefore, the generation of OH radicals is supported by adding promoters (i.e. hydrogen peroxide ( $H_2O_2$ )). The reaction of  $O_3$  with  $H_2O_2$  itself is very slow contrary to the fast reaction with its anion ( $HO_2^-$ ). This process is driven by the release of  $HO_2^{\cdot}$  and  $O_2^{\cdot-}$  that could react with  $O_3$  giving rise to OH radicals (von Sonntag and von Gunten, 2012, Staehelin and Hoigne, 1982).

For studying direct  $O_3$  reactions, it is necessary to scavenge the formed OH radicals adequately. Therefore, scavengers are necessary, which show a high reactivity towards OH radicals and that are unreactive with  $O_3$ . Suitable compounds are *tertiary* butanol (*tert.*-BuOH) or dimethyl sulfoxide (DMSO) (von Sonntag and von Gunten, 2012).

### 1.1.2 Chlorine dioxide as oxidant

Since the first discovery of chlorine dioxide ( $ClO_2$ ) in 1811 it took more than one century until it was possible to implement  $ClO_2$  use in a drinking water treatment process. The reason for this was the lack of commercially available  $NaClO_2$  (Gates, 1998, Aieta and Berg, 1986). In the beginning,  $ClO_2$  was used as substitute for chlorine for disinfection of phenol containing waters. Large excess of chlorine would be necessary in order to avoid the undesired chlorophenol formation (Gates, 2009). In case of  $ClO_2$  much lower doses could be applied and taste and odor flaws of the treated water were avoided. Additionally, it was found that chlorinated DBPs would not form at all if  $ClO_2$  is applied. However, more recent studies have shown that this assumption cannot be fully verified (Wajon et al., 1982, Rav-Acha, 1984).

Nowadays in Europe,  $ClO_2$  is regularly used for secondary disinfection of finished drinking water, i.e., prior to water distribution to the drinking water network to maintain a residual disinfection. This is done in order to maintain the water quality and prevent hygienic problems due to microbial regrowth or recontamination from deficient pipe systems (Hoigné and Bader,



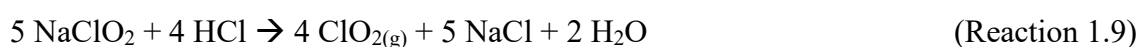
1994). In case of a fully functional distribution network, it may be even possible to renounce secondary disinfection with chlorine-based disinfectants and solely keep these options available in case of emergency as, e.g., in the Mülheim water treatment process (von Sonntag and von Gunten, 2012). Contrary to Europe, in the USA and Canada,  $\text{ClO}_2$  is often used for preoxidation of raw water for drinking water treatment (Gates, 2009, Gates, 1998).

$\text{ClO}_2$  is a highly selective oxidative and electrophilic agent. As a peculiarity, solely single electron transfer reactions have been proposed in literature of  $\text{ClO}_2$  with its reactants. High reaction rates are observed for anilines (Lee and von Gunten, 2010), neutral tertiary amines (Rosenblatt et al., 1967, Hull et al., 1967), reduced sulfur species such as thiolates (Ison et al., 2006), some polycyclic aromatic compounds (Rav-Acha and Blits, 1985), and phenolate and many of its derivatives (Hoigné and Bader, 1994, Tratnyek and Hoigné, 1994). In general, as it is also observed for the electrophile  $\text{O}_3$  (von Sonntag and von Gunten, 2012), reaction rate constants of  $\text{ClO}_2$  with weak acids, e.g., phenols or thiols, and weak bases are strongly dependent on speciation and thus on pH (Hoigné and Bader, 1994, Ison et al., 2006). Depending on the substituents of the phenolate, the reaction rate constants with  $\text{ClO}_2$  are between 5 and 9 orders of magnitude higher than for the neutral species (Tratnyek and Hoigné, 1994). It has been proposed that a single electron transfer from the deprotonated oxygen of phenolate to  $\text{ClO}_2$  initiates the oxidation of phenolate, so that, chlorite ( $\text{ClO}_2^-$ ) and a phenoxyl radical are formed (Abdighahroudi et al., 2021, Abdighahroudi et al., 2020). The phenoxyl radicals may either react with a second  $\text{ClO}_2$ , thus, leading to the formation of  $\text{HOCl}$  and *p*-benzoquinone, or rarely to *o*-benzoquinone. Additionally, the phenoxyl radicals could be subjected to irreversible coupling reactions with each other or with surrounding substrates (Wajon et al., 1982).

Key parameters of disinfection with  $\text{ClO}_2$  are often compared to those of chlorine in order to demonstrate its benefits. First,  $\text{ClO}_2$  does not show such strong pH dependency for the disinfection efficacy compared to chlorine ( $\text{pK}_a = 7.47$ ) (Furman and Margerum, 1998). In case of chlorine, only the non-dissociated species,  $\text{HOCl}$ , is effective. Second,  $\text{ClO}_2$  is equally or more efficient against some bacteria and protozoa than chlorine (USEPA, 1999). Another often-mentioned point is lower formation of chlorinated DBPs. This is especially true for trihalomethanes (THM) (Gates, 1998). It was shown that treatment of the same drinking water matrix with  $\text{ClO}_2$  yielded much less total organic halides (TOX) than in case of chlorine (Yang et al., 2013, Hua and Reckhow, 2007). The formation of TOX at all, was attributed to formation of  $\text{HOCl}$  in the reaction of  $\text{ClO}_2$  and its subsequent reaction with organic material.

However, some possible disadvantages have to be dealt with, e.g., that production costs for chlorine are lower than  $\text{ClO}_2$ . For conventional  $\text{ClO}_2$  production, storage of two to three chemicals is necessary in comparison to only one for chlorination. The operator needs to be trained more intensely and required mechanical equipment is more sophisticated (Gates, 1998, USEPA, 1999).

The generation of  $\text{ClO}_2$  requires somewhat more effort than the generation of  $\text{O}_3$ . Due to the explosive nature of  $\text{ClO}_2$ , long-term storage is undesirable. The critical aqueous concentration is  $> 10 \text{ g L}^{-1}$  and 10% in the gas phase (Gates, 1998). For large-scale applications in water treatment, mechanical generators mostly produce  $\text{ClO}_2$ . Here, mostly sodium chlorite ( $\text{NaClO}_2$ ) is mixed with either gaseous chlorine ( $\text{Cl}_2$ ) (Reaction 1.7), hypochlorous acid ( $\text{HOCl}$ ) (Reaction 1.8) or hydrochloric acid ( $\text{HCl}$ ) (Reaction 1.9).  $\text{ClO}_2$  will be formed in the course of reactions (Gates, 1998, USEPA, 1999, Aieta and Berg, 1986):



Reactions 1.7 – 1.9 represent ideal conditions without any by-product formation. Depending on the efficiency of the generator, it may also be possible that unreacted  $\text{ClO}_2^-$  remains in the solution or that chlorate ( $\text{ClO}_3^-$ ) or  $\text{HOCl}$  are formed in side reactions (Gates, 1998, USEPA, 1999). Formation of  $\text{HOCl}$ , free chlorine, may lead to enhanced formation of chlorinated DBPs (Wenk et al., 2013, Wajon et al., 1982). The elevated presence of  $\text{ClO}_2^-$  and  $\text{ClO}_3^-$  may result in an excess of threshold limit values of given regulations, e.g.,  $0.2 \text{ mg L}^{-1} \text{ClO}_2^-$  for Germany or  $1 \text{ mg L}^{-1} \text{ClO}_2^-$  for US drinking water (USEPA, 1999). Technical on-site generators are capable of reaching  $\text{ClO}_2$  production efficiencies of  $>90 \%$  with these chlorine based methods described above (Aieta and Berg, 1986). However, also a generation method, which produces chlorine-free  $\text{ClO}_2$  solution, is known in which  $\text{NaClO}_2$  is oxidized by persulfate (Uhlmann, 2012). The produced  $\text{ClO}_2$  is purged into chilled ultrapure water and remains stable if the solution is maintained cool and in the dark (Gates, 1998). This method is mostly known for bench- or pilot-scale applications. Recently, also a new variation of this bench method has become available on the market, which not introduced an elevated levels of  $\text{ClO}_2^-$ ,  $\text{ClO}_3^-$  or  $\text{HOCl}$  into the treated water due to the  $\text{ClO}_2$  generation method (Uhlmann, 2012).

## 1.2 Stoichiometric ratio and kinetics of the oxidation of compounds

The reaction of oxidants with compounds can be described by following equation:



where  $k_{\text{Ox}}$  is the second-order rate constant (kinetic) and  $\eta$  is the stoichiometric ratio that determines the moles of oxidant [Ox] consumed per mole of converted compound [M] (Nöthe et al., 2009, Tekle-Röttering et al., 2016a). If the stoichiometric ratio is  $>1$ , also formed transformation products or matrix components could contribute in oxidant consumption. For the reaction of phenol with  $\text{ClO}_2$  and  $\text{O}_3$  the stoichiometric ratio is  $>1$  (Wajon et al., 1982, Mvula and von Sonntag, 2003). In case of  $\text{ClO}_2$  with phenol the stoichiometric ratio is 2, which is explained by the first reaction of  $\text{ClO}_2$  with phenolate and second, the reaction with phenoxy radical (Wajon et al., 1982). The stoichiometric ratio of the reaction of phenol with  $\text{O}_3$  is between 1.5 and 3. Mvula and von Sonntag (2003) describe the further reaction of  $\text{O}_3$  with formed organic products but shows no direct experimental proofs which products are responsible for the high stoichiometric ratio.

Reaction rates are defined as how fast or slow a reaction is (Mortimer and Müller, 2010). A main factor influencing the reaction rate includes the concentration of the reactants, because as reactant concentration increases, the frequency of collisions increases. For this reason, the kinetic law for a chemical reaction is an equation that links the reaction rate ( $k_{\text{Ox}}$ ) (unit:  $\text{M}^{-1} \text{s}^{-1}$ ) with concentrations ([Ox], [M]) (unit: M) (Equation 1.2).

$$-\frac{d[\text{Ox}]}{dt} = k_{\text{Ox}} [\text{Ox}] \times [\text{M}] \quad (\text{Equation 1.2})$$

Hence, the main aim of a kinetic study is to determine the rate constant ( $k_{\text{Ox}}$ ) of the oxidant-compound reaction. Quantification of the rate constant is achieved by establishing the corresponding kinetic law. A first order reaction depends on the concentration of only one reactant. Other reactants can be present, but the reaction depends not on the concentration of these reactants (Mortimer and Müller, 2010). A second order reaction depends on the concentration of two first order reactants. For example, a bimolecular reaction will be second order overall and first order in each reactant (Mortimer and Müller, 2010). Commonly, the reaction of  $\text{O}_3$  and  $\text{ClO}_2$  with compounds follows second order kinetics (von Sonntag and von Gunten, 2012). If one reactant concentration is chosen in excess, its concentration does not significantly change during the reaction, and becomes constant. For example, in Equation 1.3

the compound M is in excess and links the concentrations of reactants with time (t). This approximation is called (pseudo-)first order (von Sonntag and von Gunten, 2012).

$$\ln \frac{[Ox]}{[Ox]_0} = -k_{Ox} [M] \times t = -k_{obs} \times t \quad (\text{Equation 1.3})$$

A plot of  $\ln [Ox]/[Ox]_0$  vs. time (t) yields a straight line from the slope of which  $k_{obs}$  is calculated and division by  $[M]$  yields the bimolecular rate constant  $k_{Ox}$  (Figure 1.3) (von Sonntag and von Gunten, 2012).

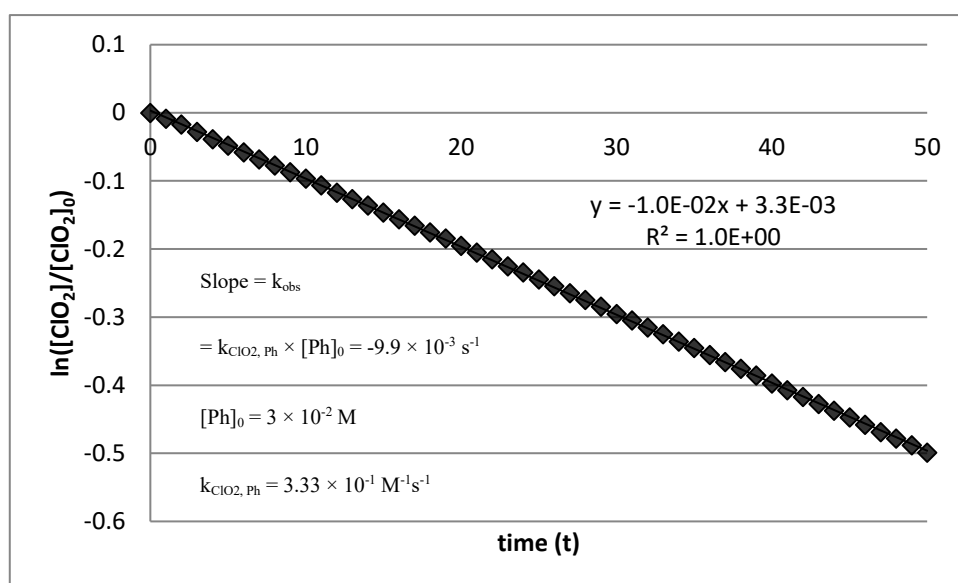


**Figure 1.3: Example plot of the determination of reaction rate constant  $k$  of the reaction of  $ClO_2$  with phenol (pH = 1.03;  $c(\text{phenol}) = 3 \times 10^{-2} \text{ M}$ ;  $c_0(ClO_2) = 3 \times 10^{-4} \text{ M}$ ;  $c(\text{sulfur acid buffer}) = 1 \times 10^{-1} \text{ M}$ ;  $T = 25^\circ\text{C}$ ).**

If the deprotonated species ( $M^-$ ) of the compound reacts faster or slower with the oxidant as the protonated species ( $MH$ ), the specific rate constants for the oxidant with both species and the degree of dissociation ( $\alpha$ ) must be included.

$$k_{Ox} = \alpha \times k_{Ox,MH} + (1 - \alpha) \times k_{Ox,M^-} \quad (\text{Equation 1.4})$$

With the  $pK_a$  of compound at hand (e.g.,  $pK_a(\text{phenol}) = 9.9$ ) one can calculate the reactivity  $pK_a$ . At the reactivity  $pK_a$ , the apparent reaction rate constant with the oxidant is the same for both species:

$$\alpha \times k_{Ox,MH} = (1 - \alpha) \times k_{Ox,M^-} \quad (\text{Equation 1.5})$$

In case the pH is higher than the reactivity  $pK_a$  the deprotonated species is the prevalent reaction partner of the oxidant. This equations shows the important of the pH value during the oxidative reactions with compounds.

### 1.3 Investigation of reaction mechanism

As described before, oxidative treatment does not usually result in full mineralization but rather leads to formation of TPs. For a comprehensive environmental assessment, it is essential to elucidate the transformation pathways. This is especially important with regard to ecotoxicological concerns, because transformation products may be more toxic than their precursors (Hübner et al., 2015, Knoop et al., 2018).

Commonly, the investigation of the transformation pathways is done by product identification. Today, high-resolution mass spectrometry (HRMS) or/and nuclear magnetic resonance spectrometry (NMR) are well-established tools in environmental analysis for screening and identification of unknown TPs (Li et al., 2017, Petrovic et al., 2007, Funke et al., 2016, Prasse and Ternes, 2016). For the identification by NMR, the TPs must be isolated from other compounds and purified. Additionally, a sufficient amount of the unknown TP is necessary (Purschke et al., 2020). Therefore, multiple separation runs of samples and collection of the same fraction must be applied. With the results of the NMR a structure proposal of the TP could be done.

By means of HRMS, the exact mass of a TP may be determined so that it is possible to derive the most probable sum formulas and, eventually, to formulate tentative TP molecule structures (García-Galán et al., 2008, Deeb et al., 2017). These structures remain tentative until the probable molecule structures have been verified by an analytical standard with regard to retention time and fragmentation spectra or other analytical techniques such NMR or infrared spectroscopy (Richardson and Kimura, 2016, Krauss et al., 2010).

Despite the advantages of HRMS and NMR, there are also some limitations to be faced (Krauss et al., 2010). Exemplarily limitations are the multiple separation runs for NMR and the need of an analytical standard or additional analytical technique (Schymanski et al., 2015, Krauss et al., 2010). Such a case may occur if isobaric substances, i.e. substances with the same exact mass, are present in an analytical run. These isobaric substances have the same molecular formula and may even share a highly similar structure. In the latter case, chromatographic separation is hardly possible and differentiation of isobaric substances becomes challenging as illustrated by

Schymanski et al. (2015) for triazine-derivative herbicides and their TPs. Fragmentation experiments, i.e. MS<sup>n</sup>-experiments, represent a possible solution to distinguish some isobaric substances (Schlüsener et al., 2015, Schymanski et al., 2015, Funke et al., 2016). Nevertheless, if different collision energies do not lead to specific fragmentation products but, e.g., only to CO<sub>2</sub> or H<sub>2</sub>O or highly similar analytes result in similar fragmentation spectra, this approach is not expedient (Krauss et al., 2010). These circumstances may pose a problem in identification of transformation pathways of oxidative processes. Due to the potential formation of isobaric TPs, the initial point of attack of the oxidant at the reactive site(s) of the detected TPs may often remain ambiguous. The oxidation of the antibiotic sulfamethoxazole by various oxidants illustrates this case (Gao et al., 2014). Additionally, several oxidative processes may lead to formation of similar TPs, which do not necessarily need to be formed by the same reaction pathways. In order to investigate the underlying mechanisms or to distinguish between several degradation processes compound-specific stable isotope analysis (CSIA) has been shown to be a useful proxy (Hofstetter et al., 2014, Elsner, 2010, Schmidt and Jochmann, 2012).

With CSIA, all compounds contained in a sample are first separated by either gas chromatography (GC) or liquid chromatography (LC). Subsequently, the separated compounds are oxidized to low molecular weight gases in an interface and the different isotopes of one element may be detected with isotope ratio mass spectrometry (IRMS) (Elsner et al., 2012, Jochmann and Schmidt, 2012). However, GC-IRMS is only applicable for compounds, which may be properly transferred to the gas phase. Derivatization has been shown to enable GC-IRMS analysis for a certain range of non-volatile compounds (Reinicke et al., 2010). In case of large molecules or if derivatization of the molecule is not possible, LC-IRMS may be an alternative. Here, carbon stable isotope values are readily determined via CO<sub>2</sub>. However, if stable isotope values for carbon ought to be determined it is inevitable that no organic solvents are used for compound separation with LC since these would significantly interfere with the analyte stable isotope values. Consequently, LC-IRMS measurements are only possible for a limited number of compound classes for which a purely aqueous phase separation is applicable. If the compounds are thermostable, a high temperature gradient for improved separation may be used as well (Kujawinski et al., 2012).

The high precision IRMS devices have a lack in sensitivity compared to HRMS instruments. Therefore, the low environmental concentration ranges which are generally detectable with HRMS are hardly amenable for IRMS measurements (Schmidt and Jochmann, 2012). For this reason, enrichment techniques have to be employed in many cases if environmental samples

are to be analyzed. For these cases, solid-phase extraction (Torrentó et al., 2019), purge and trap (Kujawinski et al., 2010, Jochmann et al., 2006) or solid-phase micro-extraction (Berg et al., 2007, Zwank et al., 2003) represent feasible solutions. Remaining matrix interferences after solid-phase extraction may substantially be reduced by a preparative LC cleanup step prior to GC-IRMS analysis (Melsbach et al., 2019, Schreglmann et al., 2013). Moreover, the successful use of custom-made molecularly imprinted polymers for selective enrichment of the target analyte, e.g. 1-H-benzotriazole, has been presented lately (Bakkour et al., 2018). These enrichment techniques have not yet been modified and validated for LC-IRMS, so that this remains a future goal in order to enable analysis of non-GC compatible compounds.

CSIA is a powerful tool to close further analytical gaps, which cannot be answered by HRMS alone. With CSIA, transformation processes in the environment or in batch experiments in the laboratory may be tracked (Elsner, 2010, Schmidt and Jochmann, 2012, Hofstetter and Berg, 2011). Additionally, it may be possible to distinguish dilution, sorption or volatilization from transformation effects. In this case, the potentially observed transformation needs to be accompanied by isotopic fractionation whereas transport or dilution processes are generally assumed to cause minor or even negligible isotope effects (Schmidt and Jochmann, 2012, Hofstetter et al., 2008).

Besides the plain distinction between dilution and transformation effects, CSIA may also provide valuable hints for identification of certain transformation mechanisms or enable distinction between several mechanisms or different oxidation processes. This is possible in certain cases because isotope fractionation is specific for each mechanism (Elsner, 2010). For the herbicide isoproturon it was shown that isotopic fractionation differed not only between abiotic and biotic hydrolysis but also depending on the respective bacterial or fungal strain responsible for biotransformation (Penning et al., 2010). Furthermore, CSIA has allowed valuable insights in the formation pathways of N-nitrosodimethylamine (Spahr et al., 2017a, Spahr et al., 2017b), degradation mechanisms of diclofenac in the environment and water treatment processes (Maier et al., 2016), oxidation of atrazine induced by the abiotic factors OH radicals, excited triplet states or direct photolysis (Hartenbach et al., 2008). Moreover, several studies have illustrated that the pH is a master variable, which significantly influences isotopic fractionation if the reactant may exist as protonated and deprotonated specie etc., e.g. during permanganate or electrochemical oxidation of *p*-methylaniline and further substituted anilines (Skarpeli-Liati et al., 2011) or photolysis of chloroanilines (Ratti et al., 2015b, Ratti et al., 2015a).

Recently, it was stated that the variety of TrOCs in the environment has reached such a high level that it is rather impossible to investigate TP formation for every single compound and identify each TP potentially formed. Instead, future research should focus on functional group behavior and oxidants, which may be applied to whole TrOCs classes in the next step (von Gunten, 2018). Consequently, this claim does not only apply to HRMS but also to CSIA analyses. Permanganate as oxidant has already been systematically studied in detail for oxidation of substituted anilines (Skarpeli-Liati et al., 2011) or several nitrotoluenes (Wijker et al., 2013) whereas CSIA regarding other chemical oxidants such as ozone (Willach et al., 2020, Maier et al., 2016) and ClO<sub>2</sub> (Willach et al., 2017) have hardly been tackled, yet. To fill this gap with systematic studies considering influences of pH or different functional groups of a compound class remains a challenging task for the future.



## **2. Chapter: Scope & Aims**

Phenols are relevant as structural units of dissolved organic matters and as trace organic compounds. Therefore, a better understanding of reaction conditions and product formation of oxidative reactions with phenol are important aspects in advanced water treatment. This work's central aim is to investigate the oxidative transformation of phenol as a probe compound with the oxidants chlorine dioxide ( $\text{ClO}_2$ ) and ozone ( $\text{O}_3$ ) under different conditions and utilizing multiple methods, including compound-specific stable isotope analysis (CSIA). Figure 2.1 represents a graphical overview that illustrates the content of the three major chapters of the presented work.

In **Chapter 3**, the focus is on the reaction of  $\text{ClO}_2$  with phenol. To that end, a concept for hypochlorous acid (HOCl) determination in the reaction of  $\text{ClO}_2$  with phenol is developed. Additionally, the formation and influence of HOCl in  $\text{ClO}_2$ -based transformation of trace organic compounds in wastewater treatment are investigated.

**Chapters 4 and 5** deal with the reaction of phenols with  $\text{O}_3$  in order to foster our understanding of the reaction mechanism. In **Chapter 4**, the stoichiometric ratio of  $\text{O}_3$  for phenol degradation, and which parameter influences it are tested. Therefore, the influence of different parameters (pH, OH radicals, organic products and superoxide) on stoichiometric ratio in the phenol reaction with  $\text{O}_3$  are compared to each other. Finally, the impact of different substituents at the phenolic ring on the stoichiometric ratio is studied (4-chlorophenol, 4-methylphenol, and 4-methoxyphenol).

In **Chapter 5**, for the first time as a proof of concept the correlation of  $\text{O}_3$  reaction kinetics with the extent of observed stable isotope fractionation is investigated at different pH values. Furthermore, the results of the phenols is compared with other electron-rich moieties (double bond (3-buten-2-ol) and triple bond (3-butyn-2-ol)).

An overall discussion and conclusion of the obtained results of this work is summarized in **Chapter 6**, and an outlook describing required future studies resulting from the presented thesis is given.

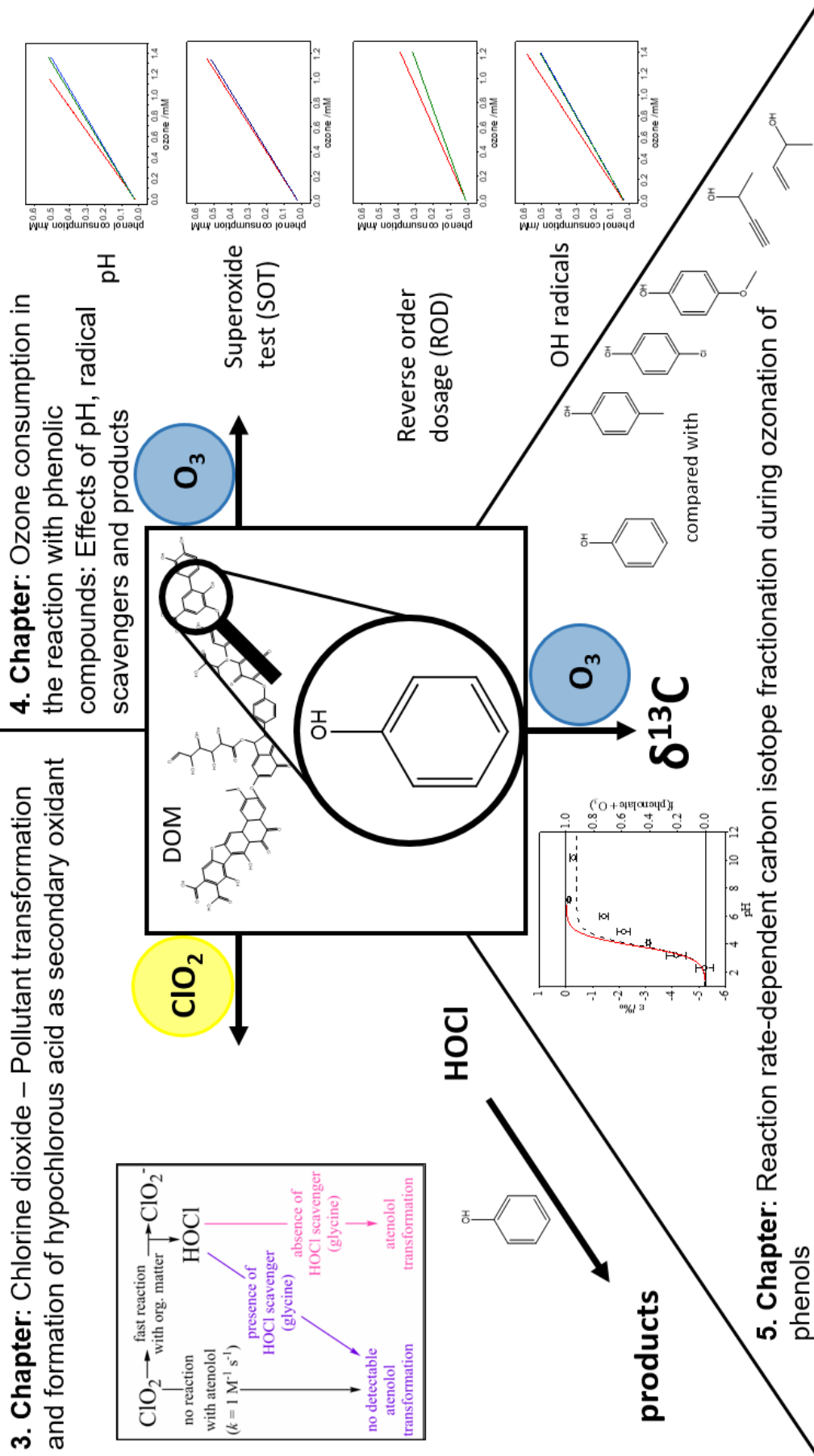


Figure 2.1: Graphical overview of the major content of this work.

# **3. Chapter: Chlorine dioxide – Pollutant transformation and hypochlorous acid formation as a secondary oxidant**

**Adapted from:** Terhalle, J., Kaiser, P., Jütte, M., Buss, J., Yasar, S., Marks, R., Uhlmann, H., Schmidt, T.C. and Lutze, H.V. (2018), *Chlorine dioxide—Pollutant transformation and formation of hypochlorous acid as a secondary oxidant*. *Environmental Science & Technology* 52(17), 9964-9971.

### 3.1 Introduction

Wastewater represents an important source of micropollutants in the environment (Hey et al., 2012). For minimizing the emissions of pollutants by wastewater treatment plant effluents, advanced treatment steps are currently implemented at many plants, in particular by ozonation and activated carbon treatment (Ebert et al., 2014). In contrast to activated carbon treatment, ozone ( $O_3$ ) also disinfects the wastewater. However, one drawback in ozonation is the formation of bromate ( $BrO_3^-$ ), a carcinogenic compound.

One alternative to ozone is chlorine dioxide ( $ClO_2$ ) that has already been used for a long time in drinking water disinfection (Gates, 2009, Huber et al., 2005). It is also a strong oxidant, which reacts if at all very slow with bromide ( $k(Br^- + ClO_2) < 0.01 M^{-1} s^{-1}$ ) (Neta et al., 1988) and results in a negligible formation of biodegradable dissolved organic carbon (BDOC) (Ramseier et al., 2011). The applicability of  $ClO_2$  for pollutant control in wastewater was demonstrated by Hey et al. (2012) who showed that more than 50 pharmaceuticals could be transformed by  $ClO_2$  in wastewater applying concentrations of  $1.25 - 20 mg L^{-1} ClO_2$  ( $1.9 \times 10^{-5} - 3.0 \times 10^{-4} M$ ). However, the overall number of pollutants, which can be transformed by  $ClO_2$ , is smaller compared to  $O_3$  mainly for two reasons. First  $ClO_2$  is more selective compared to  $O_3$  and second  $O_3$  forms highly reactive hydroxyl radicals, which can transform even very recalcitrant pollutants (such as iopamidol, atrazine or chlorobenzene) (Lee and von Gunten, 2010, von Gunten, 2003a, Huber et al., 2003).

Pollutants that react fast with  $ClO_2$  include those with activated aromatic systems (e.g., sulfamethoxazole ( $k(\text{sulfamethoxazole} + ClO_2) = 6.7 \times 10^3 M^{-1} s^{-1}$  at pH = 7.00 (Huber et al., 2005)). Other important functional groups which are reactive towards  $ClO_2$  are activated double bonds (indigotrisulfonate:  $k(\text{indigotrisulfonate} + ClO_2) > 2.5 \times 10^5 M^{-1} s^{-1}$  (Shen et al., 1987)) and activated neutral amines (protonated amines do not react with  $ClO_2$ ) (Ramseier et al., 2011, Rosenblatt et al., 1967). The reactivity of amines follows the sequence:  $k(\text{tertiary amines}) > k(\text{secondary amines}) > k(\text{primary amines})$  (Rosenblatt et al., 1967).

As with many oxidants,  $ClO_2$  also forms undesired by-products, in this case chlorite ( $ClO_2^-$ ). The maximum contaminant levels (MCL) of chlorite in drinking water ranges from  $0.2 mg L^{-1}$  ( $3 \times 10^{-6} M$ ) (Germany) to  $1 mg L^{-1}$  ( $1.5 \times 10^{-5} M$ ) (United States Environmental Protection Agency (US-EPA)). Even though there is no regulation on maximal chlorite concentrations in

### 3. Chapter: Chlorine dioxide – Pollutant transformation and hypochlorous acid formation as a secondary oxidant

---

wastewater, one may expect that it will be associated to the drinking water regulation in analogy to bromate formation in ozonation.

For the formation of by-products, the reaction of  $\text{ClO}_2$  with the wastewater matrix is important. In this context, dissolved organic matter (DOM) is a key matrix constituent, which is a complex partly polymeric material containing electron rich phenolic moieties such as hesperetin (Rook, 1977). These structures can be considered to be the main reaction partners of  $\text{ClO}_2$ . Wajon et al. (1982) postulated a reaction mechanism for the reaction of  $\text{ClO}_2$  with phenolic compounds resulting in formation of hypochlorous acid (HOCl) and  $\text{ClO}_2^-$ . The phenolic anion reacts with  $\text{ClO}_2$  to the phenoxy radical and  $\text{ClO}_2^-$ . The ensuing phenoxy radical undergoes a very fast subsequent reaction with  $\text{ClO}_2$  resulting in *p*-benzoquinone and HOCl (further details on the mechanism can be found in Chapter 3.4.1 in supporting information (SI) (Chapter 3.4). In addition, some other authors postulated the formation of HOCl during the reaction of organic compounds with  $\text{ClO}_2$  (Stewart et al., 2008, Napolitano et al., 2006, Napolitano et al., 2005).

It is important to know if and how much HOCl is formed to foster our understanding of pollutant transformation and by-product formation in  $\text{ClO}_2$ -based processes. However, experimental evidence for the formation of HOCl and a suitable approach for quantification of HOCl formation in wastewater or drinking water treatment is still lacking. Furthermore, HOCl itself can produce halogenated by-products such as undesired trihalomethanes (THMs) (MCL in drinking water is  $0.08 \text{ mg L}^{-1}$ ) (Henry, 2013). However, Hua and Reckhow (2007) reported that the application of  $\text{ClO}_2$  hardly forms THMs in drinking water purification. Although, other halogenated by-products can be formed (Hua and Reckhow, 2007, Han et al., 2017). A lot of studies reported formation of halogenated products during chlorination. When HOCl is formed in the  $\text{ClO}_2$  system, the same products can be formed (Liu and Zhang, 2014, Pan and Zhang, 2013, Jiang et al., 2017).

The present paper deals with the formation of HOCl in reaction of  $\text{ClO}_2$  with organic matter. Therefore, a new concept for HOCl determination in the reaction of  $\text{ClO}_2$  with phenol was developed. Additionally, formation and influence of HOCl in  $\text{ClO}_2$  based transformation of micropollutants in wastewater treatment were investigated.

## 3.2 Material and methods

### 3.2.1 Chemicals

All chemicals and solvents were used as received from suppliers. A complete list of all chemicals used can be found in Table 3.2 in the Chapter 3.4.

### 3.2.2 Equipment

The used equipment is summarized in Table 3.3 in Chapter 3.4.

### 3.2.3 Generation of ozone and chlorine dioxide stock solutions

For the preparation of O<sub>3</sub> stock solutions, oxygen was enriched with O<sub>3</sub> by an ozone generator (Table 3.3). That gas was bubbled into ice cooled ultrapure water. After an enrichment phase of approximately 45 minutes the O<sub>3</sub> concentration was determined by UV absorption of a 1:3-diluted O<sub>3</sub> stock solution at 258 nm,  $\epsilon_{\text{O}_3} = 2950 \text{ M}^{-1} \text{ cm}^{-1}$  (Hoigné and Bader, 1980). The O<sub>3</sub> concentration in the stock solution ranged between  $1.3 \times 10^{-3}$  -  $1.6 \times 10^{-3}$  M. Continuous purging of the stock solution with gaseous O<sub>3</sub> was required to keep the O<sub>3</sub> concentration constant.

ClO<sub>2</sub> stock solutions were prepared by mixing of 50 mL of a 0.885 M NaClO<sub>2</sub> solution with 50 mL of a 0.164 M Na<sub>2</sub>S<sub>2</sub>O<sub>8</sub> solution. Further purification steps were performed according to a chlorine-free method described by Gates (1998) (Chapter 3.4.2). The resulting concentrations were determined by UV absorption measurements of a 1:30-diluted ClO<sub>2</sub> stock solution at 359 nm,  $\epsilon_{\text{ClO}_2} = 1200 \text{ M}^{-1} \text{ cm}^{-1}$  (Hoigné and Bader, 1994). Concentrations of the ClO<sub>2</sub> stock solutions used during this study were in the range of  $8.0 \times 10^{-3}$  –  $1.6 \times 10^{-2}$  M ClO<sub>2</sub>.

### 3.2.4 Detection of hypochlorous acid in the reaction of chlorine dioxide with phenol

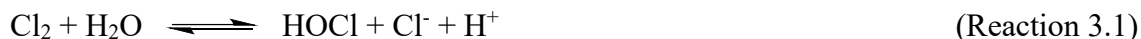
#### Experimental concept:

In brief HOCl formed in the reaction of phenol with ClO<sub>2</sub>, was scavenged by a surplus of bromide (Br<sup>-</sup>) resulting in hypobromous acid (HOBr) and chloride (Cl<sup>-</sup>). HOBr in turn, was determined by scavenging with phenol and determining the products 2- and 4-bromophenol. Detailed explanations can be obtained from Chapter 3.4.3. According to Fischbacher et al. (2015) the optimal pH for bromination of phenol by HOBr is at pH 4.00 (Chapter 3.4.8). Note that at this pH HOCl and HOBr are the most abundant chlorine and bromine species (Deborde

### 3. Chapter: Chlorine dioxide – Pollutant transformation and hypochlorous acid formation as a secondary oxidant

---

and von Gunten, 2008, Korshin, 2011). The other chlorine species (such as  $\text{Cl}_2$  and  $\text{OCl}^-$ ) are present at very small fractions at this pH. According to Deborde and von Gunten (2008) the  $\text{Cl}_2$  hydrolysis is almost complete at pH 4 in presence of 5 mM chloride (Reaction 3.1) and the pH is below the  $\text{pK}_a$  value of HOCl (see below).



Taking reaction kinetics into account, even small fractions of a highly reactive species can still be important for a chemical reaction. To that end, one cannot exclude that other free chlorine species than HOCl (i.e.,  $\text{Cl}_2$  and  $\text{Cl}_2\text{O}$ ) may also have oxidized bromide. However, the excellent recovery rates of HOCl in the validation experiments (Figure 3.14 - Figure 3.16) indicate that this does not affect the determination of HOCl. Same applies to HOBr.

#### Validation of the method

To verify that the concentration of 2- and 4-bromophenol resembled the HOCl concentration, experiments were performed in which HOCl was dosed to the reaction solution. For these experiments, the concentration of the stock solution of sodium hypochlorite ( $\text{NaOCl}$ ) was determined by measuring its UV-absorption. Therefore, an extinction coefficient of  $362 \text{ M}^{-1} \text{ cm}^{-1}$  at 292 nm of the hypochlorite anion ( $\text{OCl}^-$ ) was used (Furman and Margerum, 1998). For assuring that  $\text{OCl}^-$  is the predominant species, the pH was adjusted with NaOH to 10.0, which is considerably above the  $\text{pK}_a$  value of HOCl ( $\text{pK}_a(\text{HOCl}) = 7.47$ ) (Furman and Margerum, 1998).

For the validation experiments, three different approaches were used:

**A:** The reaction solution of phenol ( $1.0 \times 10^{-3} \text{ M}$ ), bromide ( $1.0 \times 10^{-2} \text{ M}$ ) and phosphate buffer ( $5.0 \times 10^{-3} \text{ M}$ ) was prepared and adjusted with  $\text{H}_3\text{PO}_4$  and NaOH to  $\text{pH } 4.00 \pm 0.05$ . Aliquots of 10 mL solution were filled in 20 mL headspace vials. Different volumes of the HOCl stock solution were added to this solution (30 – 190  $\mu\text{L}$ ) for final concentrations of  $2.0 \times 10^{-5} - 1.2 \times 10^{-4} \text{ M}$ .

**B:** The solution of  $1.0 \times 10^{-3} \text{ M}$  phosphate buffer was prepared and adjusted to  $\text{pH } 4.00 \pm 0.05$ . After this solution was filled in 20 mL headspace vials, different HOCl concentrations ( $2.0 \times 10^{-5} - 1.2 \times 10^{-4} \text{ M}$ ) were added to this buffer solution. At last step, a solution containing phenol and bromide was added with the final concentration of  $1.0 \times 10^{-3} \text{ M}$  phenol and  $1.0 \times 10^{-2} \text{ M}$  bromide.



### 3. Chapter: Chlorine dioxide – Pollutant transformation and hypochlorous acid formation as a secondary oxidant

---

C: Here, the same approach as in B was applied with a higher concentration of phenol ( $6.0 \times 10^{-3}$  M) and bromide ( $6.0 \times 10^{-2}$  M).

#### Dosage of chlorine dioxide

The reaction solution consisted of phenol ( $1.0 \times 10^{-3}$  M), bromide ( $1.0 \times 10^{-2}$  M) and phosphate buffer ( $5.0 \times 10^{-3}$  M). Aliquots of 10 mL solution were filled in 20 mL headspace vials. The solutions in the headspace vials were treated with 6 different dosages of ClO<sub>2</sub> (29 – 175 µL) resulting in final concentrations of  $2.0 \times 10^{-5}$  –  $1.2 \times 10^{-4}$  M ClO<sub>2</sub>. Samples were analyzed after 24 h after experiment was performed. After this reaction time, ClO<sub>2</sub> was completely consumed. Experiments were done in triplicates at each dose

#### Sample measurement:

The samples were measured by ion chromatography (Chapter 3.4.4) for the determination of chloride and chlorite and with HPLC-UV for the determination of the bromophenols (Table 3.4). Calibration of each investigated substance was integrated in each measurement sequence.

### **3.2.5 Experiments in wastewater**

Based on results of Wajon et al. (1982) HOCl might also be formed in reaction of ClO<sub>2</sub> with wastewater organic matter. To investigate the effect of HOCl on the transformation of micropollutants in oxidation with ClO<sub>2</sub> and for comparison the ClO<sub>2</sub>-based process with the ozonation, four tracer pollutants (Figure 3.7) were added to samples from a municipal wastewater effluent (DOC =  $8.11 \pm 0.12$  mg L<sup>-1</sup>, [NH<sub>3</sub>] < 0.1 mg L<sup>-1</sup>, Chapter 3.4.5) with a concentration of  $1 \times 10^{-6}$  M prior to oxidant addition. Two compounds were chosen that react fast with HOCl and slowly with ClO<sub>2</sub> (atenolol, metoprolol (Lee and von Gunten, 2010)), one pollutant that reacts fast with HOCl and ClO<sub>2</sub> (sulfamethoxazole (Lee and von Gunten, 2010)) and one that slowly reacts with HOCl and ClO<sub>2</sub> (5,6-dimethyl-1-*H*-benzotriazol). All compounds react fast with ozone. The pH of the wastewater was adjusted to a value of  $7.90 \pm 0.05$  that is typical for this wastewater. Different concentrations of oxidants were added to the wastewater ( $2.0 \times 10^{-5}$  –  $1.2 \times 10^{-4}$  M). Experiments were performed in presence and absence of  $5 \times 10^{-4}$  M glycine to assess the effect of HOCl, which may be formed *in-situ* in the application of ClO<sub>2</sub>. Glycine can selectively scavenge HOCl ( $k = 1 \times 10^5$  M<sup>-1</sup> s<sup>-1</sup> (Hoigné and Bader, 1994)) since it slowly reacts with ClO<sub>2</sub> ( $k = 1 \times 10^{-3}$  M<sup>-1</sup> s<sup>-1</sup> (Pattison and Davies, 2001)). Therefore, an effect of the glycine dose on pollutant transformation indicates the presence of

### 3. Chapter: Chlorine dioxide – Pollutant transformation and hypochlorous acid formation as a secondary oxidant

---

HOCl. Samples were measured after >24 hours after experiment was performed to provide sufficient time for complete ClO<sub>2</sub> consumption.

For investigating if other oxidants than ClO<sub>2</sub> are involved in pollutant transformation following approach was applied. Using Equation 3.1 (von Sonntag and von Gunten, 2012) pollutant abatement can be calculated on basis of oxidant exposure ( $\int[Ox]dt$ ). The exposure was determined by measuring oxidant depletion over time and calculating the time based integral. For determination of the oxidant concentration, the indigo method was used for both oxidants following the procedure described by Hoigné and Bader (1980). The exact approach is described in Chapter 3.4.6. In case of the ClO<sub>2</sub> experiment, only ClO<sub>2</sub> exposure was used and the calculated pollutant transformation was compared with experimental results.

The case that calculated data do not match with the measured data indicates that other (secondarily formed) oxidants such as HOCl are involved. The same approach was applied for O<sub>3</sub>.

$$\frac{c}{c_0} = e^{-k \times \int[Ox]dt} \quad \text{(Equation. 3.1)}$$

$c$  = concentration of the pollutant at time  $t$  [M]

$c_0$  = concentration of the pollutant at time 0 [M]

$k$  = second order reaction rate constant of the pollutant with the oxidant [M<sup>-1</sup> s<sup>-1</sup>]

$\int[Ox]dt$  = oxidant exposure in this wastewater [M × s]

The second order reaction rate constants of atenolol and sulfamethoxazole were taken from Lee and von Gunten (2010). The reaction rate constants of metoprolol and 5,6-dimethyl-1-*H*-benzotriazol (DMBT) and the oxidant exposure of ClO<sub>2</sub> and O<sub>3</sub> were determined in this study.

#### Determination of the second order reaction rate constant of DMBT with chlorine dioxide:

For the determination of the reaction rate constant of DMBT with ClO<sub>2</sub> the concept of the pseudo-first order kinetics was used which was described in “Method I” section in the SI of Dodd et al. (2006). Thereby ClO<sub>2</sub> depletion was determined in presence of DMBT ( $1 \times 10^{-3}$  M) which was present in 50 times excess over ClO<sub>2</sub> concentration ( $2 \times 10^{-5}$  M). The pH was adjusted with H<sub>3</sub>PO<sub>4</sub> and NaOH to  $8.00 \pm 0.05$  and buffered by  $5 \times 10^{-3}$  M phosphate buffer.

The solution of DMBT was added into a quartz cuvette (1 cm path length) and ClO<sub>2</sub> was directly added to that cuvette. After turning the cuvette two times upside down, the kinetics of ClO<sub>2</sub> degradation was measured by UV absorption measurements at 359 nm.

Determination of the second order reaction rate constant of metoprolol with chlorine dioxide:

It was not possible to use pseudo-first order kinetics because the 50 times excess of metoprolol over ClO<sub>2</sub> cannot be achieved, due to the low solubility of metoprolol in water. Therefore, competition kinetics was used for the determination of the reaction rate constant of metoprolol with ClO<sub>2</sub> according to “Method IV” section of the SI of Dodd et al. (2006). Here, atenolol was used as competitor. The reaction solution consisted of  $1 \times 10^{-5}$  M atenolol,  $1 \times 10^{-5}$  M metoprolol,  $1 \times 10^{-3}$  M glycine and  $1 \times 10^{-3}$  M phosphate buffer. The pH was adjusted with H<sub>3</sub>PO<sub>4</sub> and NaOH to  $8.00 \pm 0.05$  and different concentrations of ClO<sub>2</sub> were added to the reaction system ( $5 \times 10^{-6} - 3 \times 10^{-5}$  M ClO<sub>2</sub>). The concentrations of atenolol and metoprolol were measured with HPLC-UV (Table 3.4).

Sample measurement:

The samples were measured by ion chromatography (Chapter 3.4.4) for the determination of chloride, chlorite, bromide and bromate. Additionally, for the determination of the tracer pollutants in wastewater the samples were measured with HPLC-UV (Table 3.4). Calibration of each investigated substance was integrated in each measurement sequence.

### 3.3 Results and discussion

#### 3.3.1 Validation of the HOCl detection

Validation experiments were done to assure that the concentration of 2- and 4-bromophenol represent the HOCl concentration. Therefore, three different approaches were used (see Chapter 3.2.4). The comparison of these three approaches is shown in Figure 3.1. In experiment A, HOCl was dosed to the reaction solution of phenol and Br<sup>-</sup> at pH 4.00. The results of these experiment show that the dosage of HOCl does not match the yield of 2-bromophenol and 4-bromophenol (Figure 3.1 and Figure 3.13). Only  $9 \pm 1$  % of 4-bromophenol was formed with respect to the dosage of HOCl (2-bromophenol was below the limit of quantification (LOQ)). Indeed, most of HOCl formed 2,4,6-tribromophenol ( $75 \pm 2$  % average of all samples and HOCl dosages). The formation of 2,4-dibromo- and 2,4,6-tribromophenol requires 2 and 3 equivalents

of HOCl. Considering this, the sum of all bromophenols formed fairly agree with the dosage of HOCl ( $87 \pm 8\%$  recovery on average of all samples and HOCl dosages).

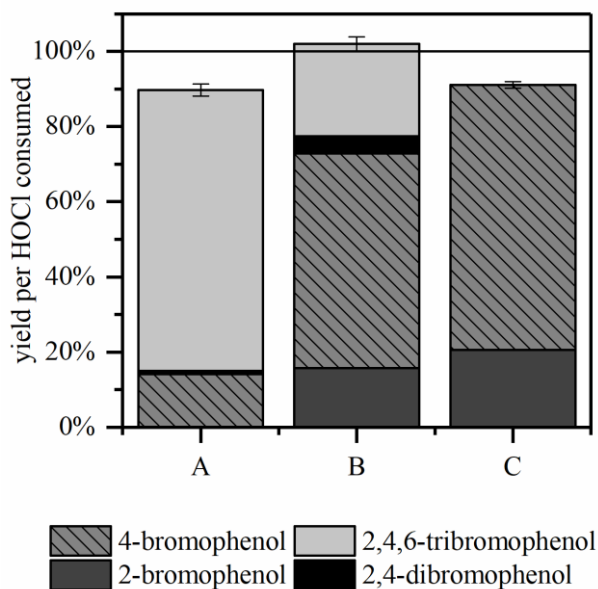


**Figure 3.1: Yield of bromophenols per HOCl consumed. A:**  $60\ \mu\text{M}$  HOCl was added to the solution of phenol ( $1.0 \times 10^{-3}\ \text{M}$ ) and bromide ( $1.0 \times 10^{-2}\ \text{M}$ ). **B:** the solution of phenol ( $1.0 \times 10^{-3}\ \text{M}$ ) and bromide ( $1.0 \times 10^{-2}\ \text{M}$ ) was added to the solution of HOCl with a concentration of  $60\ \mu\text{M}$ . **C:** The solution of phenol ( $6.0 \times 10^{-3}\ \text{M}$ ) and bromide ( $6.0 \times 10^{-2}\ \text{M}$ ) was added to the solution of HOCl with a concentration of  $60\ \mu\text{M}$  ( $\text{pH} = 4.00 \pm 0.05$ ).

The formation of multiple bromophenols can be explained as follows. After addition of HOCl to the solution containing phenol and bromide, time is needed for complete mixing of HOCl. In this mixing time, the fast reaction between HOCl of the dosed solution and bromide in the bulk solution can happen at the interface between these two solutions. However, at this interface the HOCl concentration is much higher compared to the completely mixed solution. The spots of high HOCl concentration may result in locally high HOBr concentration, which may in turn have favored formation of 2,4-di- and 2,4,6-tribromophenol. Tee et al. (1989) reported that at  $\text{pH}\ 4.00$  mono- (e.g., 2-bromophenol:  $k(\text{HOBr}) = 6.8 \times 10^5\ \text{M}^{-1}\ \text{s}^{-1}$  (Tee et al., 1989)) and di-bromophenols (2,4-dibromophenol:  $k(\text{HOBr}) = 7.24 \times 10^5\ \text{M}^{-1}\ \text{s}^{-1}$  (Tee et al., 1989)) are more reactive towards HOBr than phenol ( $k(\text{HOBr}) = 5.0 \times 10^2\ \text{M}^{-1}\ \text{s}^{-1}$  (Pinkernell and von Gunten, 2001)) by several orders of magnitude. This is due to a decrease in  $\text{p}K_a$  of the phenols with increasing degree of halogenation ( $\text{p}K_a$  (phenol) = 10;  $\text{p}K_a$  (2-bromophenol) = 8.43,  $\text{p}K_a$  (4-bromophenol) = 9.17;  $\text{p}K_a$  (2,4-dibromophenol) = 7.79) (Acero et al., 2005, Hoigné and Bader, 1994).

To prevent the excess of HOCl in the validation experiment at the interface between the dosed solution and bulk solution the following procedure was used in further experiments (approach B and C in Chapter 3.2.4). A small volume of a solution containing high concentration of phenol and bromide was added to 15 mL of HOCl solutions with different concentrations. With this approach the above described interface effect results in a local surplus of bromide and phenol suppressing multiple bromination. With a phenol and bromide concentration of  $1.0 \times 10^{-3}$  M and  $1.0 \times 10^{-2}$  M the surplus was not high enough to completely suppress multiple bromination (Figure 3.1 and Figure 3.14). At a HOCl concentration of  $6.0 \times 10^{-5}$  M, 30% of multiple brominated phenols were formed. With increasing the phenol and bromide concentration (approach C), the yield of 2,4,6-tribromophenol was indeed below LOQ (Figure 3.1 and Figure 3.15). Only at the highest HOCl concentration (120  $\mu$ M) 2,4,6-tribromophenol ( $7 \pm 1$  %) and 2,4-dibromophenol ( $3 \pm 0.3$  %) were formed. Below 120  $\mu$ M HOCl the ratio of 2-bromophenol and 4-bromophenol was the same as the ratio of 2-bromophenol and 4-bromophenol after ClO<sub>2</sub> dosage (see below). Additionally, the recovery of HOCl was nearly complete ( $90 \pm 2$  %). The results have shown that our method for determination of HOCl *via* bromophenols formation can result in different products. However, the concentration of bromine attached to the bromophenols gave a complete HOCl recovery at all experimental conditions and all combinations of products formed. This strongly corroborates that our concept allows determining HOCl formation in the reaction of ClO<sub>2</sub> with phenol. The results also indicated, that in mechanistic studies the experimental approach can have a very strong effect on the product formation. Especially in case of fast reactions, envisaged surplus of compounds under study over e.g., an oxidant may not be prevalent in case oxidant stock solution are dosed to reaction mixtures of the parent compounds. These results are similar with the results of Schreiber and Mitch (2005). They found the same phenomena in the formation of NDMA during the reaction of chloramine and hypochlorous acid. The concentration and the order of reagent addition have an influence on product formation. Shah et al. (2015) used 2,6-dichlorophenol for the determination of HOBr. This setup has the advantage that dibromophenol and tribromophenol cannot be formed. There can only one product formed (4-bromo-2,6-dichlorophenol). However, in our case the influence of the order of reagent addition on the product formation would not been recognized.

### 3.3.2 Detection of hypochlorous acid from reactions of chlorine dioxide with phenol

As explained above, formation of bromophenols indicates presence of HOCl. Indeed, bromophenols were observed. The yield of the sum of 4- and 2-bromophenol was  $42 \pm 3 \%$  regardless the  $\text{ClO}_2$  dose. 4-bromophenol was the main product with  $35 \pm 2 \%$  (Figure 3.12). Multiple bromination was not observed. This can be explained as follows. At first  $\text{ClO}_2$  reacts with phenol with a slow second order reaction rate constant ( $k = 49 \text{ M}^{-1} \text{ s}^{-1}$ , at pH 4) to  $\text{ClO}_2^-$  and HOCl. This reaction is slow enough to provide sufficient time for mixing. After complete mixing, HOBr is formed in a follow-up reaction from reaction of HOCl with bromide and thus, experience a surplus of phenol likewise the validation experiment C.

Since the yield of bromophenols represents the yield of HOCl, it can be included in the chlorine mass balance of  $\text{ClO}_2$  (Figure 3.2a). Therefore, with  $62 \pm 4 \%$  of  $\text{ClO}_2^-$  and  $42 \pm 3 \%$  of HOCl the chlorine balance is complete. In the reaction of HOCl with  $\text{Br}^-$ , stoichiometric concentrations of  $\text{Cl}^-$  are formed. Hence, the sum of  $\text{Cl}^-$  and  $\text{ClO}_2^-$  must also resemble the concentration of dosed  $\text{ClO}_2$ . This is shown in Figure 3.2b corroborating the experimental concept, albeit slightly exceeding the chlorine mass balance. These results are consistent with the postulated reaction mechanism of Wajon et al. (1982) (Figure 3.5).

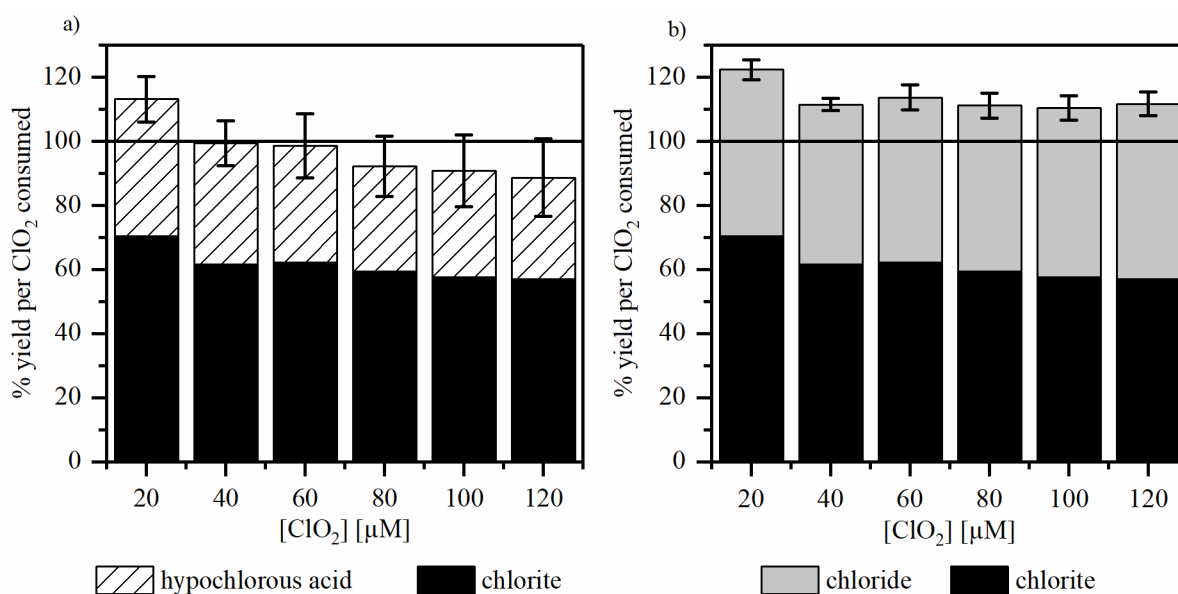


**Figure 3.2:** a) Yield of chlorite and hypochlorous acid and b) yield of chlorite and chloride in the reaction of phenol with  $\text{ClO}_2$  in presence of bromide at pH 4.00 ( $[\text{phenol}] = 1 \times 10^{-3} \text{ M}$ ,  $[\text{bromide}] = 1 \times 10^{-2} \text{ M}$ ,  $[\text{phosphate buffer}] = 5 \times 10^{-3} \text{ M}$ , different  $\text{ClO}_2$  dosages,  $T = 25^\circ\text{C}$ , in ultrapure water). The horizontal lines mark the 100 % yield and the error bars are the standard deviation of the triplicates.

### 3.3.3 Pollutant transformation in ClO<sub>2</sub> based wastewater treatment

For interpreting the transformation of micropollutants upon dosage of ClO<sub>2</sub> to wastewater, it is necessary to know the associated reaction rate constants. Table 3.1 compiles the reaction rate constants of the micropollutants, which were investigated in the present study.

**Table 3.1: Second order rate constants of the compounds under study at pH 8, exception DMBT pH 7\*.**

Compound	$k$ (ClO <sub>2</sub> ) [M <sup>-1</sup> s <sup>-1</sup> ]	Ref.	$k$ (HOCl) [M <sup>-1</sup> s <sup>-1</sup> ]	Ref.
Atenolol (ATL)	1.0	(Yang et al., 2013, Lee and von Gunten, 2010)	$3.5 \times 10^4$	(Lee and von Gunten, 2010, Yang et al., 2013)
5,6-dimethyl-1- <i>H</i> -benzotriazol (DMBT)	$4.5 \times 10^{-1}$	This study	$1.2 \times 10^2$ *	Calculated from (Nika et al., 2017)
Metoprolol (MET)	1.3	This study	$4.5 \times 10^4$	
Sulfamethoxazole (SMX)	$7.9 \times 10^3$	(Lee and von Gunten, 2010)	$5.7 \times 10^2$	(Lee and von Gunten, 2010)

The reaction rate constants indicate that atenolol, metoprolol and DMBT react slowly with ClO<sub>2</sub> and cannot be readily transformed by ClO<sub>2</sub>. However, the high reaction rate constant of SMX with ClO<sub>2</sub> suggests that this compound is readily transformed by ClO<sub>2</sub> which was also shown by Lee and von Gunten (2010).

Figure 3.3 shows the experimentally determined and calculated transformation of atenolol in wastewater. With the oxidant exposure for a ClO<sub>2</sub> dosage of  $5 \times 10^{-5}$  M at hand (further details see Chapter 3.4.7) the transformation of atenolol is calculated to be only 1 %. This contradicts the experimental data displaying a transformation of 40 %. The higher degree of transformation suggests the formation of a secondary oxidant. As previously stated it is possible, that during the reaction of ClO<sub>2</sub> with organic matter HOCl is formed which reacts very fast with atenolol ( $k = 3.5 \times 10^4 \text{ M}^{-1} \text{ s}^{-1}$  (at pH 8)) (Lee and von Gunten, 2010). It has to be mentioned that atenolol transformed by HOCl may reform atenolol upon further reaction. This was observed in presence of a reductive agent (e.g., thiosulfate (Lee and von Gunten, 2010)) and may also happen with other chloramines. Presence of HOCl can be investigated by addition of a selective scavenger, which predominantly reacts with HOCl. Glycine is such a selective scavenger and further experiments were performed in presence of  $5 \times 10^{-4}$  M glycine. In presence of glycine, 7 % of atenolol was transformed, after dosage of  $5 \times 10^{-5}$  M ClO<sub>2</sub>, which fairly matches the calculated transformation based on the ClO<sub>2</sub> exposure.



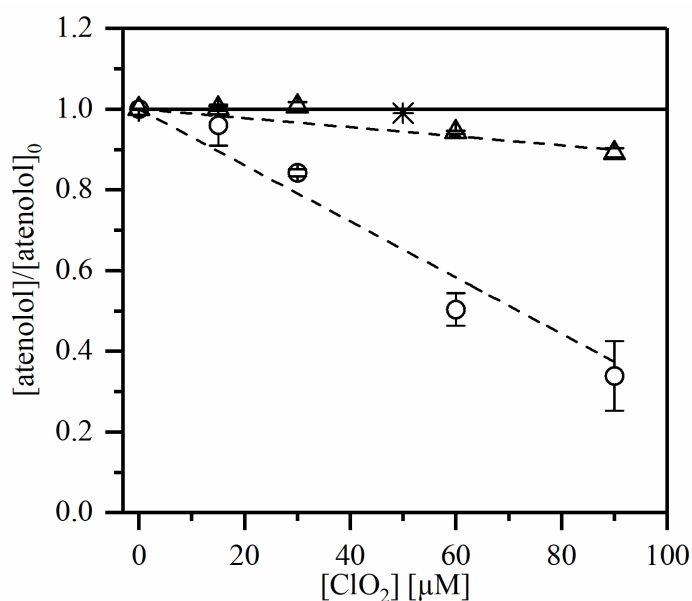


**Figure 3.3:** Transformation of atenolol by ClO<sub>2</sub> in absence (circles) and presence (triangles) of glycine. The predicted value was calculated with equation 1 and the exposure of ClO<sub>2</sub> (star) (dashed line: linear regression forced through x/y = 0/1, [atenolol]<sub>0</sub> = 1 × 10<sup>-6</sup> M, [glycine] = 5 × 10<sup>-4</sup> M, DOC = 8.11 ± 0.12 mg L<sup>-1</sup>; [NH<sub>3</sub>] < 0.1 mg L<sup>-1</sup>; pH = 7.90 ± 0.05, T = 22°C, error bars are the standard deviation of the triplicates, recovery = 99 ± 5 %, reaction time > 24 h).

With the results of Figure 3.3 at hand, the fraction of atenolol transformed by HOCl can be calculated (ClO<sub>2</sub> based treatment) (Equation 3.2). Thus, 83 % of the transformed atenolol can be attributed to reactions with HOCl and 17 % to reactions with ClO<sub>2</sub> (Figure 3.20). In sum, these results strongly suggest that intrinsically formed HOCl was most important for the transformation of atenolol.

$$\% \text{ transformation by HOCl} = \frac{\text{transformation in absence of glycine} - \text{transformation in presence of glycine}}{\text{transformation in absence of glycine}} \quad (\text{Eq. 3.2})$$

Metoprolol showed a similar behavior (Figure 3.20). 47 % and 9 % of metoprolol were transformed in absence and presence of glycine, respectively, at a dose of 5 × 10<sup>-5</sup> M ClO<sub>2</sub>. In Figure 3.20 the relative contribution of HOCl and ClO<sub>2</sub> regarding the metoprolol transformation is shown. 81 % of the transformed metoprolol can be attributed to reactions with HOCl and 19 % to reactions with ClO<sub>2</sub>. Thus, HOCl has also a strong influence on the transformation of metoprolol. The similar behavior of the results of atenolol and metoprolol can be explained by the similar structures of the two compounds, having the same functional groups. Both compounds probably react with ClO<sub>2</sub> and HOCl at their secondary amine. Since, activation of the nitrogen by the methyl groups is rather weak, the reactivity towards ClO<sub>2</sub> is small. However,

HOCl reacts fast with nearly all amines. Indeed, even ammonia which is slowly degraded by even strong oxidants such as  $O_3$  ( $k(NH_3 + O_3) = 2.2 \times 10^1 M^{-1} s^{-1}$  (Neta et al., 1988)) is rapidly converted to chloramines by HOCl. Thus, the formation of HOCl in  $ClO_2$  based water treatment may increase the overall number of pollutants, which can be transformed in this process. The system becomes more complex in presence of  $Br^-$ , which can scavenge HOCl resulting in HOBr (Kumar and Margerum, 1987). Many organic compounds react with HOBr even faster than with HOCl. Thus, HOBr may become important for pollutant transformation in application of  $ClO_2$  as well (Acero et al., 2005, Criquet et al., 2015).

The transformation of SMX (Figure 3.22) was not affected by the presence of glycine. This corroborates that at the present experimental conditions, glycine did not affect the  $ClO_2$  concentration and that HOCl did not contribute to SMX transformation. This can be explained by a lower reactivity of SMX with HOCl ( $k(SMX + HOCl) = 5.7 \times 10^2 M^{-1} s^{-1}$  (Lee and von Gunten, 2010)) compared with  $ClO_2$  ( $k(SMX + ClO_2) = 7.9 \times 10^3 M^{-1} s^{-1}$  (Lee and von Gunten, 2010)). Additionally, the concentration of  $ClO_2$  is higher than the concentration of HOCl.

The comparison of wastewater ozonation with the application of  $ClO_2$  reveals that SMX was transformed better in the latter process, even though  $O_3$  reacts 2 orders of magnitudes faster with SMX ( $k(SMX + O_3) = 5.7 \times 10^5 M^{-1} s^{-1}$  (Lee and von Gunten, 2010)) than  $ClO_2$  ( $k(SMX + ClO_2) = 7.9 \times 10^3 M^{-1} s^{-1}$  (Lee and von Gunten, 2010)). With the dosage of  $3 \times 10^{-5} M$ ,  $ClO_2$  transformed 96 % and  $O_3$  only 58 % of SMX. This result can be explained by the higher exposure of  $ClO_2$  in wastewater (Chapter 3.4.9), which compensated the lower reactivity of SMX with  $ClO_2$  compared to  $O_3$ . These results readily agree with the study of Lee and von Gunten (2010) on SMX transformation.

Furthermore, the reaction of DMBT was studied (Figure 3.23). Nika et al. (2017) reported that DMBT reacts slowly with  $ClO_2$  and HOCl. The transformation of DMBT by  $ClO_2$  was ~1 % in experiments in presence and absence of glycine. These results confirmed the slow reaction rate constants with  $ClO_2$  and HOCl.

The above results strongly suggest that HOCl may indeed be formed during  $ClO_2$  based wastewater treatment and subsequently may contribute to the transformation of micropollutants that slowly react with  $ClO_2$ . A further example from literature is ciprofloxacin (CIP). Hey et al. (2012) reported a > 90 % transformation of CIP in wastewater in the  $ClO_2$  application at a small  $ClO_2$  dosage of  $1.8 \times 10^{-5} M$  ( $1.25 mg L^{-1}$ ) even though CIP reacts slowly with  $ClO_2$

( $k(\text{CIP} + \text{ClO}_2) = 7.9 \text{ M}^{-1} \text{ s}^{-1}$  (Wang et al., 2010)). The experimentally determined transformation of atenolol in absence of glycine allows calculating the exposure of HOCl after solving Equation 3.1 for exposure. Then exposure can be calculated from atenolol transformation (reaction of  $\text{ClO}_2$  were neglected). With the exposure of  $\text{ClO}_2$  and HOCl at hand, the transformation of CIP in the wastewater of the present study can be estimated (using Equation 3.1 again). At a dosage of  $1.5 \times 10^{-5} \text{ M ClO}_2$  the HOCl exposure in the wastewater was  $2.3 \times 10^{-6} \text{ M} \times \text{s}$  ( $> 24 \text{ h}$  after  $\text{ClO}_2$  dosage). The estimated transformation of CIP in the present wastewater was 82 % by HOCl ( $k(\text{CIP} + \text{HOCl}) = 7.6 \times 10^5 \text{ M}^{-1} \text{ s}^{-1}$  (Deborde and von Gunten, 2008)) and 9 % by  $\text{ClO}_2$  (Figure 3.20). Hence, CIP would also be readily transformed upon  $\text{ClO}_2$  dosage in the wastewater of the present study, however, mainly by its reaction with HOCl. The high transformation degree of CIP reported by Hey et al. (2012) also suggests that HOCl formation played an important albeit unnoted role in their experiments.

Comparing the oxidative wastewater treatment based on  $\text{ClO}_2$  with that based on  $\text{O}_3$  shows, that  $\text{ClO}_2$  is a much more selective oxidant. On the one hand, the high selectivity of  $\text{ClO}_2$  may result in a better removal of certain pollutants (e.g., SMX, see above). On the other hand, this will reduce the overall number of micropollutants, which can be transformed by  $\text{ClO}_2$ . This is demonstrated by Figure 3.4, which shows the transformation of atenolol, metoprolol, SMX and DMBT in wastewater treated by  $\text{ClO}_2$  and ozone, respectively. Ozone is capable of transforming all compounds with a similar efficiency, with SMX being somewhat better transformed than the other compounds. In contrast,  $\text{ClO}_2$  covers a large range of transformation efficiencies. This is because  $\text{O}_3$  may react by very different pathways (i.e., electron transfer, 1,2-cycloaddition and oxygen transfer), enabling a fast reaction with several functional groups. Furthermore, hydroxyl radicals are formed in the reaction of  $\text{O}_3$  with organic matter, which can transform a large variety of pollutants (von Sonntag and von Gunten, 2012, Fischbacher et al., 2013, Buxton et al., 1988). Beside pollutant transformation, formation of by-products such as  $\text{ClO}_2^-$  or  $\text{BrO}_3^-$  should be considered. The dose of  $3.0 \times 10^{-5} \text{ M ClO}_2$  resulted in an exceedance of the US-EPA drinking water standard of  $\text{ClO}_2^-$  ( $1 \text{ mg L}^{-1}$ ). With this dosage, micropollutants such as SMX can be largely transformed ( $>90 \%$ ). Ozonation formed  $\text{BrO}_3^-$  to a level above the drinking water standard with a dose of  $1.2 \times 10^{-4} \text{ M}$  and a lower ozone dose has to be recommended for avoiding elevated  $\text{BrO}_3^-$  concentrations. A dose of  $9.0 \times 10^{-5} \text{ M}$  may enable safe use of ozone in this particular wastewater sample, which also results in a nearly complete transformation of the pollutants under study ( $> 90 \%$ ). However, these pollutants react fast with ozone and other pollutants may be transformed to a smaller extent.

### 3. Chapter: Chlorine dioxide – Pollutant transformation and hypochlorous acid formation as a secondary oxidant

The applicability of  $\text{ClO}_2$  depends on the relevance of  $\text{ClO}_2^-$  and how it would be regulated in wastewater treatment, as well as on the formation of undesired chlorinated by-products. In both aspects, there is currently a lack of information for a feasibility statement. Furthermore, the presence of  $\text{HOCl}$  was not taken into account in process studies using  $\text{ClO}_2$  as oxidant so far. This may have caused a bias on reaction- and disinfection kinetics determined in the past and should be considered when using such data. In Addition, the knowledge of presences of other oxidative species like  $\text{HOCl}$  or  $\text{HOBr}$  next to  $\text{ClO}_2$  might be useful for the detection of new by-products during the treatment with  $\text{ClO}_2$ .

The present study has shown that the reaction of  $\text{ClO}_2$  with matrix constituents can result in formation of other oxidants. In that regard  $\text{HOCl}$  and  $\text{HOBr}$  can be formed which may react with ammonia to another oxidative species, i.e., halamines. The complex interplay of all reactive species in real water matrices requires further research in future studies.

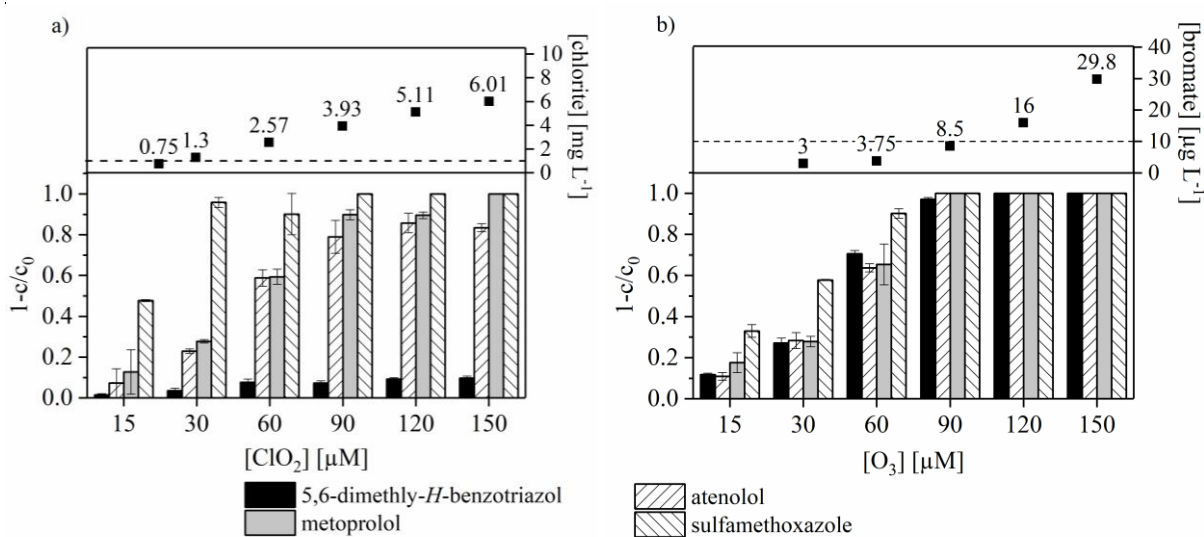


**Figure 3.4:** a) Transformation of micropollutants in wastewater after different  $\text{ClO}_2$  dosage and formation of chlorite (absence of glycine). b) Transformation of micropollutants in wastewater after different  $\text{O}_3$  dosages and formation of bromate ( $[\text{micropollutant}]_0 = 1 \times 10^{-6} \text{ M}$ ,  $\text{DOC} = 8.3 \pm 1 \text{ mg L}^{-1}$ ,  $\text{pH} = 7.80 \pm 0.05$ ,  $T = 20^\circ\text{C}$ ,  $[\text{Br}]_0 = 225.5 \pm 2.7 \mu\text{g L}^{-1}$ ,  $[\text{NH}_3] < 0.1 \text{ mg L}^{-1}$ , error bars are the standard deviation of the triplicates; recovery rate = 82 – 102 %). Filled squares show the concentration of formed chlorite (4a) and bromate (4b).

### 3.4 Supporting Information

#### 3.4.1 Reaction mechanism of phenol with chlorine dioxide

Wajon et al. (1982) postulated a reaction mechanism for the reaction of ClO<sub>2</sub> with phenol (Figure 3.5). In reactions of ClO<sub>2</sub> with phenol the phenolate is the most important species, since the neutral phenol species react slowly with ClO<sub>2</sub> ( $k(\text{ClO}_2 + \text{phenol}) = 0.4 \text{ M}^{-1} \text{ s}^{-1}$  (Hoigné and Bader, 1994)), while the anionic species reacts fast ( $k(\text{ClO}_2 + \text{phenolate}) = 4.9 \times 10^7 \text{ M}^{-1} \text{ s}^{-1}$  (Hoigné and Bader, 1994)). With the pK<sub>a</sub> of phenol at hand (pK<sub>a</sub>(phenol) = 10.0 (Hoigné and Bader, 1994)) one can calculate the reactivity pK<sub>a</sub>, which gives the fraction of species reacting with e.g., an oxidant. In case pH equals the reactivity pK<sub>a</sub> the apparent reaction rate with the oxidant is the same for both species:  $[\text{phenol}] \times k_{\text{phenol} + \text{ClO}_2} = [\text{phenolate}] \times k_{\text{phenolate} + \text{ClO}_2}$  (activity coefficients = 1.0). With this assumption, the concentration in the Henderson-Hasselbalch equation can be replaced by the reaction rate constants of the two species. This modification is shown in Equation 3.3:

$$\text{reactivity } pk_a = pk_a - \log\left(\frac{k_{\text{phenolate} + \text{ClO}_2}}{k_{\text{phenol} + \text{ClO}_2}}\right) \quad (\text{Equation 3.3})$$

In case the pH is higher than the reactivity pK<sub>a</sub> the deprotonated species is the prevalent reaction partner. A reactivity pK<sub>a</sub> of 1.91 was calculated for the reaction of ClO<sub>2</sub> with phenol. Hence, at pH > 1.91, ClO<sub>2</sub> reacts mainly with the phenolate. The phenolic anion reacts with ClO<sub>2</sub> to a phenoxy radical and chlorite (ClO<sub>2</sub><sup>-</sup>). The ensuing phenoxy radical undergoes a very fast second reaction with ClO<sub>2</sub> resulting in *p*-benzoquinone and hypochlorous acid (HOCl). This implies that ClO<sub>2</sub><sup>-</sup> and HOCl may be formed as by-products in the reaction with phenol.

3. Chapter: Chlorine dioxide – Pollutant transformation and hypochlorous acid formation as a secondary oxidant

---

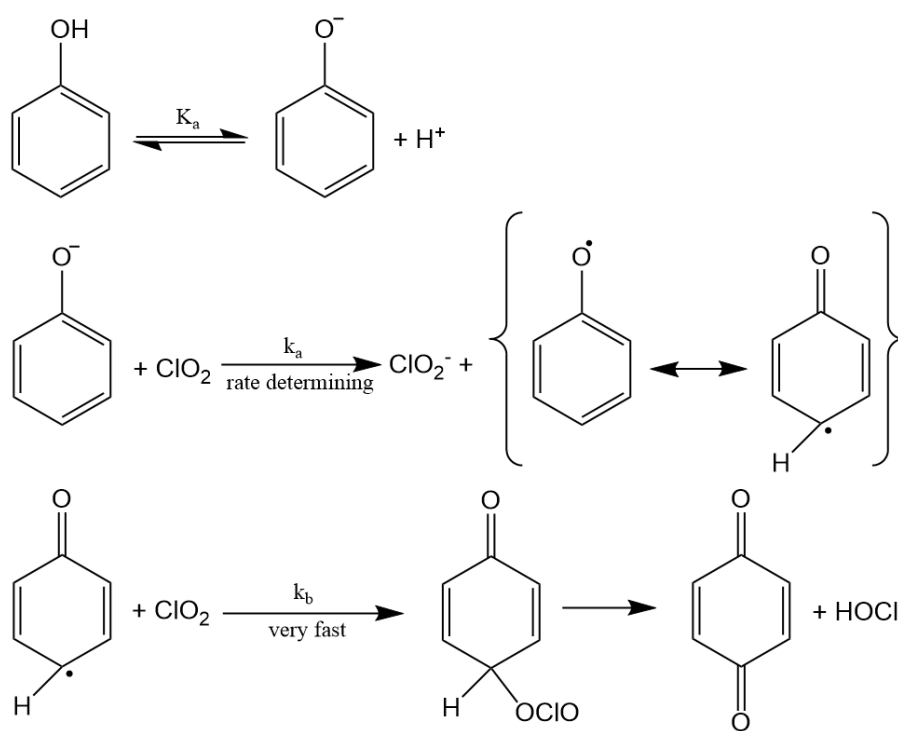


**Figure 3.5: Reaction mechanism of the reaction between phenol and chlorine dioxide (modified from Wajon et al. (1982)).**

3. Chapter: Chlorine dioxide – Pollutant transformation and hypochlorous acid formation as a secondary oxidant

**Table 3.2: Chemicals and wastewater used in Chapter 3.**

Substance	Structural formula	Purity	Manufacturer
2,4,6-tribromophenol ( $pK_a = 5.93$ )	$Br_3C_6H_2OH$	99 %	Sigma-Aldrich (Taufkirchen, Germany)
2,4-dibromophenol ( $pK_a = 7.79$ )	$Br_2C_6H_3OH$	95 %	Sigma-Aldrich
2-bromophenol ( $pK_a = 8.44$ )	$BrC_6H_4OH$	98 %	Sigma-Aldrich
4-bromophenol ( $pK_a = 9.36$ )	$BrC_6H_4OH$	99 %	Sigma-Aldrich
5,6-dimethyl-1- <i>H</i> -benzotriazol ( $pK_a = 9.28$ )	$C_8H_9N_3 \times H_2O$	$\geq 99$ %	Sigma-Aldrich
ammonium molybdate (para) tetrahydrate	$(NH_4)_6Mo_7O_{24} \times 4H_2O$	99 %	Alfa Aesar (Karlsruhe, Germany)
atenolol ( $pK_a = 9.6$ )	$C_{14}H_{22}N_2O_3$	$\geq 98$ %	Sigma-Aldrich
glycine ( $pK_a = 9.78$ )	$NH_2CH_2COOH$	$\geq 99$ %	Sigma-Aldrich
( $\pm$ )-metoprolol (+)-tartrate salt ( $pK_a = 9.7$ )	$(C_{15}H_{25}NO_3)_2 \times C_4H_6O_6$	$\geq 98$ %	Sigma-Aldrich
nitrogen	$N_2$	$> 99$ %	Air Liquide (Oberhausen, Germany)
phenol ( $pK_a = 10$ )	$C_6H_5OH$	99 %	Sigma Aldrich
potassium bromate	$KBrO_3$	99.5 %	Fluka (Taufkirchen, Germany)
potassium iodide	$KI$	$\geq 99$ %	Fluka
sodium bromide	$NaBr$	$\geq 99$ %	Fluka
sodium chloride	$NaCl$	99.5 %	Bernd Kraft (Duisburg, Germany)
sodium chlorite	$NaClO_2$	80 %	Sigma-Aldrich
sodium hypochlorite ( $pK_a = 7.47$ )	$NaOCl$	4 %	Sigma Aldrich
sulfamethoxazole ( $pK_a = 5.6$ )	$C_{10}H_{11}N_3O_3S$	analytical standard	Fluka
potassium dihydrogen phosphate	$KH_2PO_4$	99 %	AppliChem
ortho-phosphoric acid	$H_3PO_4$	85 % p. a.	AppliChem
	<b>pH</b>	<b>DOC</b>	
wastewater effluent	$7.99 \pm 0.07$	$8.11 \pm 0.12$ mg L <sup>-1</sup>	

3. Chapter: Chlorine dioxide – Pollutant transformation and hypochlorous acid formation as a secondary oxidant

**Table 3.3: Used equipment**

Name	Components	Description	Manufacturer
HPLC/UV	Pump	LC-20AT	Shimadzu (Duisburg, Germany)
	UV/VIS-detector	SPD-20A	Shimadzu
	Auto sampler	SIL-20A	Shimadzu
	Software	LabSolutions (Version 1.25 SP4)	Shimadzu
	Column oven	CTO-10AS	Shimadzu
	Column	ProntoSil 120 C18 5µm 250 x 4,0 mm	Bischoff (Leonberg, Germany)
	Communication element	CBM-20A	Shimadzu
	Degasser	DGU-20A <sub>5</sub>	Shimadzu
IC	Equipment	881 Compact IC pro	Metrohm (Filderstadt, Germany)
	Pump	Standard	Metrohm
	Detector	IC Conductivity Detector	Metrohm
		UV-Detector	Metrohm
	Sample loop	20 µL and 1 mL	
	Column	Metrosep A Supp 5- 250/4.0	Metrohm
		Metrosep A Supp 16 250/4.0	Metrohm
	Auto Sampler	863 Compact	Metrohm
	Post-column reactor	Wille et al. (2010)	Metrohm
Software	MagIC Net	Metrohm	
UV/vis- spectrometer	UV-1650 PC		Shimadzu
pH meter	827 pH		Metrohm



### 3. Chapter: Chlorine dioxide – Pollutant transformation and hypochlorous acid formation as a secondary oxidant

---

O <sub>3</sub> generator	BMT 802X		BTM Messtechnik (Berlin, Germany)
ultrapure water generator	Purelab ultra		ELGA (Celle, Germany)
TOC-Analyzer	TOC 5000A		Shimadzu

#### 3.4.2 Chlorine dioxide production and handling

To produce a chlorine free aqueous ClO<sub>2</sub> solution the persulfate-chlorite method was used. This method is based on the reaction between sodium persulfate (Na<sub>2</sub>S<sub>2</sub>O<sub>8</sub>) and sodium chlorite (NaClO<sub>2</sub>) and was described by Gates (1998) (Reaction 3.2):

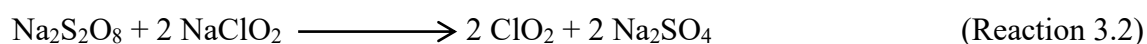
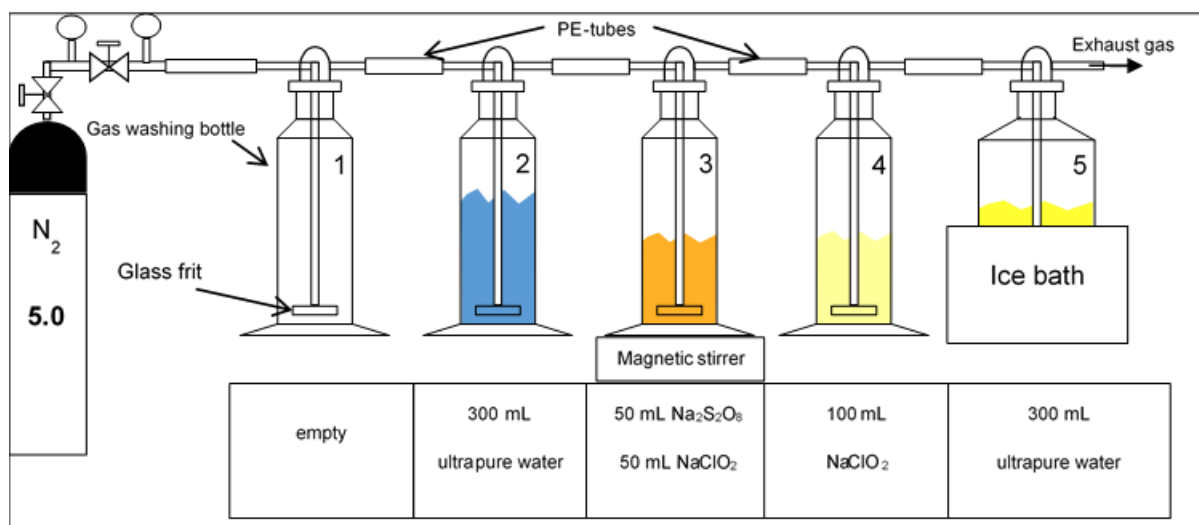


Figure 3.6 shows the apparatus, which was used for ClO<sub>2</sub> production. It consists of a series of five gas washing bottles, which are connected with PE tubes to a nitrogen gas supply. In this apparatus, ClO<sub>2</sub> is produced according to Reaction 3.2 in bottle No. 3 and transferred via bottle No. 4 into the ice cooled bottle No. 5, which is filled with 300 mL ultrapure water. Within a reaction time of ca. 2 hours the ClO<sub>2</sub> concentration in bottle No. 5 steadily increases to a value of ca.  $1.0 \times 10^{-2} - 1.5 \times 10^{-2}$  M. For buffering any back pressure which may occur in case the nitrogen gas flow is turned off, an empty bottle was installed as the first bottle (No. 1). Bottle No. 2 was filled with fresh ultrapure water for washing the nitrogen gas. Bottle No. 4 was filled with a 0.111 M NaClO<sub>2</sub> solution for scavenging of HOCl which might be formed in bottle No. 3 as by-product. HOCl can be removed by its reaction with ClO<sub>2</sub><sup>-</sup> ( $k(\text{HOCl} + \text{ClO}_2^- \text{H}^+) = 1.06 \times 10^6 \text{ M}^{-2} \text{ s}^{-1}$  (Peintler et al., 1990)) yielding ClO<sub>2</sub> and Cl<sup>-</sup> (Gates, 1998). The reaction solution in bottle No. 3 was prepared by filling 50 mL of a 0.885 M NaClO<sub>2</sub> aqueous solution into this bottle. The reaction was then started by addition of 50 mL of 0.168 M Na<sub>2</sub>S<sub>2</sub>O<sub>8</sub> aqueous solution. The reaction solution was continuously stirred during the whole production time.

3. Chapter: Chlorine dioxide – Pollutant transformation and hypochlorous acid formation as a secondary oxidant



**Figure 3.6: Apparatus for ClO<sub>2</sub> production (bottle No.3: 50 mL 0.885 M NaClO<sub>2</sub> + 50 mL Na<sub>2</sub>S<sub>2</sub>O<sub>8</sub>; bottle No. 4: 100 mL 0.111 M NaClO<sub>2</sub>).**

The concentration of ClO<sub>2</sub> in the fifth bottle was measured by UV-absorption at 359 nm. Therefore, 0.1 mL ClO<sub>2</sub> solution was added with a glass syringe to 2.9 mL ultrapure water in a 1 cm cuvette (1:30 dilution). The dilution was necessary to keep the absorption below 1 cm<sup>-1</sup> and thus to use the linear range of the UV-measurement. The diluted solution has an absorption of 0.4 - 0.6 cm<sup>-1</sup> ( $\epsilon_{359} = 1200 \text{ M}^{-1} \text{ cm}^{-1}$  (Gates, 1998));  $[\text{ClO}_2] = 1.0 - 1.5 \times 10^{-2} \text{ M}$ ). To make sure that the solution in the cuvette was homogeneously mixed the cuvette was turned to head two times. The concentration was calculated with the Lambert-Beer-law (Equation 3.4):

$$E_{359} = \epsilon_{359} \times c \times d \quad (\text{Equation 3.4})$$

$E_{359}$  = extinction at the wavelength of 359 nm

$\epsilon_{359}$  = molar extinction coefficient at 359 nm [ $\text{M}^{-1} \text{ cm}^{-1}$ ]

$c$  = concentration of ClO<sub>2</sub> [M]

$d$  = path length of the cuvette [cm]

After finishing the ClO<sub>2</sub> production, the solution was filled in amber glass bottles with ground glass joint. These bottles were filled up without leaving any headspace and stored dark and cool (5 – 9 °C). Furthermore, it is very important to handle the solution carefully because ClO<sub>2</sub> can be explosive at a high concentration (Gates, 2009).

Stored cool, dark and without headspace, the ClO<sub>2</sub> solution could be used for one month with a loss of < 20 % of ClO<sub>2</sub>. If the loss was higher than 20 %, a fresh ClO<sub>2</sub> solution was prepared.

### 3. Chapter: Chlorine dioxide – Pollutant transformation and hypochlorous acid formation as a secondary oxidant

During and after use of the ClO<sub>2</sub> stock solution a significant amount of ClO<sub>2</sub> is lost via transfer from liquid to gas phase (Henry constant (K<sub>H</sub>) ~0.8 atm M<sup>-1</sup> (20°C) (Huber et al., 2005)). Therefore, the concentration of the ClO<sub>2</sub> stock solution was determined by UV-absorption before each experiment.

#### Dosing of ClO<sub>2</sub> solution:

The ClO<sub>2</sub> solution must be cooled during the use of ClO<sub>2</sub> for preventing loss of ClO<sub>2</sub> into the gas phase. Additionally, the dosing of ClO<sub>2</sub> by regular pipettes is unsuitable because of the headspace in the pipette tips. Hence, for the dosage of ClO<sub>2</sub> solutions, high precision glass syringes (Hamilton syringe) were used.

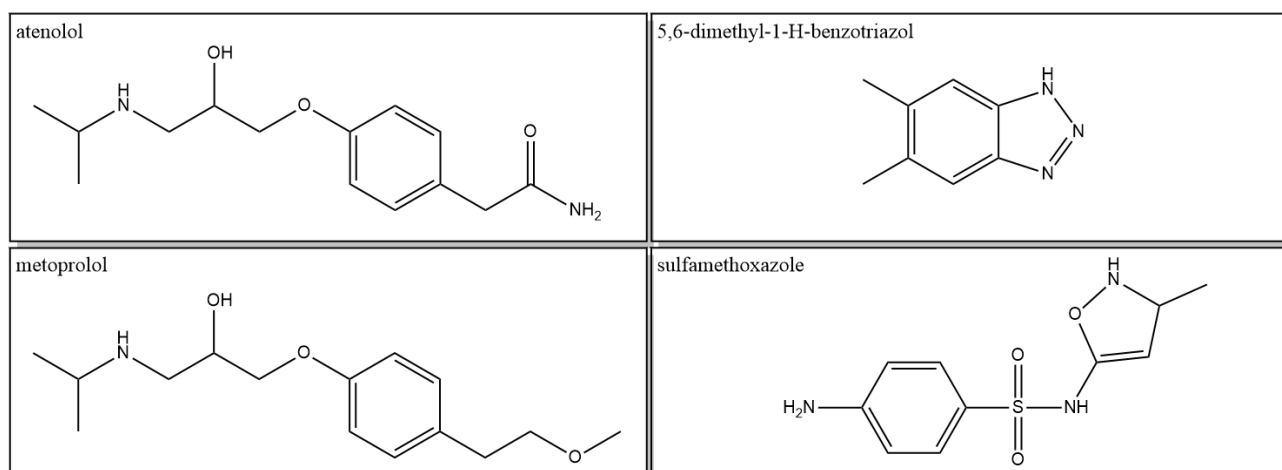


**Figure 3.7: Structure of the organic compounds under study.**

### 3.4.3 Detection of hypochlorous acid in the reaction of chlorine dioxide with phenol

HOCl formed in the reaction of phenol with  $\text{ClO}_2$  (Figure 3.5 reaction path (a)) was scavenged by a surplus of bromide ( $\text{Br}^-$ ) (10 mM) resulting in hypobromous acid (HOBr) and chloride ( $\text{Cl}^-$ ) (Figure 3.5 reaction path (b)). HOBr in turn, was determined by scavenging with phenol and determining the products 2- and 4-bromophenol (reaction path (c) and (d)). Assuming quantitative scavenging of HOCl by  $\text{Br}^-$  and HOBr by phenol, the yield of bromophenols corresponds to the amount of HOCl formed. The reaction of HOCl with  $\text{Br}^-$  ( $k(\text{HOCl} + \text{Br}^-) = 1.32 \times 10^3 \text{ M}^{-1} \text{ s}^{-1}$  (pH = 4.00) (Kumar and Margerum, 1987)) is four orders of magnitudes faster than the reaction of HOCl with phenol ( $k(\text{phenol} + \text{HOCl}) = 3.82 \times 10^{-1} \text{ M}^{-1} \text{ s}^{-1}$  (pH = 4.00) (Criquet et al., 2015)). Since, the concentration of  $\text{Br}^-$  is 10 times higher than the concentration of phenol, HOCl was quantitatively scavenged by  $\text{Br}^-$ . Corresponding experiments were performed at pH 4.00 because a quantitative yield of bromophenols from the reaction of HOBr with phenol can only be achieved at this pH (Fischbacher et al., 2015).

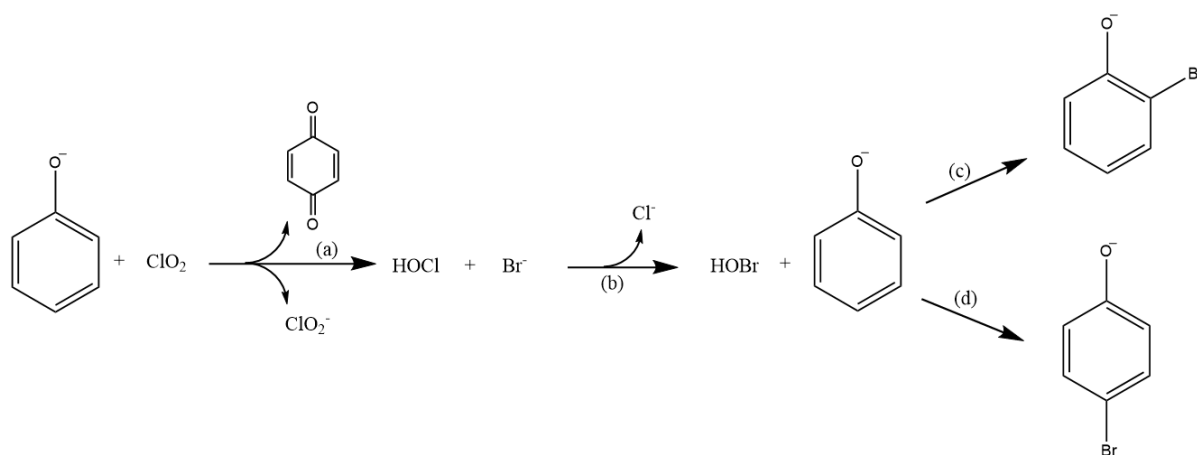


**Figure 3.8: Formation of bromophenols in reaction of  $\text{ClO}_2$  with phenol in the presence of bromide.**

3. Chapter: Chlorine dioxide – Pollutant transformation and hypochlorous acid formation as a secondary oxidant

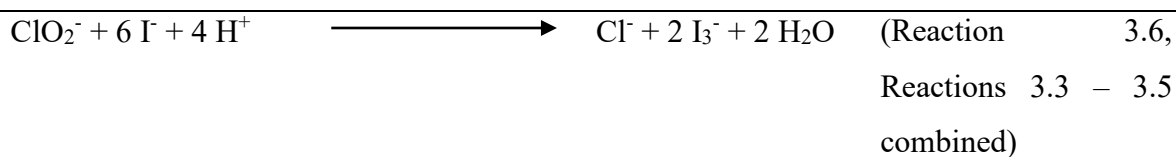
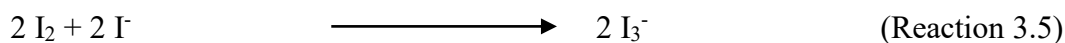
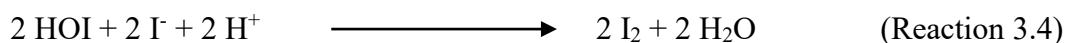
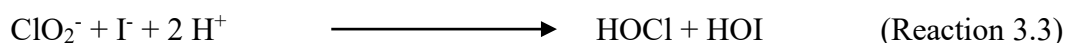
### 3.4.4 HPLC- and IC-methods

In Table 3.4, HPLC-UV methods for the determination of the organic compounds are shown.

**Table 3.4: HPLC-UV methods**

Compound, in brackets: retention time [min]	Inj.- vol. [ $\mu\text{L}$ ]	Eluent	Eluent flow [ $\text{mL min}^{-1}$ ]	Detected wave- length [nm]
2- bromophenol (15.7) 4-bromophenol (16.7) phenol (10.0) 2,4-dibromphenol (21.2) 2,4,6-tribromphenol (24.3)	50	Eluent was composed of acetonitrile (ACN) and water, (pH ca. 6-7). In the eluent program below: proportions of the organic solvent are shown and the remaining fraction corresponds to water. 0-18 min gradient from 30 to 70 % ACN 18-20 min isocratic at 70 % ACN 20-21 min gradient from 70 to 30 % ACN 21-30 min isocratic at 30 % ACN (equilibration for starting conditions)	0.7	240 270
metoprolol (17.6)	50	Isocratic: 35 % MeOH/ 65 % H <sub>2</sub> O (pH 2, with HCl adjusted) runtime 25 min	0.5	234
atenolol (9.5)	50	Isocratic: 20 % MeOH/ 80 % H <sub>2</sub> O (pH 2, with HCl adjusted) runtime 20 min	0.5	234
5,6-dimethyl-1- <i>H</i> - benzotriazol (17.9)	50	Isocratic: 50 % MeOH/ 50 % H <sub>2</sub> O (pH 2, with HCl adjusted) runtime 25 min	0.5	270
sulfamethoxazole (9.9)	50	Isocratic: 40 % MeOH/ 60 % H <sub>2</sub> O (pH 2 adjusted with HCl) runtime 20 min	0.5	270

In Table 3.5, the IC-methods for the detection of  $\text{ClO}_2^-$ ,  $\text{Cl}^-$ , bromide ( $\text{Br}^-$ ) and bromate ( $\text{BrO}_3^-$ ) are shown. For a sensitive determination of  $\text{ClO}_2^-$  and  $\text{BrO}_3^-$ , a post-column reaction was additionally used. The concept is described for the  $\text{ClO}_2^-$  detection, but the  $\text{BrO}_3^-$  reactions are similar, only the stoichiometry is different.  $\text{ClO}_2^-$  oxidized iodide ( $\text{I}^-$ ) to triiodide ( $\text{I}_3^-$ ) under acidic conditions (Reactions 3.3 – 3.6) (Lengyel et al., 1996). Ammonium heptamolybdate-tetrahydrate ( $\text{Mo(VI)}$ ) acted as a catalyst for Reaction 3.3. Triiodide is detected by UV absorption at 352 nm ( $\epsilon_{352, \text{I}_3^-} = 22900 \text{ M}^{-1}\text{cm}^{-1}$  (Alexander, 1962)). This method allows a sensitive and selective  $\text{ClO}_2^-$  and  $\text{BrO}_3^-$  detection. However, other compounds may also form  $\text{I}_3^-$  (e.g., nitrite) hence one has still to check for interferences using this method.



### 3.4.5 Dissolved Organic Carbon analysis

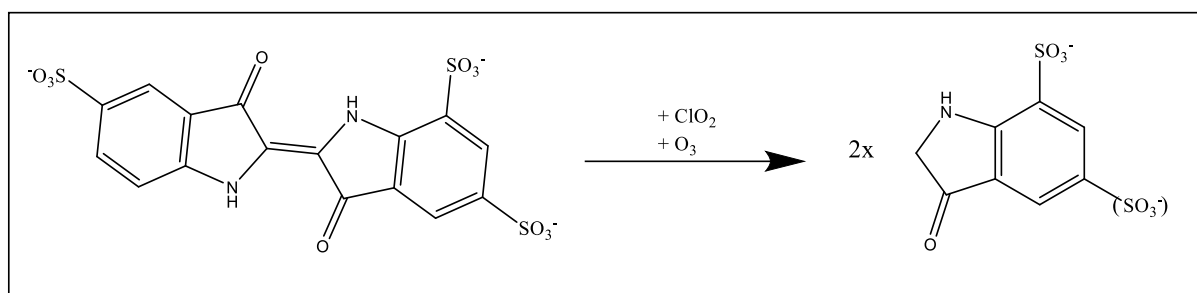
The dissolved organic carbon (DOC) was determined by the non-purgeable organic carbon (NPOC). Therefore, the wastewater sample was filtrated through a 25 mm PTFE syringe filter (0.45  $\mu\text{m}$ , S/N 160707036, BGB, Germany) and the pH value was adjusted between pH 2 and 3 with hydrochloric acid (37%, Bernd Kraft). The measurements were accomplished by a TOC-Analyzer (TOC 5000A, Shimadzu). For the quantification a calibration with potassium hydrogen phthalate (99%, Alfa Aesar) in the range of 1 to 50  $\text{mg L}^{-1}$  were performed. The time of purging with nitrogen was 5 minutes.

Table 3.5: IC- methods with the post-column reaction system (CD = Conductivity detector, n. a. = not applicable)

Compound	Inj.- Vol. [ $\mu\text{L}$ ]	Eluent; in brackets: column	Eluent flow [ $\mu\text{L min}^{-1}$ ]	retention time CD [min]	Post-column reaction solution	Eluent flow [ $\text{mL min}^{-1}$ ]	Detected wave- length [nm]	retention time UV- detector [min]
chlorite	20	$3.2 \times 10^{-3} \text{ M Na}_2\text{CO}_3$ + $1.0 \times 10^{-3} \text{ M NaHCO}_3$ (Metrosep A Supp 5 250/4.0)	0.7	7.0	$2.7 \times 10^{-1} \text{ M KI}$ + $5 \times 10^{-2} \text{ M } (\text{NH}_4)_6\text{Mo}_7\text{O}_{24} \times 4 \text{ H}_2\text{O}$ + $1 \times 10^{-1} \text{ M H}_2\text{SO}_4$	0.2	352	7.6
chloride				8.5				n. a.
bromate	500	$7.5 \times 10^3 \text{ M Na}_2\text{CO}_3$ + $7.5 \times 10^{-4} \text{ M NaOH}$ (Metrosep A Supp 16 250/4.0)	0.7	13.5				14.5
bromide				21.6				n. a.

### 3.4.6 Experiments for determining oxidant depletion

Indigo trisulfonate, a dark-blue dye ( $\epsilon_{600} = 20000 \text{ M}^{-1} \text{ cm}^{-1}$ ), reacts with  $\text{ClO}_2$  or  $\text{O}_3$  to isatinesulfonic acid, a slightly yellow substance ( $\epsilon_{600} = \text{negligible}$ ) (Figure 3.9). In case of  $\text{O}_3$ , the bridging double bond of indigo trisulfonate is oxidized (Hoigné and Bader, 1980). Also,  $\text{ClO}_2$  is expected to attack the double bond, however, the exact reaction mechanism is not known yet.



**Figure 3.9: Reaction of indigo trisulfonate with chlorine dioxide and ozone.**

#### Depletion of chlorine dioxide

10 mL of the wastewater was aliquoted in 20-mL headspace vials after the pH measurement and the residual  $\text{ClO}_2$  concentration was determined for every reaction time in an individual experiment. The approach is shown in Figure 3.10. The sample was mixed for 10 seconds after the dosage of  $\text{ClO}_2$ . Thereby three different concentrations of  $\text{ClO}_2$  were added to the samples i.e.,  $2 \times 10^{-5} \text{ M}$ ,  $5 \times 10^{-5} \text{ M}$  and  $1 \times 10^{-4} \text{ M}$ . For quenching the residual  $\text{ClO}_2$  after a certain reaction time, indigo trisulfonate was added at different dosages, depending on the dose of  $\text{ClO}_2$  (the higher the  $\text{ClO}_2$  dose the higher the indigo trisulfonate dose). Two different indigo trisulfonate concentrations were added:  $5 \times 10^{-5} \text{ M}$  indigo trisulfonate for experiments applying  $2 \times 10^{-5} \text{ M}$   $\text{ClO}_2$  and  $5 \times 10^{-5} \text{ M}$   $\text{ClO}_2$  and  $1 \times 10^{-4} \text{ M}$  indigo trisulfonate was used in case of a dosage of  $1 \times 10^{-4} \text{ M}$   $\text{ClO}_2$ . Indigo trisulfonate was added after 16 different reaction times to cover an overall reaction time of 20 minutes. The absorption of the remaining indigo trisulfonate was determined at 600 nm. A reference without  $\text{ClO}_2$  is important because the difference of the indigo concentration in the reference and in the sample shows the concentration of residual  $\text{ClO}_2$ .

The reaction stoichiometry of  $\text{ClO}_2$  and indigo trisulfonate is ca. 2:1 (Hoigné and Bader, 1980). However, no exact value on the reaction stoichiometry was available. Therefore, calibrations



of  $\text{ClO}_2$  with indigo trisulfonate were done. Figure 3.11 shows a slope of  $0.498 \pm 0.007$  indicating that indeed 2 molecules of  $\text{ClO}_2$  are consumed per 1 molecule indigo trisulfonate bleached. By multiplying the extinction coefficient of indigo trisulfonate with the slope in Figure 3.10 one arrives at the response factor for quantification of  $\text{ClO}_2$  using the indigo method ( $9955 \text{ M}^{-1}\text{cm}^{-1}$ ).

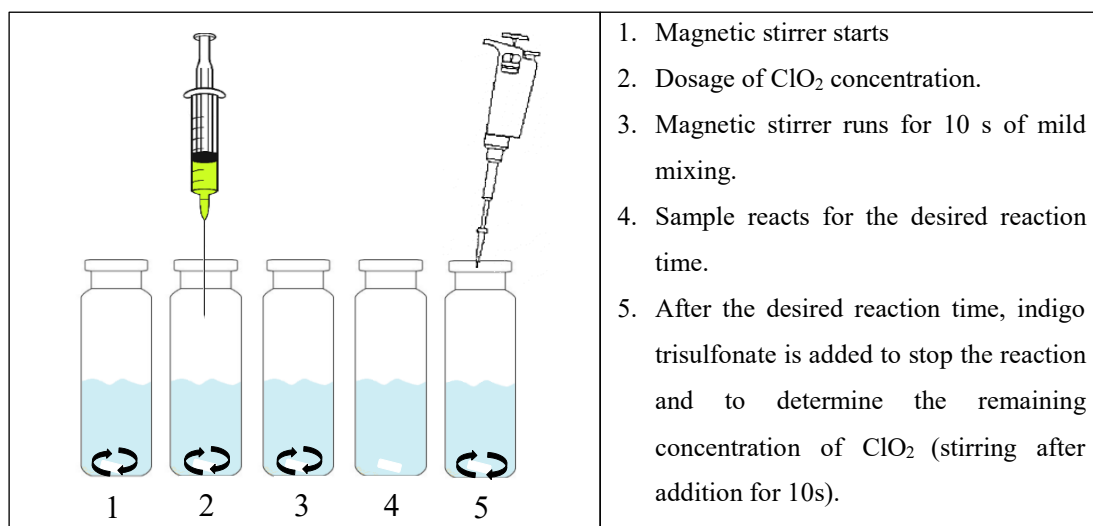


Figure 3.10: Experimental approach for the depletion experiment of  $\text{ClO}_2$ .

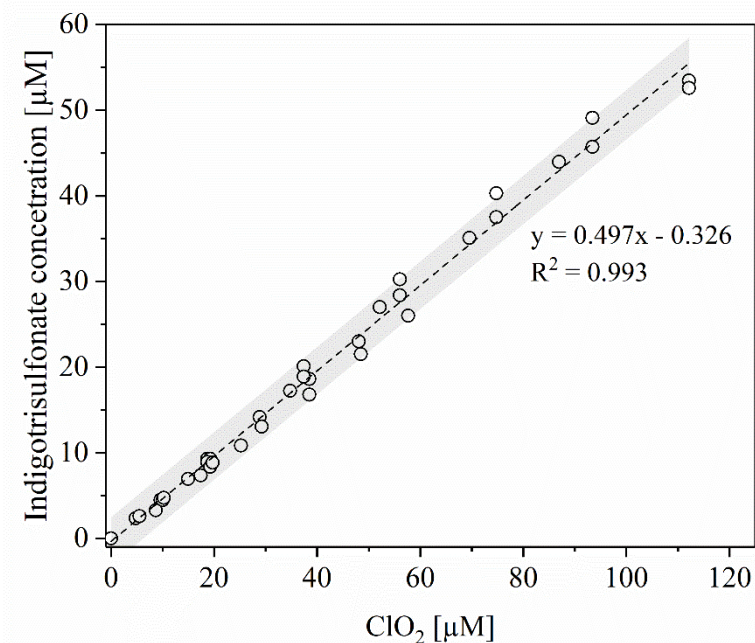


Figure 3.11: Calibration of indigo trisulfonate method for  $\text{ClO}_2$  determination (grey area = 95 % confidence interval).

### Depletion of ozone

Another setup was used for measuring ozone depletion in wastewater. The wastewater was filled in a 250-mL screw neck bottle, equipped with a magnetic stirrer and a dispenser for rapid sampling. Three different  $O_3$  concentration were investigated:  $2 \times 10^{-5}$  M,  $5 \times 10^{-5}$  M and  $1 \times 10^{-4}$  M. Samples were taken at regular intervals after the dosage of ozone. For this, a volume of 10 mL of the sample was transferred by the dispenser into a tube which contained indigo trisulfonate.  $7 \times 10^{-5}$  M indigo trisulfonate was added for experiments applying  $2 \times 10^{-5}$  M  $O_3$  and  $5 \times 10^{-5}$  M  $O_3$ .  $8.7 \times 10^{-5}$  M indigo trisulfonate was used in case of a dosage of  $1 \times 10^{-4}$  M  $O_3$ . For a good mixing, the tube was turned over one time after sampling. All samples containing samples that were treated, with  $ClO_2$  as well as reference samples (without addition of  $ClO_2$ ) were measured by UV/vis- spectrometry at a wavelength of 600 nm. According to Hoigné and Bader (1980)  $O_3$  reacts with indigo trisulfonate with a stoichiometry of 1 and the extinction coefficient of  $20000 \text{ M}^{-1}\text{cm}^{-1}$  was used for determining the amount of ozone needed to bleach the indigo dye.

#### **3.4.7 Chloride concentration**

In the Validation experiment, a high concentration of bromide was used (10 mM). In addition, chloride can be added to the reaction solution with the dosage of this concentration. To see this contamination with chloride, blank samples (without  $ClO_2$ ) were measured. The chloride concentration of the blank sample was subtracted from the chloride concentration in the samples with  $ClO_2$ . The blank concentration of chloride is  $4.2 \mu\text{M}$ .

#### **3.4.8 Bromophenol formation**

The experiments were done at pH 4.00. According to Fischbacher et al. (2015) this is the optimal pH for the bromination of phenol by HOBr. In addition experiments at pH 7.00 were done. In Figure 3.12 the formation of 4- and 2- bromophenol is shown. The yield of bromophenol was small (max. 7 % per consumed  $ClO_2$ ). In comparison, the formation of bromophenol at pH 4.00 is shown in Figure 3.13. The sum of both bromophenol is between 38-48 % per consumed  $ClO_2$ . This corroborates the results of Fischbacher et al. (2015).

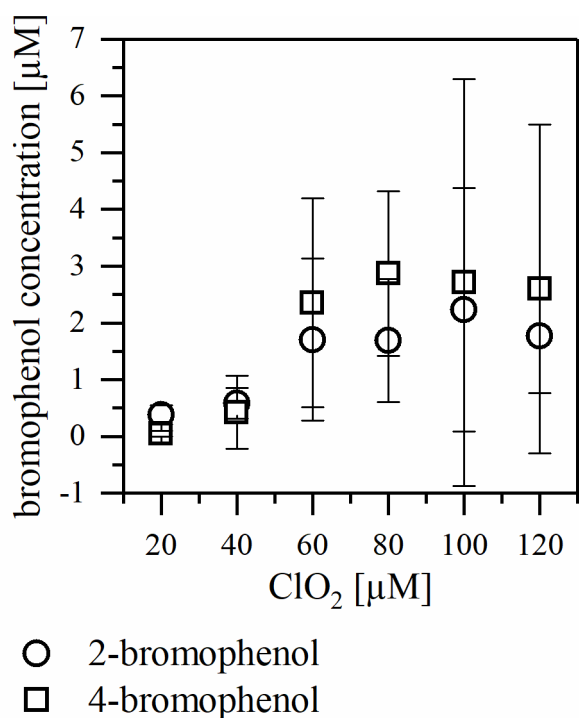


Figure 3.12: Formation of the bromophenols by the reaction of phenol + bromide + ClO<sub>2</sub> at pH 7.00 ([phenol] = 1 × 10<sup>-3</sup> M; [bromide] = 1 × 10<sup>-2</sup> M; [phosphate-buffer] = 5 × 10<sup>-3</sup> M; different ClO<sub>2</sub> dose)

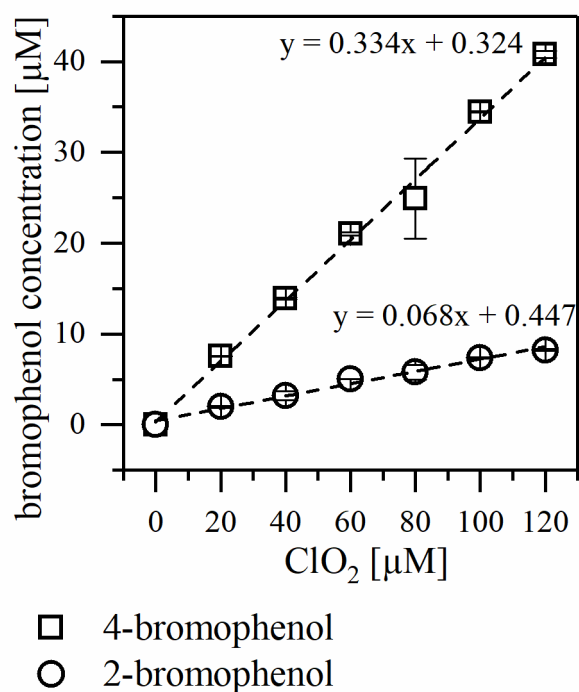
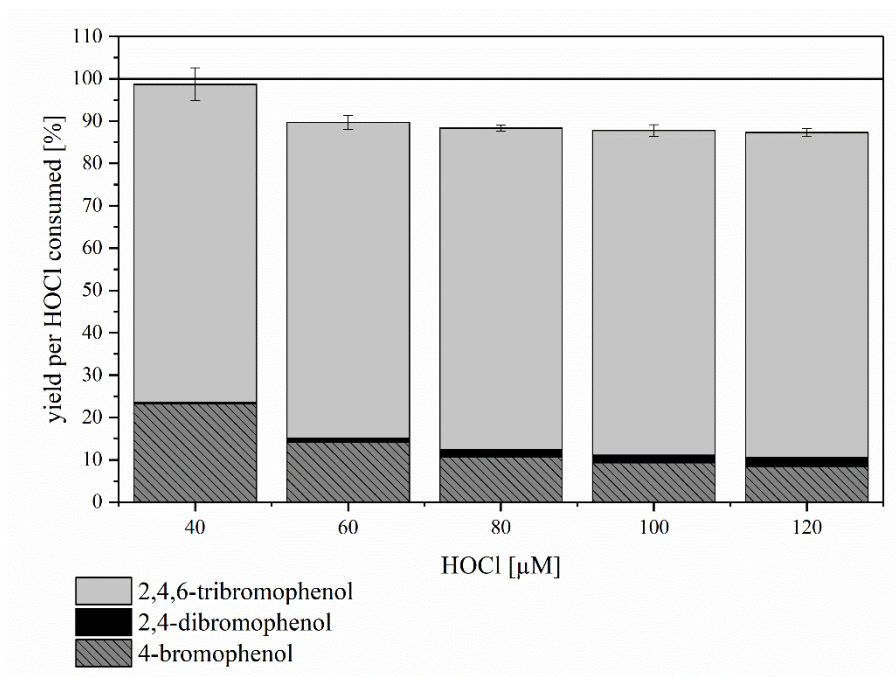
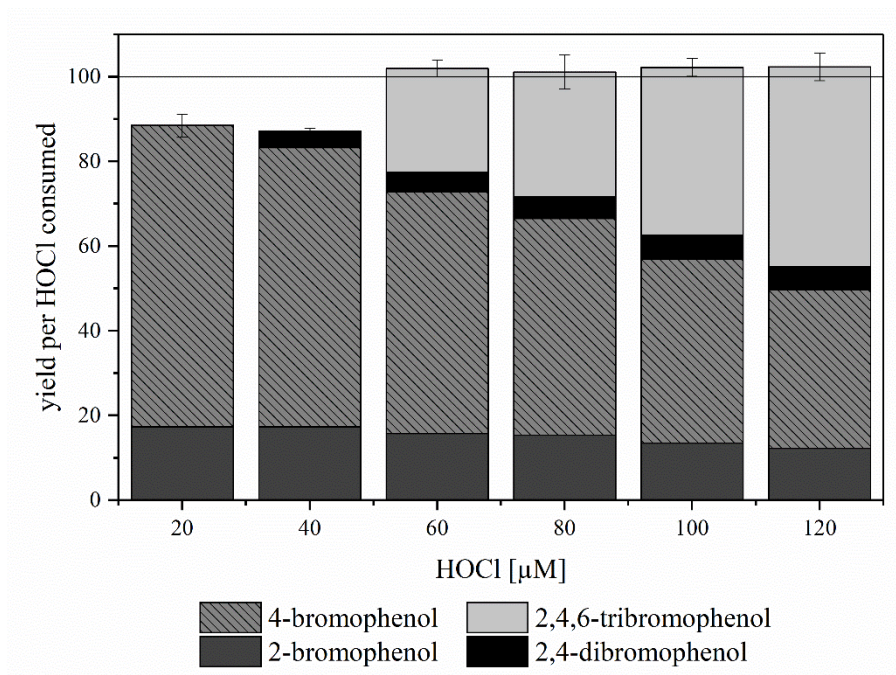


Figure 3.13: Formation of the bromophenols by the reaction of phenol + bromide + ClO<sub>2</sub> at pH 4.00 ([phenol] = 1 × 10<sup>-3</sup> M; [bromide] = 1 × 10<sup>-2</sup> M; [phosphate-buffer] = 5 × 10<sup>-3</sup> M; different ClO<sub>2</sub> dose)



**Figure 3.14:** Yield of the bromophenols in the reaction of phenol with HOCl in presence of bromide at pH 4.00 without addition of glycine ([phenol] =  $1 \times 10^{-3}$  M, [bromide] =  $1 \times 10^{-2}$  M; [phosphate buffer] =  $1 \times 10^{-3}$  M, pH = 4, T = 20 °C). The horizontal line marks the 100 % yield, 2-bromophenols were found but the values are below the limit of quantification = 10.89  $\mu\text{M}$ .



**Figure 3.15:** Yield of bromophenols at the dosage of phenol and bromide to HOCl dilutions (final concentrations [phenol] =  $1.0 \times 10^{-3}$  M and [bromide] =  $1.0 \times 10^{-2}$  M; HOCl concentration ranged between  $2.0 \times 10^{-5}$  –  $1.2 \times 10^{-4}$  M; pH = 4,00).

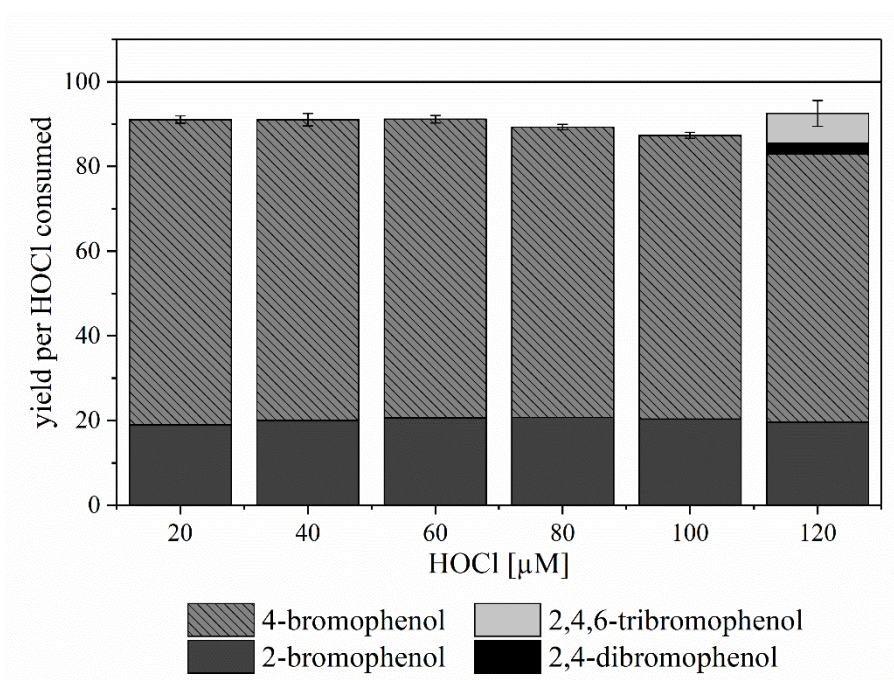


**Figure 3.16: Yield of bromophenols at the dosage of phenol and bromide to HOCl dilutions (final concentrations [phenol] =  $6.0 \times 10^{-3}$  M and [bromide] =  $6.0 \times 10^{-2}$  M; HOCl concentration ranged between  $2.0 \times 10^{-5}$  –  $1.2 \times 10^{-4}$  M; pH = 4,00).**

### 3.4.9 Determination of oxidant exposure

Three depletion experiments were performed with different oxidant concentrations. In the case of  $\text{ClO}_2$ , a dose of  $2 \times 10^{-5}$  M resulted in a complete  $\text{ClO}_2$  consumption prior to the first possible sample (i.e., 20 seconds), while a dose of  $1 \times 10^{-4}$  M  $\text{ClO}_2$  resulted in a residual concentration of  $1 \times 10^{-5}$  M even after 24 hours of reaction time (Figure 3.17). In these two cases, it was not possible to calculate an oxidant exposure for the complete depletion of  $\text{ClO}_2$ . However, a dose of  $5 \times 10^{-5}$  M  $\text{ClO}_2$  resulted in an optimal life time of  $\text{ClO}_2$  for calculating the oxidant exposure ( $3.2 \times 10^{-2}$  M  $\times$  s (Figure 3.17a)).

Analogous experiments were performed for  $\text{O}_3$ .  $\text{O}_3$  has a much shorter life time compared to  $\text{ClO}_2$ . The two depletion curves for doses of  $2 \times 10^{-5}$  M and  $5 \times 10^{-5}$  M  $\text{O}_3$  resulted in a complete  $\text{O}_3$  depletion after few seconds of reaction (Figure 3.19). Only at a dose of  $1 \times 10^{-4}$  M, free  $\text{O}_3$  was present and measurable (Figure 3.17b). The  $\text{O}_3$  exposure was calculated to be  $2.0 \times 10^{-3}$  M  $\times$  s.

The different degradation kinetics of  $\text{ClO}_2$  and  $\text{O}_3$  can be explained by the high selectivity of  $\text{ClO}_2$ .  $\text{ClO}_2$  is more stable in the wastewater matrix than  $\text{O}_3$  which increases the chances of reactions of  $\text{ClO}_2$  with pathogens and pollutants. This can compensate slow reaction kinetics of

pollutants with  $\text{ClO}_2$  and in case pollutants react fast with  $\text{ClO}_2$  very small dosages may be required. This was demonstrated by Lee and von Gunten (2010) for different pollutants. They have shown that for the degradation of  $17\alpha$ -Ethinylestradiol in wastewater, a lower dosage of  $\text{ClO}_2$  ( $3 \times 10^{-6}$  M) was required than of  $\text{O}_3$  ( $1 \times 10^{-5}$  M) to achieve one log unit of degradation.

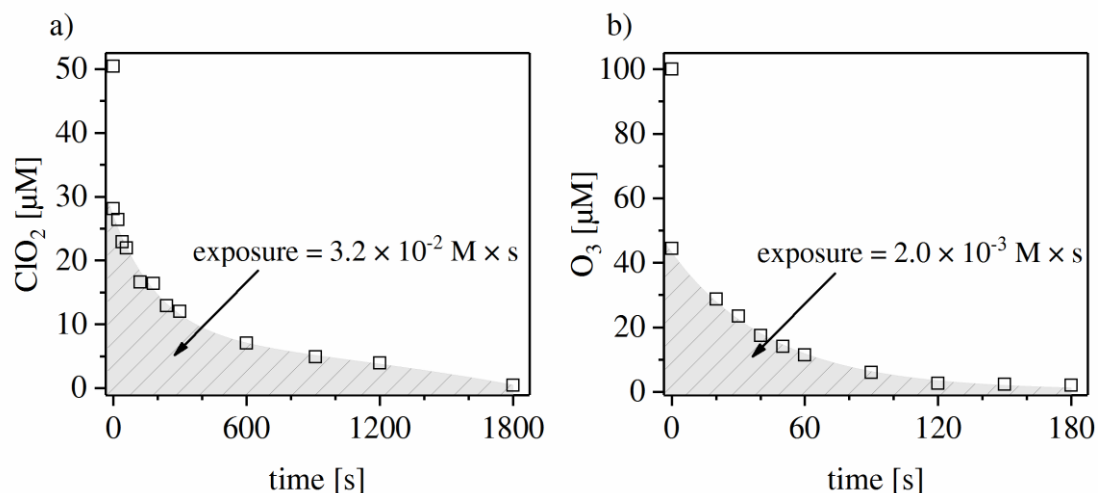


**Figure 3.17: Depletion curve of a)  $5 \times 10^{-5}$  M  $\text{ClO}_2$  and b)  $1 \times 10^{-4}$  M  $\text{O}_3$  in wastewater. Oxidant concentration was determined with the indigo method. The marked area below the depletion curve represents the exposure of  $\text{ClO}_2$  ( $3.2 \times 10^{-2}$  M  $\times$  s) and  $\text{O}_3$  ( $2.0 \times 10^{-3}$  M  $\times$  s) ( $\text{pH} = 7.90 \pm 0.05$ ,  $\text{DOC} = 8.11 \pm 0.12$  mg  $\text{L}^{-1}$ ,  $T = 22^\circ\text{C}$ ).**

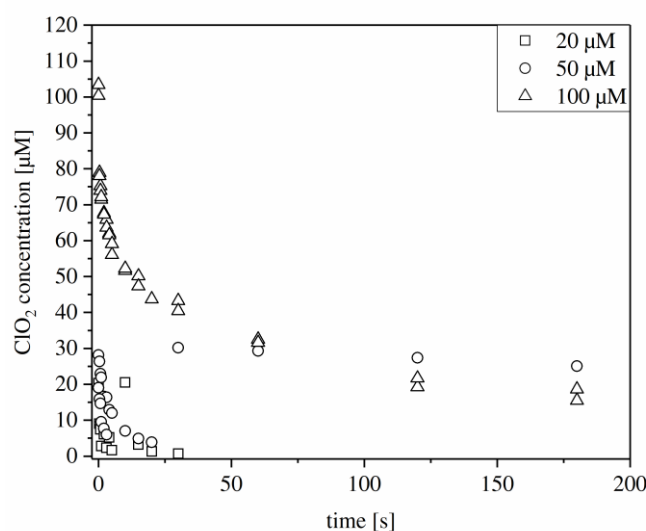


**Figure 3.18: Depletion curves of three initial chlorine dioxide concentrations in the present wastewater. Chlorine dioxide concentration was determined by indigo method ( $\text{pH} = 7.90 \pm 0.05$ ;  $T = 22^\circ\text{C}$ ).**

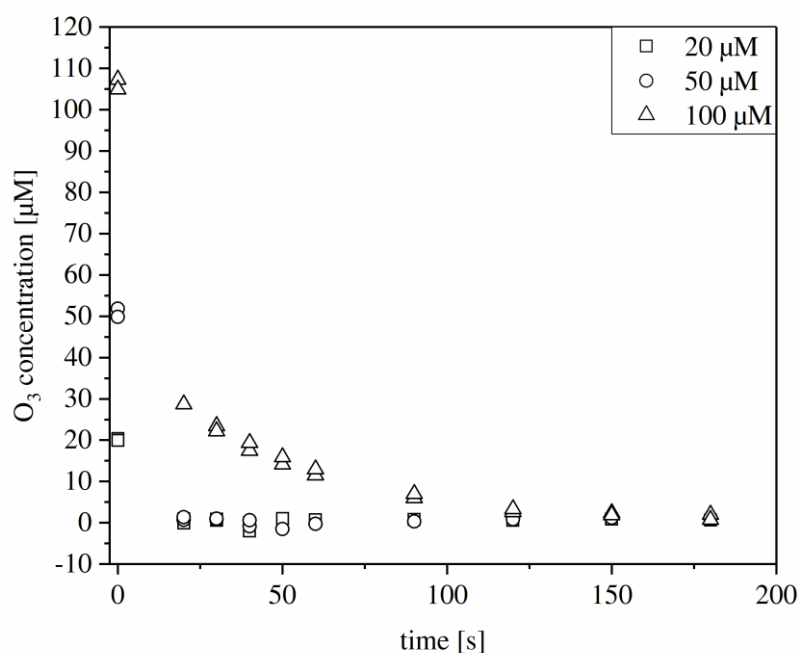


**Figure 3.19: Depletion curve of three initial ozone concentration in the present wastewater. Ozone concentration was determined by indigo method (pH = 7.90 ±0.05; T = 22°C).**

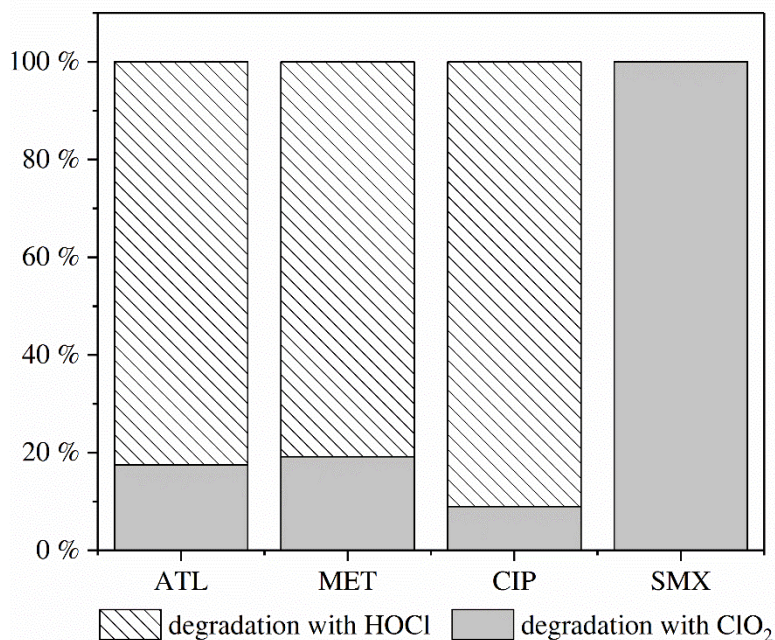


**Figure 3.20: Ratio of the micropollutant transformation related to reactions with HOCl and to reactions with ClO<sub>2</sub> (ATL= atenolol; MET = metoprolol; CIP = ciprofloxacin; SMX = sulfamethoxazole).**

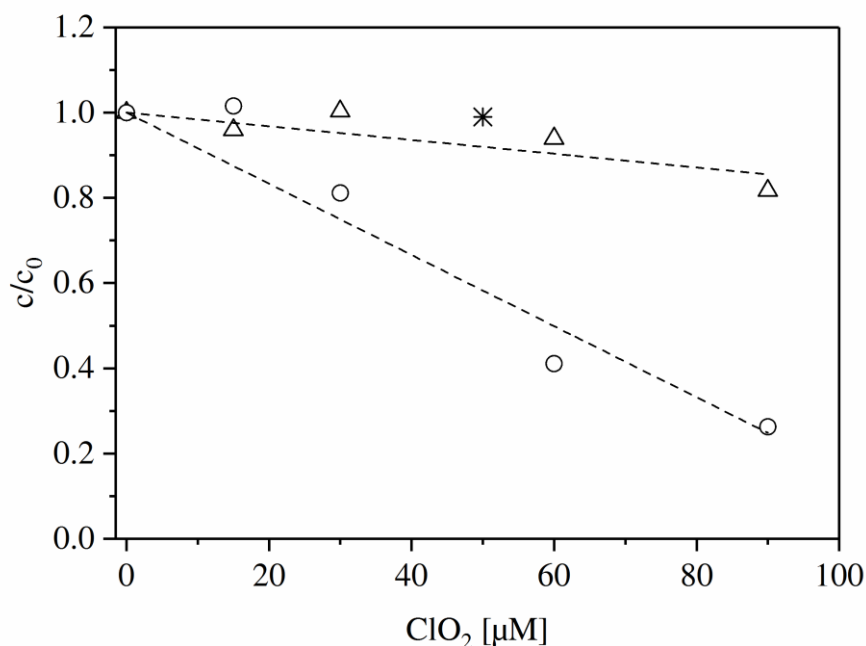


**Figure 3.21: Transformation of metoprolol with ClO<sub>2</sub> in absence (circles) and in presence of glycine (triangles). The calculated values were calculated with equation 1 (main text) (star), dashed line: linear regression forced through  $x/y = 0/1$  ([metoprolol]<sub>0</sub> =  $1 \times 10^{-6}$  M, pH =  $7.90 \pm 0.05$ , T =  $22^\circ\text{C}$ , recovery =  $92 \pm 8$  %).**

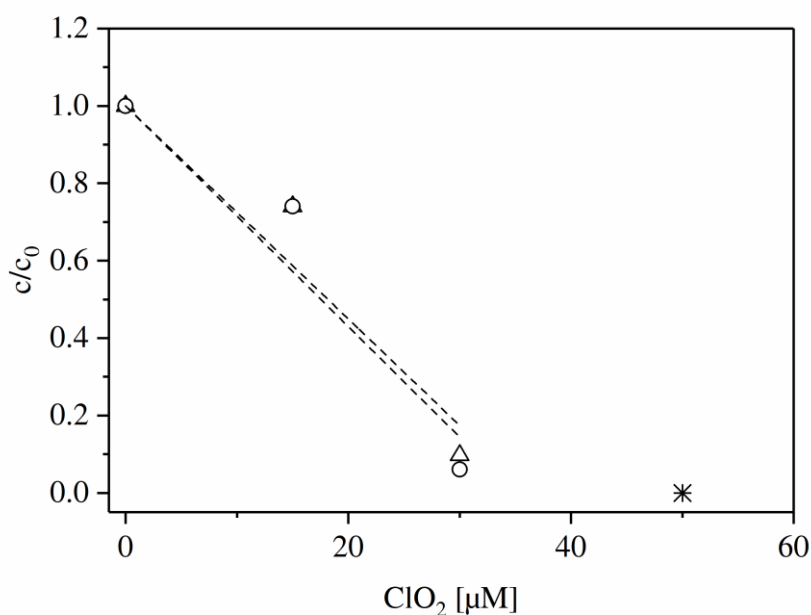


**Figure 3.22: Transformation of sulfamethoxazole with ClO<sub>2</sub> in absence (circles) and in presence of glycine (triangles). The predicted degradation was calculated with equation 1 (main text) (star), dashed line: linear regression forced through  $x/y = 0/1$  ([SMX]<sub>0</sub> =  $1 \times 10^{-6}$  M, DOC =  $8.11 \pm 0.12$  mg L<sup>-1</sup>, pH =  $7.90 \pm 0.05$ , T =  $22^\circ\text{C}$ , recovery =  $99 \pm 1$  %).**



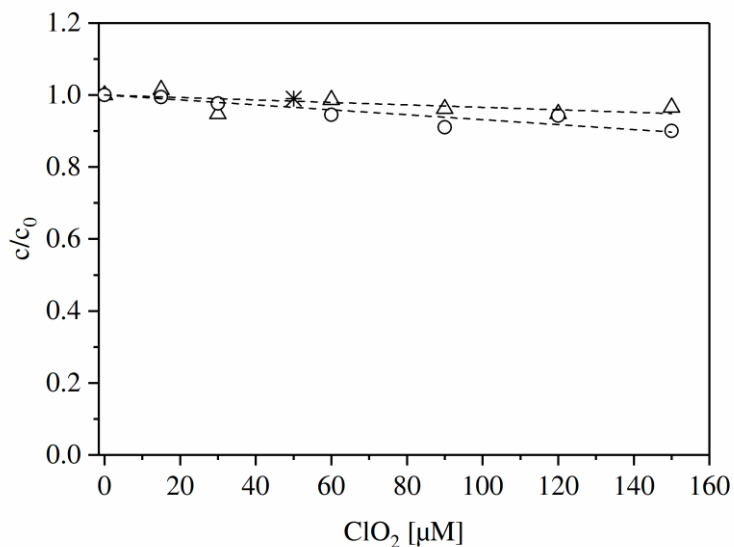


**Figure 3.23:** Transformation of 5,6-dimethyl-1-*H*-benzotriazol with ClO<sub>2</sub> in absence (circles) and in presence of glycine (triangles). The predicted degradation was calculated with equation 1 (main text) (star), dashed line: linear regression forced through  $x/y = 0/1$  ( $[DMBT]_0 = 1 \times 10^{-6}$  M, DOC =  $8.11 \pm 0.12$  mg L<sup>-1</sup>, pH =  $7.90 \pm 0.05$ , T = 22°C; recovery =  $98 \pm 5$  %).

# **4.Chapter: Ozone consumption in the reaction with phenolic compounds: Effects of pH, radical scavengers and products**

**Adapted from:** Terhalle, J., Tintrop, L.K., Nikutta, S.E., Krzeczesa D.L., Schmidt, T.C. and Lutze, H.V. (2022) *Ozone consumption in the reaction with phenolic compounds: Effects of pH, radical scavengers and products*. Submitted to Chemosphere 02.2022.

## 4.1 Introduction

Phenolic structures are common moieties in trace organic compounds (TrOCs) and dissolved organic matter (DOM) (von Gunten, 2018). The content of oxidizable phenols in DOM is between 2.3 and 2.9 mM phenol/g C (Tentscher et al., 2018). Hence, in wastewater, a DOM concentration of 10 mg/L results in a phenol concentration of ~10 – 13  $\mu$ M (Tentscher et al., 2018). The reaction of phenol with ozone ( $O_3$ ) has already been investigated in many studies (Mvula and von Sonntag, 2003, Ramseier and von Gunten, 2009, Konstantinova et al., 1991, Singer and Gurol, 1983). The postulated reaction mechanisms of Mvula and von Sonntag (2003) suggest that one mole of  $O_3$  reacts with one mole of phenol (Figure 4.1). Thereby,  $O_3$  may react at different sites: i.e., attack of  $O_3$  at the *ortho*-position of phenol and attack of  $O_3$  at the *para*-position (Figure 4.1, Reaction 1). After  $O_3$  addition at these sites, it may form a 1,2-cyclo adduct and initiate the Criegee Reaction (Reaction 2), form superoxide (Reaction 3), transfer oxygen under formation of singlet oxygen (Reaction 4) and may abstract an electron under formation of an ozonide radical anion ( $O_3^{\cdot-}$ ) (Reaction 5). Furthermore, an outer sphere electron transfer is possible, requiring a preceding  $O_3$  addition (Reaction 6). The products from these reactions are *p*-benzoquinone (Reaction 3), catechol (Reaction 4), *cis,cis*-muconic acid (Reaction 2) or hydroquinone (Reaction 3, 5, 6) (Mvula and von Sonntag, 2003). The  $O_3$  consumption of this reaction mechanism has been described by Mvula and von Sonntag (2003) to be > 1 per phenol degraded. Therefore,  $O_3$  consumption can be presented as mole phenol degraded per mole consumed  $O_3$  as done by Mvula and von Sonntag (2003) (e.g., 0.48 mole of phenol was degraded per mole of  $O_3$ ) or as mole  $O_3$  per mole degraded substance (e.g., 2.1 moles of  $O_3$  was needed for degradation per mole of phenol). In this study, the second definition is used.

Mvula and von Sonntag (2003) have shown an  $O_3$  consumption of 2.1 at pH 7 and with a decreasing pH, the  $O_3$  consumption increased to 3.0 (pH 3), in absence of a radical scavenger. Additionally, with increasing pH, the  $O_3$  consumption decreased to 1.7 (pH 10). They explained their observation with excessive consumption of  $O_3$  by the primary organic products, which react considerably faster with  $O_3$  than phenol at pH 3 and 7. At pH 10, however, formed reaction products have about the same reaction kinetics as phenol and do not contribute in  $O_3$  consumption as will be explained below (note that concentration of products are lower than the concentration of phenol) (Tentscher et al., 2018, Mvula and von Sonntag, 2003). The reaction

4. Chapter: Ozone consumption in the reaction with phenolic compounds: Effects of pH, radical scavengers and products

of phenol with  $O_3$  is largely depending on pH because the neutral phenol reacts six orders of magnitude slower than the deprotonated phenol (phenolate) (Mvula and von Sonntag, 2003).

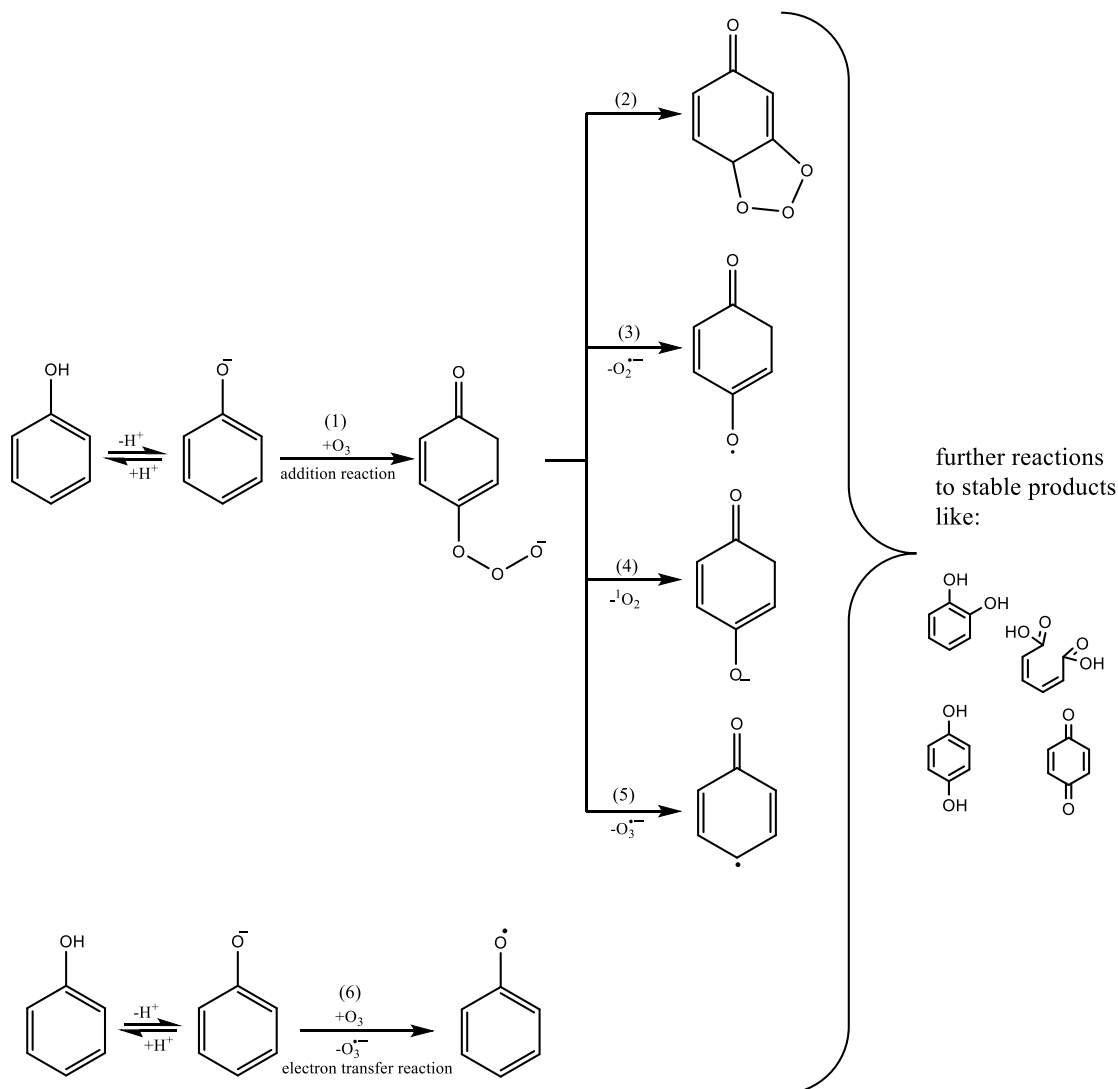


**Figure 4.1: Reaction steps of ozone with phenol at *para*-position; Further reaction to adduct formation (2), superoxide formation (3), singlet oxygen formation (4) and electron transfer reaction (5 and 6) (modified from Mvula and von Sonntag (2003)).**

With pH values  $> 4$  (reactivity  $pK_a$ ), the reaction kinetic of phenol increases by one order of magnitude per pH unit. However, the high reaction kinetics of the neutral species of the products (see Table 4.5) results in way higher reactivity  $pK_a$  (e.g., reactivity  $pK_a(\text{catechol}) = 7.56$ ) and reaction kinetics remain unchanged at  $pH < 7$ . Hence, with decreasing pH, the competition for  $O_3$  between the precursors and the reaction products increase (see further information in Chapter 4.5). Indeed, Figure 4.6 shows that the reaction kinetics of reaction products with  $O_3$  are 2 - 3 orders of magnitude faster than the reaction with phenol at pH 3. However, at pH 7, phenol reacts 3 - 4 orders of magnitude faster with  $O_3$  than at pH 3. Hence

at pH 7, organic reaction products react with similar kinetics as phenol, but can be neglected contributing to  $O_3$  scavenging due to their low concentrations. Yet, it remains unclear how an  $O_3$  consumption  $>1$  at pH 7 can be explained.

Other studies reported similar values for the  $O_3$  consumption of phenol, 2.2 at pH 7 and 2.6 at pH 3, both in the presence of hydroxyl radical scavengers (*tertiary*-butanol and dimethyl sulfoxide) (Ramseier and von Gunten, 2009). Ramseier and von Gunten (2009) underline the reformation of phenolate (Figure 4.2). Thereby, the formed phenoxyl radical (Reaction 6) reacts with the hydroquinone anion (formed product) by a one-electron transfer, resulting in a phenolate and hydroquinone radical (Reaction 8). The newly formed phenolate is able to consume further  $O_3$ .

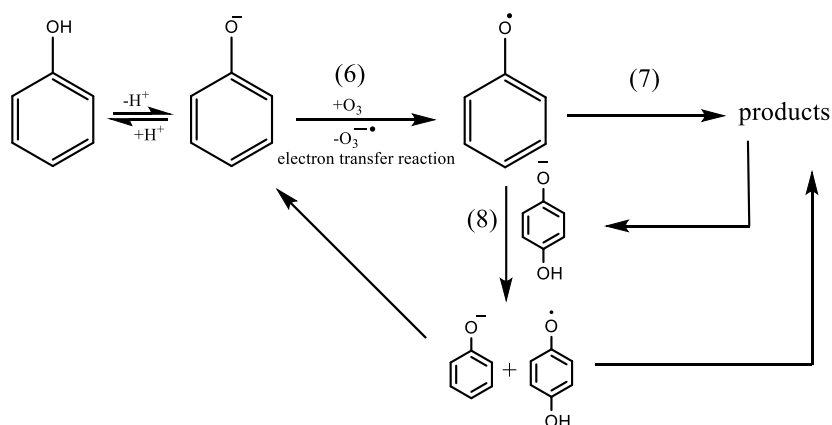


**Figure 4.2: Ozone-consuming chain reaction due to reformation of phenolate per reaction of the phenoxyl radical with the hydroquinone anion (modified from Mvula and von Sonntag (2003))**

Tentscher et al. (2018) support the hypothesis of Mvula and von Sonntag (2003), in that formed reaction products may compete with phenol, at  $pH > 7$ . However, all previous works cannot fully explain an elevated  $O_3$  consumption of  $> 1$  at  $pH > 7$ , since organic products are not relevant for  $O_3$  decomposition any more (see above) (Mvula and von Sonntag, 2003, Ramseier and von Gunten, 2009, Tentscher et al., 2018).

The reaction of the products with  $O_3$  distorts the overall  $O_3$  consumption. These reactions could be suppressed with a high excess of phenol. In this case,  $O_3$  can only react with phenol and results in one mole phenol being degraded with one mole  $O_3$ . However, the use of high phenol concentrations is not possible because the determination of the degree of degradation of phenol is not possible (the difference of  $c$  to  $c_0$  is too small). To overcome the problem, the concept of

#### 4. Chapter: Ozone consumption in the reaction with phenolic compounds: Effects of pH, radical scavengers and products

---

Chapter 3 was used. In Chapter 3, the order of dosages was changed: Commonly, the oxidant is added to a solution with the compound under study. Just after dosage and prior to complete mixing an interface forms between the compound under study (e.g., phenol) containing bulk solution and the O<sub>3</sub> stock solution. At this interface, the oxidant is present in excess compared to the compound under study, which favors reaction of O<sub>3</sub> with formed organic reaction products. In Chapter 3, the compound under study was added to a solution with diluted oxidant. This reversed order of dosages results in an excess of the compound under study to the oxidant at the reaction interface. As a result, the oxidant may only react with the compound under study and not with the primary products. This experimental concept was not systematically used to investigate the effect of primary products on oxidant depletion, yet.

A further hypothesis is that other reactive species, in addition to O<sub>3</sub> and OH radicals are formed, which can consume O<sub>3</sub>. One possible species is the selective reactive species superoxide (O<sub>2</sub><sup>•-</sup>). O<sub>2</sub><sup>•-</sup> is formed in the reaction of OH radicals with organic compounds (e.g., *tert.*-BuOH or phenol (see Figure 4.1 Reaction 5 and Chapter 4.5.3) (Mvula and von Sonntag, 2003, von Sonntag and von Gunten, 2012). O<sub>2</sub><sup>•-</sup> reacts faster with O<sub>3</sub> ( $1.5 \times 10^9 \text{ M}^{-1} \text{ s}^{-1}$ ) than the phenolate (Sehested et al., 1983). The influence of O<sub>2</sub><sup>•-</sup> on the O<sub>3</sub> consumption was not investigated in other studies, yet.

This study investigates the influence of different parameters on O<sub>3</sub> consumption in the reaction of phenols with O<sub>3</sub>: First, the impact of the hydroxyl radical formation and the comparison of different pH values were investigated. Second, the role of the primary organic transformation products on the O<sub>3</sub> consumption was tested using the concept of Chapter 3. Finally, the impact of the O<sub>2</sub><sup>•-</sup> formation on O<sub>3</sub> consumption was studied. Thereby 4-chlorophenol (deactivating substituent), phenol, 4-methylphenol (activating substituents) and 4-methoxyphenol (activating substituents) were used as compound under study.

## 4.2 Material and methods

### 4.2.1 Chemicals

All chemicals and solvents were used as received from suppliers. A complete list of all used chemicals is shown in Table 4.3.

### 4.2.2 Equipment

The used equipment and methods are summarized in Table 4.4.

### 4.2.3 Generation of ozone stock solution

For the preparation of O<sub>3</sub> stock solutions, oxygen was enriched with O<sub>3</sub> by an O<sub>3</sub>-generator (Table 4.4). In brief, the gaseous O<sub>3</sub> was bubbled into ice-cooled ultrapure water. After an enrichment phase of approximately 45 minutes, the O<sub>3</sub> concentration was determined by UV absorption of a 1:3-diluted O<sub>3</sub> stock solution at 258 nm,  $\epsilon_{O_3} = 3200 \text{ M}^{-1} \text{ cm}^{-1}$  (Hoigné and Bader, 1980). The O<sub>3</sub> concentration in the stock solution ranged between  $1.6 \times 10^{-3} - 1.8 \times 10^{-3} \text{ M}$ . Continuous purging of the stock solution with gaseous O<sub>3</sub> was required to keep the O<sub>3</sub> concentration constant.

### 4.2.4 Experimental part

#### 4.2.4.1 Influence of pH values

With varying pH value, the ratio of the phenolic reacting species is changing. Figure 4.3 shows the fraction of phenol and phenolate (red and blue lines) over the pH range 1 to 12. Additionally, the fraction of O<sub>3</sub>, which reacts with phenol and phenolate, was plotted vs. pH (pink and green lines). From pH 1 to pH 9, the fraction of phenolate is below 10%. However, already at pH 5, 90% of O<sub>3</sub> reacts with phenolate. Only below pH 3, the reaction of phenolate contributes by < 10%. Both O<sub>3</sub> reactions, with phenol and phenolate, are combined in  $k_{\text{obs}}$  (orange line). With increasing pH,  $k_{\text{obs}}$  increases because phenolate (e.g.,  $k(\text{O}_3 + \text{phenolate}) = 1.4 \times 10^9 \text{ M}^{-1} \text{ s}^{-1}$ ) (Mvula and von Sonntag, 2003) reacts six orders of magnitude faster with O<sub>3</sub> than phenol (e.g.,  $k(\text{O}_3 + \text{phenol}) = 1.3 \times 10^3 \text{ M}^{-1} \text{ s}^{-1}$ ) (Mvula and von Sonntag, 2003). Therefore, the experiments for phenol were performed at pH 2, 7, and 11.

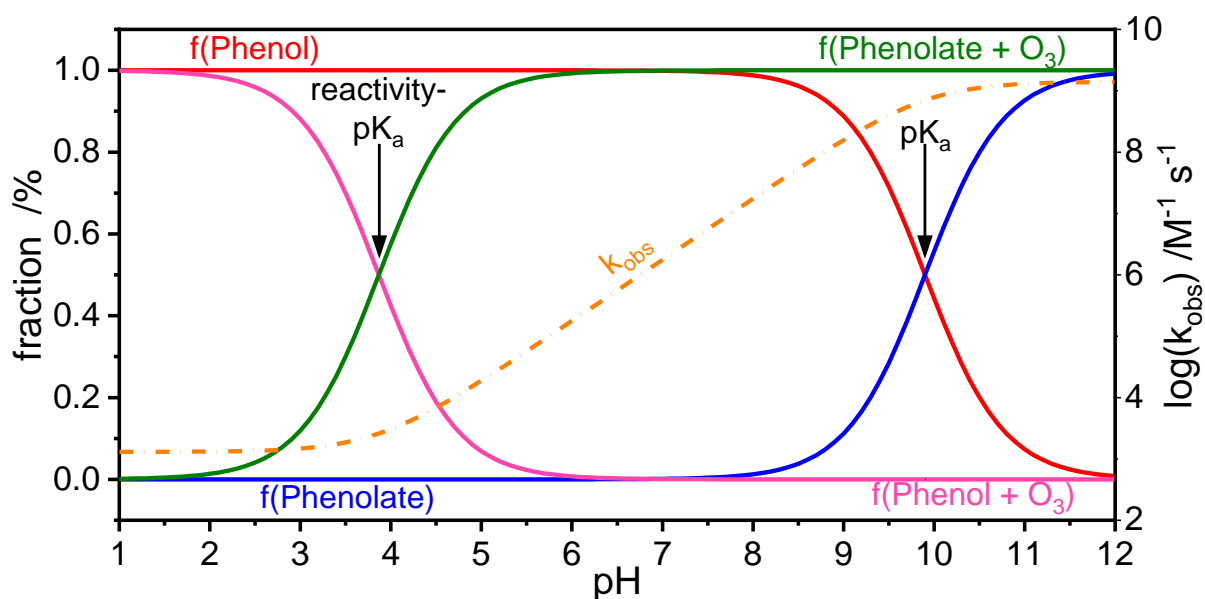


**Figure 4.3:** Fraction of phenol (red line) and phenolate (blue line) at different pH values. Additionally, the reacting fraction of  $O_3$  with phenol (pink line) and phenolate (green line) is shown. The crossing point of the fractions shows the  $pK_a$  value, and the crossing point of the reacting fraction is called the reactivity- $pK_a$ . The  $k_{obs}$  is plotted on a logarithmic scale against the pH values (orange line).

All reaction solutions consisted of  $5 \times 10^{-4}$  M phenol and  $1 \times 10^{-1}$  M phosphate buffer. The phosphate buffer species were varied and the pH was adjusted to 2, 7, and 11. After determining the concentration of the  $O_3$  stock solution and before the addition of  $O_3$ , the reaction solution was diluted with ultrapure water. This dilution results in equal liquid sample volumes. The reaction solutions were treated with six different dosages of  $O_3$  (final concentration range between  $2.5 \times 10^{-4}$  M and  $1.5 \times 10^{-3}$  M). All samples were analyzed more than 12 h after the experiment was performed. After this reaction time,  $O_3$  was consumed entirely. Experiments were performed in triplicates at each dose. Calibration of phenol was integrated into each measurement sequence. The concentration of phenol was measured by HPLC-UV (Table 4.4).

#### 4.2.4.2 Influence of the OH radical scavenger

OH radicals are formed during the reaction of  $O_3$  with phenol and subsequently react with phenol and  $O_3$ , too. Therefore, OH radicals may influence the determined  $O_3$  consumption. For the investigation of the influence of the OH radicals, experiments were done as described in Chapter 4.2.4.1. The difference to Chapter 4.2.4.1 was the addition of  $1.25 \times 10^{-1}$  M *tert.*-butanol (*tert.*-BuOH) to each sample. *Tert.*-BuOH was added to scavenge  $\geq 95\%$  of the formed



OH radicals (for calculations of scavenger concentrations cf. Willach et al. (2020) and Lutze et al. (2015)). Phenol concentration was measured by HPLC-UV (Table 4.4).

#### 4.2.4.3 Reverse order dosage (ROD)

For the reverse order dosage (ROD), one has to take care of how the sample and dosing agent are prepared: Phosphate buffer and *tert.*-BuOH (same concentration as in chapter 4.2.4.2) was mixed in a vial (Solution A). At first, O<sub>3</sub> was added to solution A, and after 10 s solution B, consisting of phenol, phosphate buffer, and *tert.*-BuOH, was added to solution A. This procedure creates an excess of phenol over O<sub>3</sub> at the reaction interface. Thus, O<sub>3</sub> should react exclusively with phenol, and products formed should not contribute to O<sub>3</sub> consumption. The ROD concept was done at pH 7 and 11 because at these pH values the reaction rate constant of phenol is faster than the reaction rate constants of the formed products.

#### 4.2.4.4 Superoxide test (SOT)

O<sub>2</sub><sup>•-</sup> is a product of the reaction of O<sub>3</sub> with organic compounds and reacts fast with O<sub>3</sub> ( $k = 1.5 \times 10^{-9} \text{ M}^{-1} \text{ s}^{-1}$ ) (Sehested et al., 1983, von Sonntag and von Gunten, 2012). In the superoxide test (SOT), methanol (MeOH) ( $3.6 \times 10^{-3} \text{ M}$ ) was used as an OH radical scavenger to investigate its influence on phenol consumption since it results in excessive O<sub>2</sub><sup>•-</sup> formation. Upon the reaction of OH radicals with MeOH the O<sub>2</sub><sup>•-</sup> exposure can be significantly increased (Fischbacher et al., 2015). The MeOH concentration was chosen to scavenge  $\geq 95\%$  of the OH radicals.

#### 4.2.4.5 Determination of the OH radical yield in the reaction of phenol with ozone

The OH radical yield was determined using dimethyl sulfoxide (DMSO) as radical scavenger. DMSO reacts slowly with O<sub>3</sub> ( $k = 1.8 \text{ M}^{-1} \text{ s}^{-1}$  (Reisz et al., 2014)), while its reaction with OH radicals is fast ( $k = 7 \times 10^9 \text{ M}^{-1} \text{ s}^{-1}$  (Buxton et al., 1988)). Thereby, DMSO forms methane sulfinic acid (MSIA) upon the reaction with OH radicals. MSIA reacts further with oxygen to methane sulfonic acid (MSOA). Reactions are shown in Chapter 4.5.1. Both acids were measured by ion chromatography. The sum of MSIA and MSOA represents 92% of the OH radicals. So the yield of the OH radicals is calculated by the following equation (Veltwisch et al., 1980):

$$[OH^{\bullet}] = \frac{[MSIA] + [MSOA]}{0.92} \quad (\text{Equation 4.1})$$

#### 4.2.4.6 Experiments with substituted phenols

The substituted phenols (4-chlorophenol (ClPh), 4-methylphenol (MePh) and 4-methoxyphenol (MxPh)) were added in the reaction solutions (analyte + buffer + radical scavenger). Initial analyte concentration was  $5 \times 10^{-4}$  M for both experiments, ozonation with and without radical scavenging.  $1 \times 10^{-2}$  M phosphate buffer and  $1.25 \times 10^{-1}$  M of *tert.*-BuOH for ClPh,  $1.95 \times 10^{-1}$  M for MePh, and  $4.45 \times 10^{-1}$  M for MxPh were added to the sample to achieve at least 95 % scavenging of OH radicals (Willach et al., 2020, Lutze et al., 2015). Experiments were performed at four pH values:

- 1.) >1 pH-unit below the reactivity p*K*<sub>a</sub> of phenols under study,
- 2.) at the reactivity p*K*<sub>a</sub> of phenols under study,
- 3.) at pH 7 and,
- 4.) >1 pH-unit above the p*K*<sub>a</sub> of phenols under study.

The speciation of the substituted phenols is shown in Figure 4.7 - Figure 4.9 in Chapter 4.5.2. The pH values under investigation were: ClPh: 2.2 / 3.2 / 7.0 / 11.0; MePh: 2.2 / 5.3 / 7.0 / 12.0; MxPh: 2.2 / 5.8 / 7.0 / 12.0.

All samples were analyzed after more than 12 h reaction time to guaranty full turnover of O<sub>3</sub>. Experiments were performed in triplicates at each dose and each pH value. Calibration of each investigated compound was integrated into each measurement sequence.

### 4.3 Results and discussion

The O<sub>3</sub> consumption of all experiments with phenol is summarized in Figure 4.4 and Table 4.1. Additionally, in Table 4.1, the values of Mvula and von Sonntag (2003) and Ramseier and von Gunten (2009) are given for comparison. Analyzing the results shown in Figure 4.4 and Table 4.1 reveals three observations:

- a) Phenol has an O<sub>3</sub> consumption > 1 at all pH values
- b) *Tert.*-BuOH as scavenger did not have strong effect on the O<sub>3</sub> consumption
- c) MeOH resulted in a strong increase of O<sub>3</sub> consumption.

These observations imply the following interpretations: Organic reaction products cannot be the only reason for the elevated O<sub>3</sub> consumption. Since, at pH 11, the reaction rate of phenol is

nearly diffusion controlled and organic reaction products cannot significantly compete with phenolate for O<sub>3</sub>.

The small influence of *tert.*-BuOH indicates that also OH radicals, which are formed in the reaction between phenol and O<sub>3</sub> (Table 4.1 and Figure 4.10 - Figure 4.12), have a small influence on the O<sub>3</sub> consumption, even though OH radicals could react with O<sub>3</sub>. This can be explained by the fast reaction kinetics of OH radicals with phenol ( $k = 1.4 \times 10^{10} \text{ M}^{-1} \text{ s}^{-1}$  (Buxton et al., 1988)), which are thus scavenged by phenol. On the one hand, this should reduce the O<sub>3</sub> consumption, since phenol is degraded by O<sub>3</sub> and OH radicals. On the other hand, the reaction of OH radicals with phenol forms carbon centered radicals, which in turn give rise to reactive oxygen species, which may react with O<sub>3</sub> more selectively such as O<sub>2</sub><sup>•-</sup> (von Sonntag et al., 1997a, von Sonntag and von Gunten, 2012).

The strong effect of MeOH in the SOT experiment indicates that O<sub>2</sub><sup>•-</sup>, which is formed in the reaction of OH radicals with MeOH, can indeed compete with phenolate for O<sub>3</sub>. In the presence of MeOH, more O<sub>3</sub> is needed to degrade one mole of phenol. At pH 7, O<sub>3</sub> consumption increased from 2.4 (*tert.*-BuOH) to 3.2 (MeOH) (note that at this pH O<sub>2</sub><sup>•-</sup> reacts 850 times faster than phenol with O<sub>3</sub>, see Table 4.2). At pH 11, a slight increase of O<sub>3</sub> consumption from 3.6 (*tert.*-BuOH) to 4.2 (MeOH) can be observed, which could be related to the fact that O<sub>2</sub><sup>•-</sup> reacts 1.2 times faster than phenolate with O<sub>3</sub> and thus, increase the O<sub>3</sub> consumption. The SOT showed that O<sub>2</sub><sup>•-</sup> could indeed be important for the depletion of O<sub>3</sub> in the phenol system even at alkaline conditions, with phenolate being fully deprotonated and thus most reactive.

To corroborate that the formed organic products may not be most important for the O<sub>3</sub> consumption the ROD experiment by Chapter 3 (see also Chapter 4.2.4.3) was applied. The results of the ROD are shown in Figure 4.4 (black squares) and Table 4.1. Figure 4.4 shows that excess of phenol during dosage still results in an elevated O<sub>3</sub> consumption (2.3). It is noteworthy that in the ROD experiment the O<sub>3</sub> consumption significantly increased from 1.9 (pH 2) to 2.3 (pH 7). Furthermore, ROD also shows that, at pH 11, the O<sub>3</sub> consumption further increases (ROD O<sub>3</sub> consumption at pH 11: 3.6), which disagrees with the common approach (O<sub>3</sub> consumption at pH 11: 2.9).

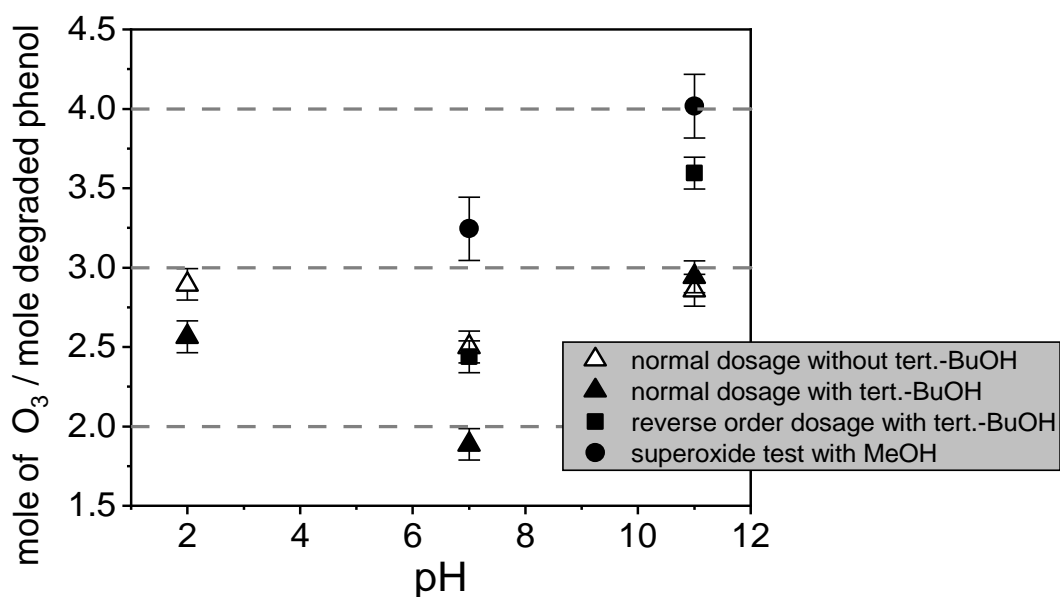


**Figure 4.4:** The  $O_3$  consumption in the reaction with phenol at different pH values, different OH radicals scavengers, and different dosages. Normal dosage is the addition of  $O_3$  to the reaction solution of phenol, phosphate buffer, and *tert.*-BuOH. Reverse order dosage: Adding the reaction solution of phenol, phosphate buffer, and *tert.*-BuOH to a mixture of  $O_3$ , phosphate buffer, and *tert.*-BuOH. Superoxide test: Using methanol instead of *tert.*-BuOH as OH radical scavenger.

**Table 4.1:** Moles of  $O_3$  per mole degraded phenol at three different pH values. Right column: ratio of  $O_3$  concentration to phenol concentration.

	pH 2	pH 7	pH 11	$O_3$ / phenol
Mvula and von Sonntag (2003)(without <i>tert.</i> BuOH)	3.0	2.1	1.7	0.25 – 0.8
Mvula and von Sonntag (2003) (with <i>tert.</i> BuOH)	---	2.4	---	0.25 – 0.8
Ramseier and von Gunten (2009) (with <i>tert.</i> BuOH)	2.6	2.2	---	0.07 – 0.9
This Study (without <i>tert.</i> BuOH)	2.9	2.5	2.9	0.5 – 3.0
This Study (with <i>tert.</i> BuOH)	2.6	1.9	2.9	0.5 – 3.0
This study (ROD)	---	2.3	3.6	0.5 – 3.0
This Study (SOT)	---	3.2	4.0	0.5 – 3.0
OH radical yield	37%	25%	30%	0.5 – 3.0

Finally, the influence of substituents on the O<sub>3</sub> consumption was investigated. Therefore, three substituted phenols were chosen: ClPh, with chloride as an electron-withdrawing substituent, MePh, and MxPh, with CH<sub>3</sub> and OCH<sub>3</sub> as electron-donating substituents. In addition, different pH values were selected to take the influence of the corresponding species (protonated/deprotonated) into account. An overview of the results is shown in Figure 4.5.

Due to the chlorine substituent, ClPh reacts slower with O<sub>3</sub> than phenol (reaction rate constants are shown in Table 4.2). Nevertheless, the O<sub>3</sub> consumption at pH 2 without *tert.*-BuOH was similar to phenol (2.9). This value does not change with increasing pH value (pH 3.2: 2.9; pH 7: 3.0; pH 11: 3.0), which is shown in Figure 4.5B. If the OH radicals are scavenged, the consumption decreases largely at pH 7 (2.9) and 11 (2.1) (Figure 4.5A).

According to Tentscher et al. (2018), benzoquinones and catechol are formed when ClPh reacts with O<sub>3</sub> at pH 3. At this pH value, these two products react faster with O<sub>3</sub> than ClPh (benzoquinone reacts 4 times faster and catechol 830 times faster) (see Table 4.2). At pH 7, the yield of the two products increases. However, the reaction rate constant of ClPh increases much more with pH than the reaction rate constants of benzoquinone and catechol. Hence, at pH 7,  $k_{\text{obs}}$  of O<sub>3</sub> plus benzoquinone and catechol are considerably lower than  $k_{\text{obs}}$  of O<sub>3</sub> plus ClPh, and the fraction of O<sub>3</sub> reacting with ClPh compared to the reaction products increases, which can explain the decrease in O<sub>3</sub> consumption. For pH 11, the product yield is unknown, but the O<sub>3</sub> consumption is similar to pH 7, indicating that the influence of the products did not change.

The situation is different with the other two substituted phenols. The methyl- or methoxy-group in *para*-position increases the electron density in the phenolic ring and thus the reaction rate with O<sub>3</sub> becomes faster. At pH 2, the O<sub>3</sub> consumption was 1.8 (MePh) and 2.0 (MxPh) (Figure 4.5A and Table 4.2). In contrast to ClPh, the O<sub>3</sub> consumption of these activated phenols slightly increases (Figure 4.5) with increasing pH value. A reaction of O<sub>3</sub> with formed reaction products may also explain the higher O<sub>3</sub> consumption at low pH. At pH  $\geq$  7, the O<sub>3</sub> consumption of all phenols is very similar, which may indicate that primary O<sub>2</sub><sup>•-</sup> formation (Figure 4.1, Reaction 3) is the main driver of O<sub>3</sub> consumption, since especially at pH 7 O<sub>2</sub><sup>•-</sup> reacts much faster than conceivable products (Table 4.2).

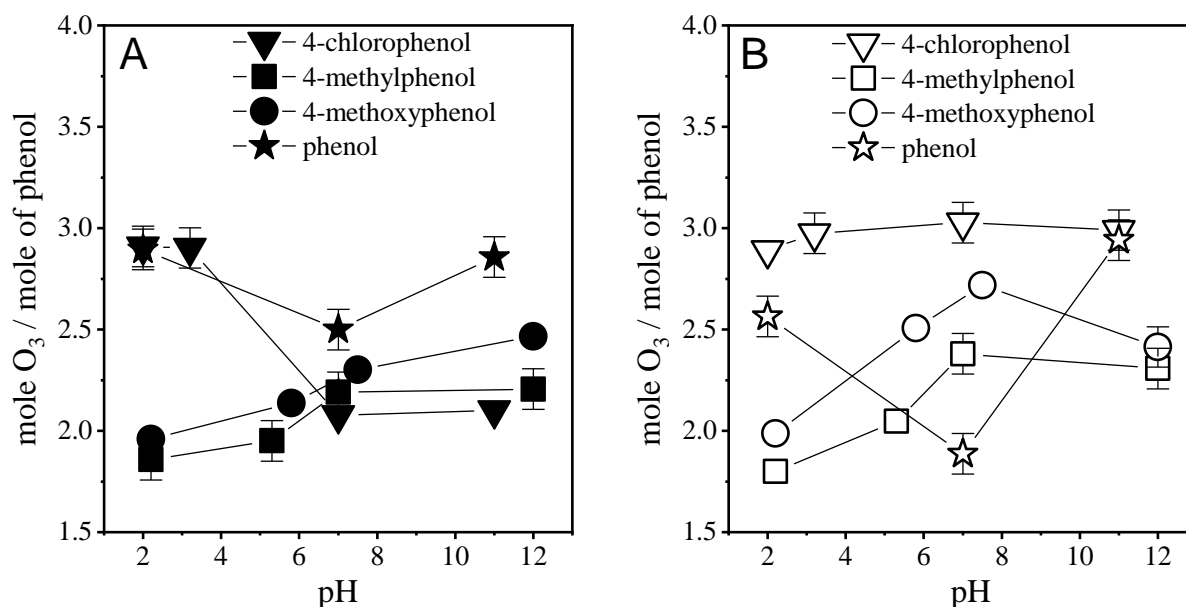


**Figure 4.5:** O<sub>3</sub> consumption during the reaction of O<sub>3</sub> with phenol (stars), 4-chlorophenol (triangle), 4-methylphenol (square), and 4-methoxyphenol (circle) at different pH values. **A:** in the presence of *tert.*-BuOH and **B:** In the absence of *tert.*-BuOH.

According to Tentscher et al. (2018), MePh mainly forms cyclodienones and catechol. However, the yield changes with increasing pH value. For example, the amount of formed cyclodienones decreases, and catechol formation increases with pH. Since Catechol reacts way faster with O<sub>3</sub> than cyclodions and somewhat faster than with MePh it may contribute in O<sub>3</sub> stoichiometric ratio. These results show that even with the substituted phenols, the O<sub>3</sub> consumption is >1, which is not explainable with the reaction of the formed organic products, since their reaction rate is about the same. Here also superoxide may play a role in O<sub>3</sub> consumption.

4. Chapter: Ozone consumption in the reaction with phenolic compounds: Effects of pH, radical scavengers and products

**Table 4.2: Reaction rate constants of the compounds under study with O<sub>3</sub> at different pH values (upper part), the reaction rate constants of phenol products (organic and inorganic) with O<sub>3</sub> (middle part), and yield of the main products of the substances under study with O<sub>3</sub> at pH 7 (lower part); note that the reactivity pK<sub>a</sub> values of hydroquinone, catechol and cis,cis-muconic acid are > 10, hence k<sub>app</sub> hardly changes at the below given pH range (2-12).**

Compounds	pH 2 [M <sup>-1</sup> s <sup>-1</sup> ]	pH 7 [M <sup>-1</sup> s <sup>-1</sup> ]	pH 11/ pH12 [M <sup>-1</sup> s <sup>-1</sup> ]
Phenol (Hoigné and Bader, 1983b)	1.32 x 10 <sup>3</sup>	1.76 x 10 <sup>6</sup>	1.30 x 10 <sup>9</sup>
4-chlorophenol (Hoigné and Bader, 1983b)	6.25 x 10 <sup>2</sup>	2.49 x 10 <sup>6</sup>	5.86 x 10 <sup>8</sup>
4-methylphenol (Tentscher et al., 2018)	3.00 x 10 <sup>4</sup>	1.63 x 10 <sup>6</sup>	2.67 x 10 <sup>9</sup>
4-methoxyphenol (Tentscher et al., 2018)	4.70 x 10 <sup>5</sup>	7.25 x 10 <sup>6</sup>	9.48 x 10 <sup>9</sup>
Formed products	Reaction rate constant [M <sup>-1</sup> s <sup>-1</sup> ]		
Hydroquinone (Gurol and Nekouinaini, 1984)	For all pH values 2.30 x 10 <sup>6</sup>		
Catechol (Gurol and Nekouinaini, 1984)	For all pH values 5.20 x 10 <sup>5</sup>		
cis,cis-muconic acid (Mvula and von Sonntag, 2003)	For all pH values 2.40 x 10 <sup>4</sup>		
Benzoquinone (Mvula and von Sonntag, 2003)	2.50 x 10 <sup>3</sup>		
OH radicals (Sehested et al., 1984)	1.10 x 10 <sup>8</sup>		
Superoxide (Sehested et al., 1983)	1.50 x 10 <sup>9</sup>		
Compounds	Yield of main reaction products at pH 7		
phenol	benzoquinone (30 % (Tentscher et al., 2018)) catechol (15 % (Tentscher et al., 2018))		
4-chlorophenol	benzoquinone (20 % (Tentscher et al., 2018)) catechol (12 % (Tentscher et al., 2018))		
4-methylphenol	catechol (12 % (Tentscher et al., 2018)) cyclohexenone (22 % (Tentscher et al., 2018)) benzoquinone (2 % (Tentscher et al., 2018))		
4-methoxyphenol	benzoquinone (12 % (Tentscher et al., 2018)) hydroquinone (12 % (Tentscher et al., 2018))		

#### 4.4 Conclusion

At pH 11, superoxide is the product, which reacts faster than the investigated phenols. Thus, the  $O_3$  consumption, which is  $> 1$  in all experiments, cannot solely depend on the reaction of  $O_3$  with the formed organic products. Hence, another reaction partner may contribute to  $O_3$  consumption, i.e., superoxide. This could be further investigated by using a selective  $O_2^{\cdot-}$ -scavenger such as tetranitromethane, which would also allow to determine the  $O_2^{\cdot-}$  yields or by directly dosing of  $O_2^{\cdot-}$  (using  $KO_2$ ). However, these experiments are beyond the scope of this study and should be subjected in further studies.

#### 4.5 Supporting information

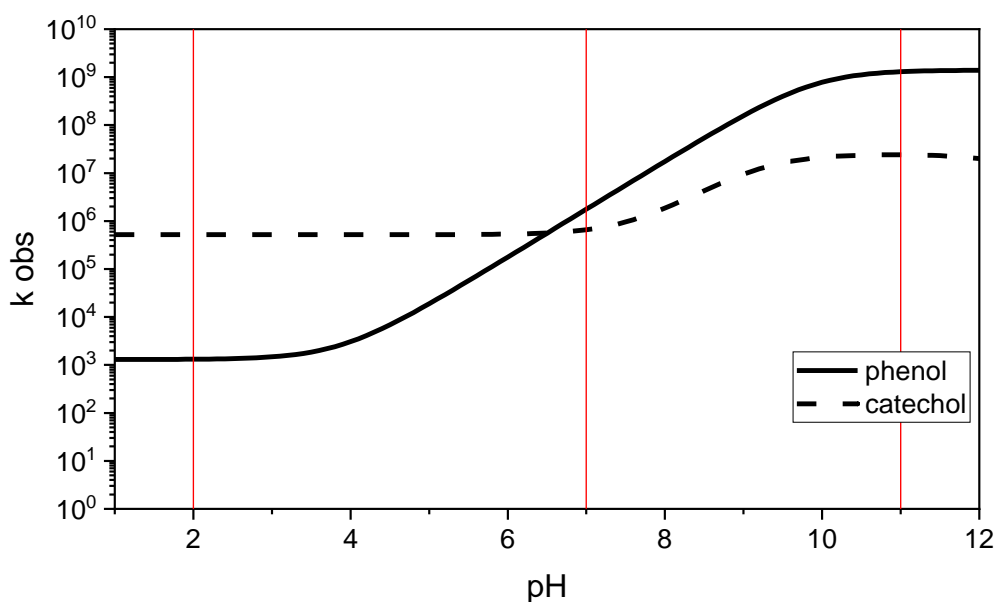


**Figure 4.6: Observed reaction rate constant ( $k_{obs}$ ) of phenol and catechol vs. pH. Red lines present the pH values under study.**



4. Chapter: Ozone consumption in the reaction with phenolic compounds: Effects of pH, radical scavengers and products

**Table 4.3: Chemicals used in the present study**

Substance	Structural formula	Purity	Manufacturer
phenol ( $pK_a = 9.98$ )	$C_6H_5OH$	99 %	Merck (Darmstadt, Germany)
4-methylphenol ( $pK_a = 10.3$ )	$C_6H_4OHCH_3$	$\geq 99\%$	Merck
4-chlorophenol ( $pK_a = 9.38$ )	$C_6H_4OHCl$	$\geq 99\%$	Merck
4-methoxyphenol ( $pK_a = 10.21$ )	$C_6H_4OHOCH_3$	$\geq 98.5\%$	Merck
sodium chloride	$NaCl$	99.5 %	Bernd Kraft (Duisburg, Germany)
sodium hydroxide	$NaOH$	99 %	VWR Chemicals (Langenfeld, Germany)
dipotassium hydrogen phosphate	$K_2HPO_4$	$\geq 99\%$	AppliChem (Steinheim, Germany)
sodium dihydrogen phosphate	$NaH_2PO_4$	$\geq 99\%$	AppliChem
<i>ortho</i> -phosphoric acid	$H_3PO_4$	85 % p. a.	AppliChem
<i>tert.</i> -butanol	$C_4H_9OH$	$\geq 99.5\%$	Merck (Darmstadt, Germany)
oxygen gas	$O_2$	1.0	Air Liquide
methanol (MeOH)	$CH_3OH$	99.9%	Fisher Scientific (Karlsruhe, Germany)
sodium methanosulfinic (MSIA)	$CH_3SOOH$	95.0 %	Alfa Aesar (Loughborough, England)
methanosulfonic acid (MSOA)	$CH_3SO_2OH$	99.0 %	Merck (Darmstadt, Germany)
dimethyl sulfoxide (DMSO)	$(CH_3)_2SO$	99.0 %	Merck (Darmstadt, Germany)

4. Chapter: Ozone consumption in the reaction with phenolic compounds: Effects of pH, radical scavengers and products

**Table 4.4: Used equipment**

Name	Components	Description	Manufacturer
HPLC/UV	Pump	LC-20AT (isocratic flow was used = 0.3 mL/min)	Shimadzu (Duisburg, Germany)
	UV/VIS-detector	SPD-20A (250-280 nm)	Shimadzu
	Autosampler	SIL-20A	Shimadzu
	Software	LabSolutions (Version 1.25 SP4)	Shimadzu
	Column oven	CTO-10AS	Shimadzu
	Column	Kinetex EVO C18 2.6 µm 50 x 2.1 mm	Phenomenex
	Communication element	CBM-20A	Shimadzu
	Degasser	DGU-20A <sub>5</sub>	Shimadzu
	Eluent (phenol)	H <sub>2</sub> O (pH 2)/ACN: 75%/25%	
	Eluent (ClPh)	H <sub>2</sub> O (pH6)/ACN: 87.5%/12.5%	
	Eluent (MePh)	H <sub>2</sub> O (pH6)/ACN: 87.5%/12.5%	
	Eluent (MxPh)	H <sub>2</sub> O (pH6)/MeOH: 87.5%/12.5%	
IC	Pump	883 Basic IC Plus (Flow: 1 ml/min)	Metrohm
	Injector	883 Basic IC Plus	Metrohm
	Autosampler	863 Compact Autosampler	Metrohm
	Conductivity detector	883 Basic IC Plus	Metrohm
	Software	MagICNet 3.2	Metrohm
	Column	Metrosep A Supp 4, 250/4,0	Metrohm
	Sample loop	20 µL	Metrohm
	Eluent	0.36 mM Na <sub>2</sub> CO <sub>3</sub> /0.34 mM NaHCO <sub>3</sub>	

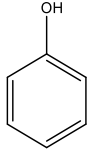
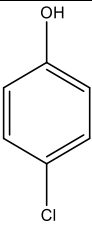
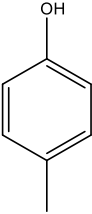
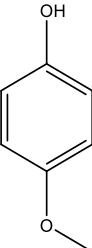
4. Chapter: Ozone consumption in the reaction with phenolic compounds: Effects of pH, radical scavengers and products

---

UV-spectrometer		UV-1800 240 V IVDD US	Shimadzu
balance			Sartorius
pH meter	827 pH		Metrohm
O <sub>3</sub> generator	BMT 802X		BTM Messtechnik (Berlin, Germany)
ultrapure water generator	Purelab ultra		ELGA (Celle, Germany)

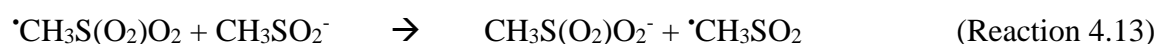
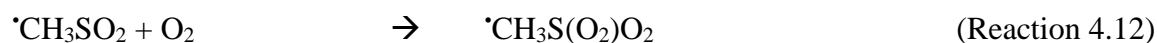
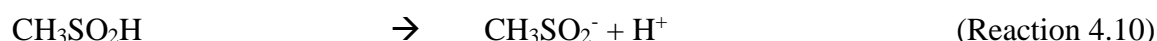
4. Chapter: Ozone consumption in the reaction with phenolic compounds: Effects of pH, radical scavengers and products

**Table 4.5: Structure, reaction rate constants and  $pK_a$  values of the compounds under study.**

Name		$k(\text{neutral species with ozone}) / \text{M}^{-1} \text{s}^{-1}$	$k(\text{anionic species with ozone}) / \text{M}^{-1} \text{s}^{-1}$	$pK_a$
phenol		$1.3 \times 10^3$	$1.4 \times 10^9$	9.98
4-chlorophenol		$6.0 \times 10^2$	$6.0 \times 10^8$	9.38
4-methylphenol		$3.0 \times 10^4$	$3.2 \times 10^9$	10.3
4-methoxyphenol		$4.7 \times 10^5$	$1.1 \times 10^{10}$	10.21

#### 4.5.1 Measurement of methansulfonic acid and methansulfinic acid

In the reaction of OH radicals with dimethyl sulfoxide (DMSO, (CH<sub>3</sub>)<sub>2</sub>SO), methansulfinic acid (MSIS; CH<sub>3</sub>SOH) is formed first (Reaction 4.9 – 4.10) and in follow up reaction (Reactions 4.11 – 4.14) methansulfonic acid (MSOS, CH<sub>3</sub>SO<sub>3</sub><sup>-</sup>) is formed (Sehested and Holcman, 1996, Steiner and Babbs, 1990, Veltwisch et al., 1980):



MSIS and MSOS were measured with ion chromatography. The phosphate buffer needs 70 min to eluate from the column, so after performing four samples with 15 min run time, a water sample for the eluation of the buffer was introduced.

#### 4.5.2 Species diagram of the substituted phenol:

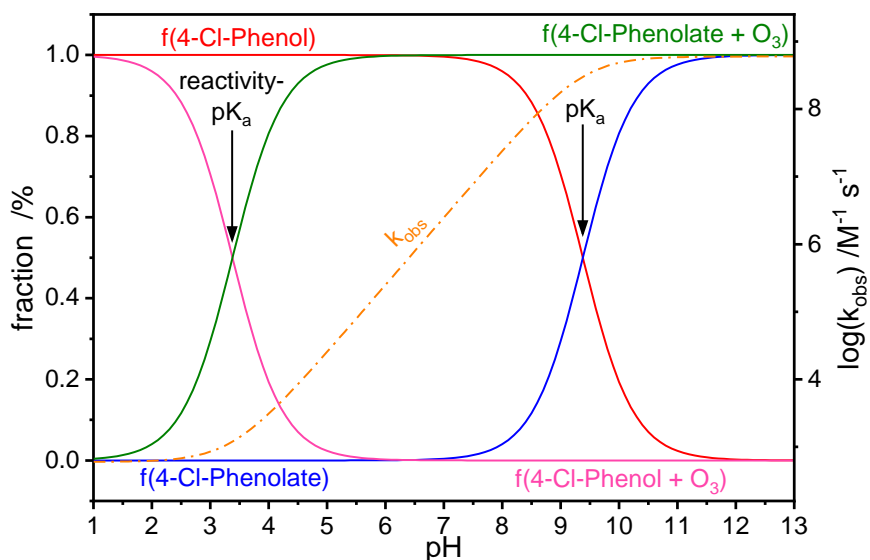


**Figure 4.7:** Fraction of 4-chlorophenol (red line) and the fraction of 4-chlorophenolate (blue line) at different pH values. Additionally, the reacting fraction of ozone with neutral species (pink line) and anionic species (green line) is shown. The crossing point of the fractions shows the  $pK_a$  value and the crossing point of the reacting fraction are called the reactivity- $pK_a$ . The  $k_{obs}$  is plotted on a logarithmic scale against the pH values (orange line).

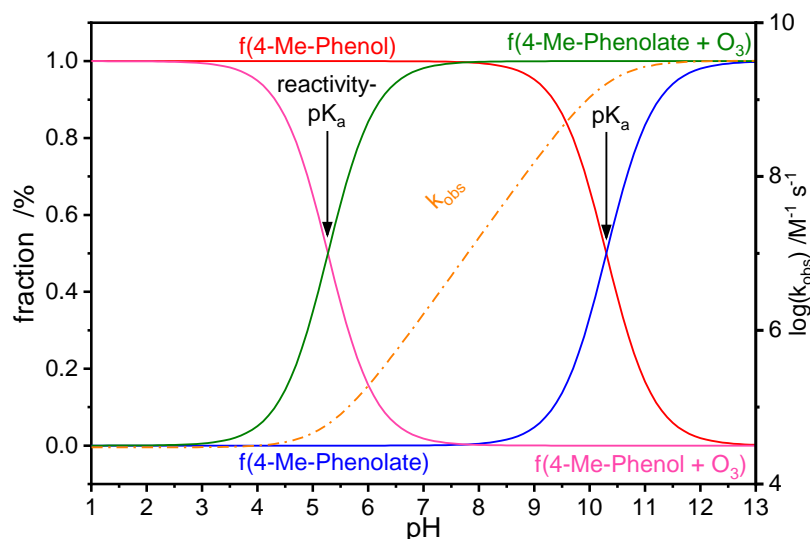


**Figure 4.8:** Fraction of 4-methylphenol (red line) and the fraction of 4-methylphenolate (blue line) at different pH values. Additionally, the reacting fraction of ozone with neutral species (pink line) and anionic species (green line) is shown. The crossing point of the fractions shows the  $pK_a$  value and the crossing point of the reacting fraction are called the reactivity- $pK_a$ . The  $k_{obs}$  is plotted on a logarithmic scale against the pH values (orange line).

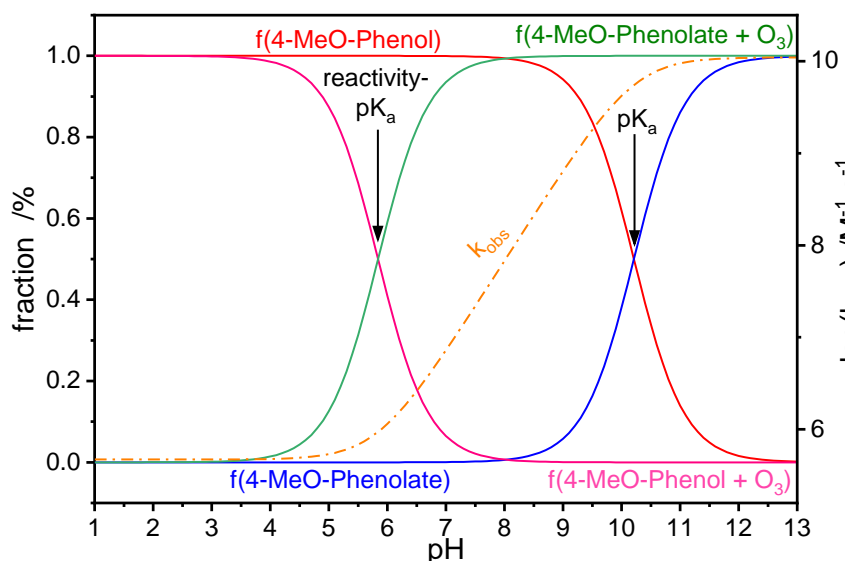


**Figure 4.9:** Fraction of 4-methoxyphenol (red line) and the fraction of 4-methoxyphenolate (blue line) at different pH values. Additionally, the reacting fraction of ozone with neutral species (pink line) and anionic species (green line) is shown. The crossing point of the fractions shows the pK<sub>a</sub> value and the crossing point of the reacting fraction are called the reactivity-pK<sub>a</sub>. The k<sub>obs</sub> is plotted on a logarithmic scale against the pH values (orange line).

#### 4.5.3 OH radical formation in the reaction of phenol

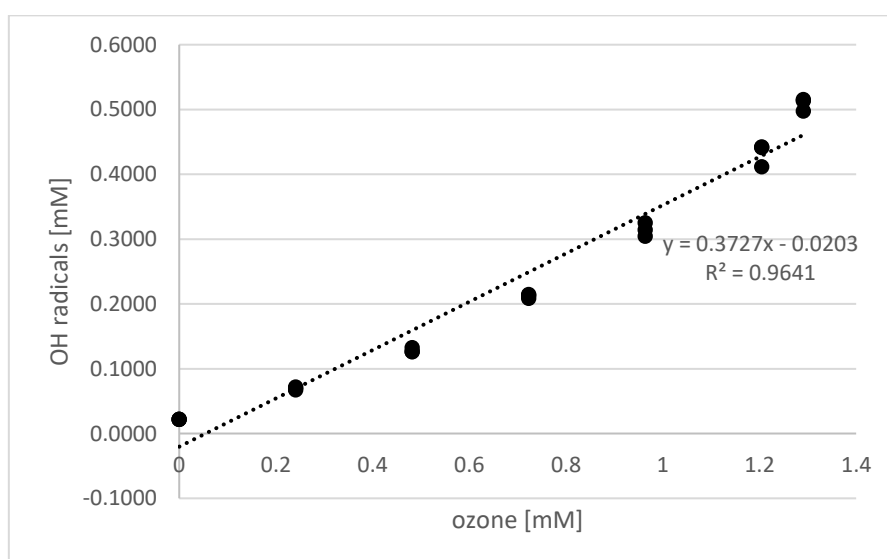


**Figure 4.10:** Concentration of OH radicals plotted against ozone concentration at pH 2. OH radicals were determined by DMSO-method (see above).

4. Chapter: Ozone consumption in the reaction with phenolic compounds: Effects of pH, radical scavengers and products

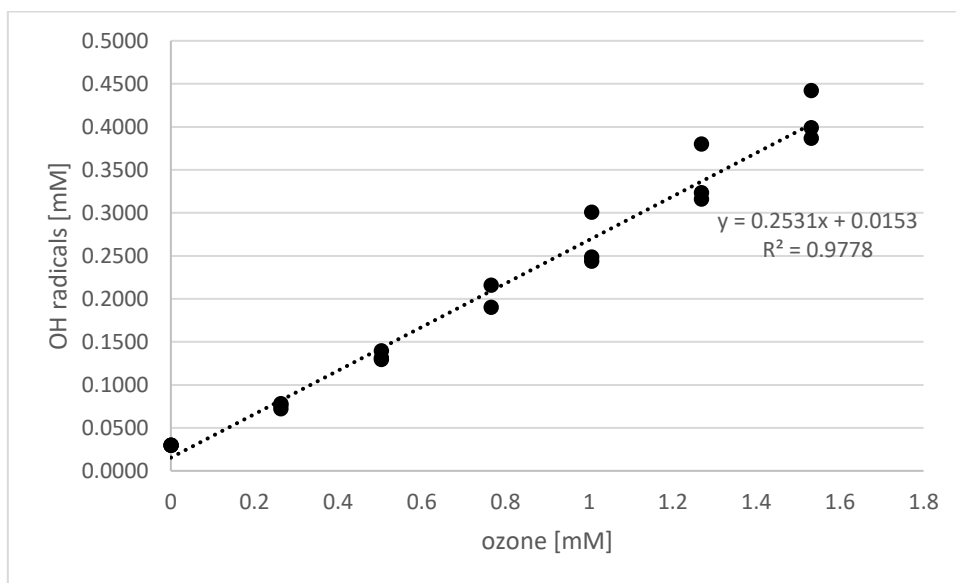


**Figure 4.11: Concentration of OH radicals plotted against ozone concentration at pH 7. OH radicals were determined by DMSO-method (see above).**

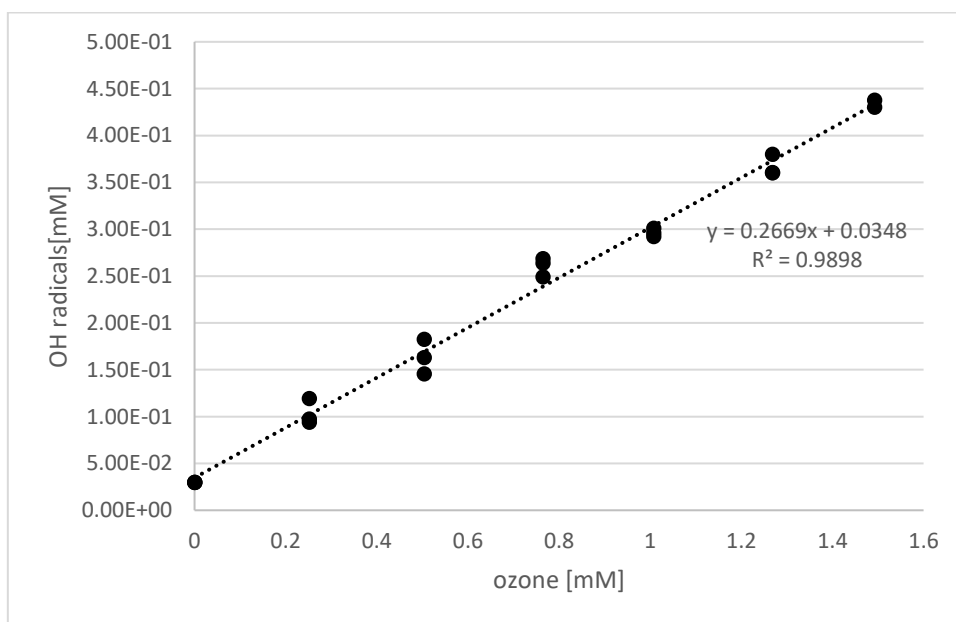
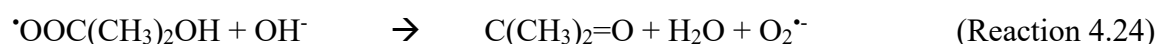
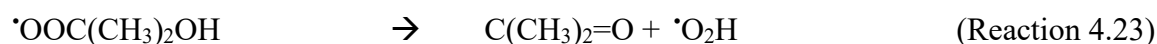
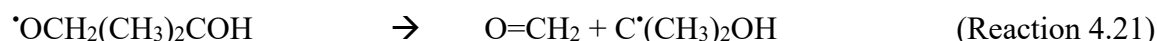
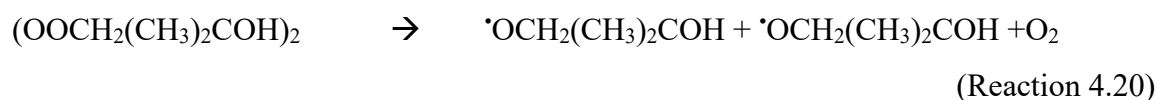
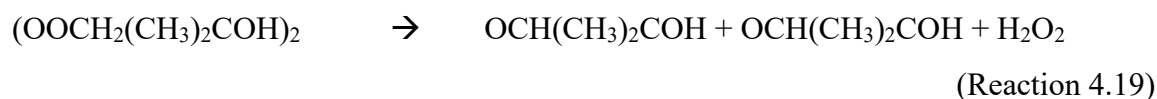
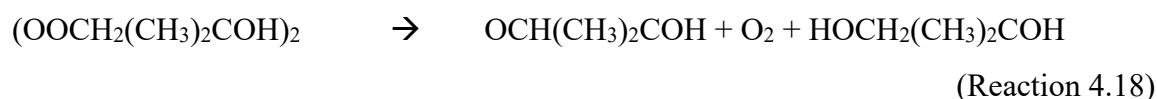
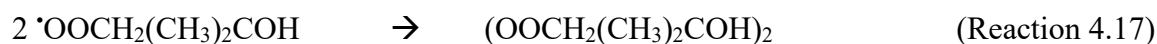
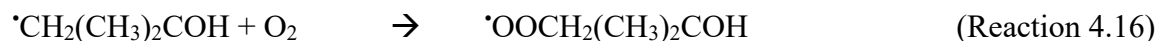
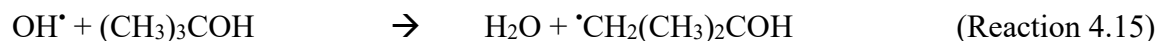


**Figure 4.12: Concentration of OH radicals plotted against ozone concentration at pH 11. OH radicals were determined by DMSO-method (see above).**

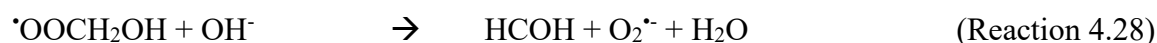
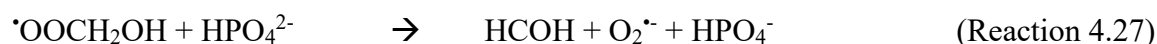


#### 4.5.4 Formation of superoxide

Source: *tert.*-Butanol ((CH<sub>3</sub>)<sub>3</sub>COH)



Source: Methanol (CH<sub>3</sub>OH)



## **5. Chapter: Reaction rate-dependent carbon isotope fractionation during ozonation of phenols**

**Adapted from:** Terhalle, J., Nikutta, S.E., Krzeczieska, D.L., Lutze, H.V., Jochmann, M.A., Schmidt, T.C., (2022), *Linking reaction rate constants and isotope fractionation of ozonation reactions using phenols as probes*. Water Research 210, 117931.

## 5.1 Introduction

Ozone (O<sub>3</sub>) is a powerful oxidant, which reacts rapidly with electron-rich moieties such as activated alkenes, amines and aromatic rings (von Gunten, 2003b). These moieties are commonly present in dissolved organic matter (DOM) and trace organic compounds (TrOCs) (Tentscher et al., 2018). However, full mineralization of TrOCs is seldomly achieved. Thus the formation of transformation by-products (TPs) is an essential issue in the application of O<sub>3</sub> for disinfection and abatement of TrOCs (von Sonntag and von Gunten, 2012). In many cases, TPs are more biodegradable and less toxic than their parent compound, but in some cases, they are even more toxic and environmentally harmful (Hübner et al., 2015, Knoop et al., 2018). A prominent case in point is the formation of nitrosamines in ozone applied wastewater treatment (von Gunten, 2018). Due to these possible adverse effects of ozonation, in-depth knowledge of the involved processes and reaction mechanism, especially about the formation of TPs is mandatory. In many cases, this cannot be done by product studies alone because on the one hand different reaction mechanisms may form the same TPs and on the other hand possible isobaric TPs cannot be distinguished or verified (Schmidt and Jochmann, 2012). In such cases, compound-specific isotope analysis (CSIA) can be applied as a complementary tool.

The measurement of isotopic fractionation of TrOCs can give insights into the reaction mechanisms as it allows distinguishing between different degradation processes of TrOCs (Maier et al., 2016, Elsner, 2010, Hunkeler et al., 2008). When using CSIA, the natural abundance isotope ratio of compounds is measured. During the course of a degradation reaction, the isotopic value changes and thus an isotopic fractionation can be observed. It has to be noted that during a reaction, the electronic structure of the molecule and the potential energy surfaces will not change and only the rate of the reaction is affected. Such an isotopic fractionation has its origin in different bond dissociation energies of the heavy and light isotopologues, involved. This difference in isotopologue energy results in differing reaction rates, which is called a kinetic isotope effect (KIE). For small molecules in which all isotopes are located in the same reactive position, the isotopic fractionation in terms of a fractionation factor  $\alpha_{\text{kin}}$  is directly related to the KIE by:

$$\alpha = \frac{l_k}{h_k} = \frac{1}{KIE} \quad (\text{Equation 5.1})$$

Where  $l_k$  is the rate constant of the light isotope and  $h_k$  that of the heavy, respectively. In cases, in which non-reacting positions and intramolecular competition have to be taken into account,

it is possible to estimate KIE from kinetic isotopic fractionation factors in terms of apparent kinetic isotope effects (AKIE). If  $k^L/k^H > 1$  we talk about a normal isotope effect, and in case of  $k^L/k^H < 1$  the isotope effect is inverse. In case of a carbon, normal isotope effect, the lighter isotope (e.g.,  $^{12}\text{C}$ ) reacts faster than the heavier isotope (e.g.,  $^{13}\text{C}$ ). Consequently, the ratio of  $^{13}\text{C}$  to  $^{12}\text{C}$  in the remaining compound fraction increases as the reaction proceeds (Elsner et al., 2005). Hence, CSIA is a tool that allows fostering the fundamental understanding of reaction mechanisms, which is important for predicting TPs. A case in point is the reaction of sulfamethoxazole (SMX) with  $\text{O}_3$ .  $\text{O}_3$  can attack SMX either at the aromatic ring or at the anilinic nitrogen. Products of these reactions would have the same exact masses and are difficult to distinguish by high-resolution mass spectrometry. However, by using CSIA, it could be shown that at pH 8,  $\text{O}_3$  presumably attacks at the nitrogen since no C-isotopic fractionation was observed. Additionally, there was a change in the mechanism at pH 3, as indicated by a significant C-isotopic fractionation (Willach et al., 2017). Furthermore, Maier et al. (2014) investigated the oxidation of diclofenac by different model systems.  $\text{O}_3$  can attack diclofenac at the secondary amine or the aromatic ring. They determined for ozonation an inverse nitrogen isotope fractionation and no significant isotope fractionation of carbon, although they found products for the attack at the aromatic ring (i.e., diclofenac-2,5-iminoquinone). The inverse nitrogen isotope fractionation confirmed the attack at the aromatic ring (Maier et al., 2014). SMX and diclofenac are compounds with more than one reactive position, which results in a complex system. Another study of Willach et al. (2020) investigated the ozonation of smaller compounds (benzene derivatives), which have only the aromatic ring as the point of attack. For benzene and some of its derivatives, an enrichment of the heavy carbon isotope in the reactions with  $\text{O}_3$  was found. These results show that the reaction of aromatic compounds with  $\text{O}_3$  may result in carbon isotopic fractionation (Willach et al., 2020). In the present study we used phenols as well-investigated probe compounds representing DOM. DOM in a typical concentration of  $10 \text{ mg L}^{-1}$  contains phenolic moieties at between  $10 - 13 \text{ }\mu\text{M}$ , which leads to these moieties being the main reaction partners of  $\text{O}_3$  in water treatment (Tentscher et al., 2018). Additionally, phenolic moieties are part of many TrOCs in natural water and wastewater effluents, but the concentration is typically much lower than in DOM (Tentscher et al., 2018, von Gunten, 2018). The reaction of phenol with  $\text{O}_3$  involves only carbon atoms. It has been investigated by many studies and a reaction mechanism has been postulated (Tentscher et al., 2018, Mvula and von Sonntag, 2003, Ramseier and von Gunten, 2009). The mechanism is described in Chapter 5.5.1.  $\text{O}_3$  reacts fast with the deprotonated phenol (referred as phenolate below) ( $k(\text{phenolate}) = 1.4 \times 10^9 \text{ M}^{-1} \text{ s}^{-1}$  (Mvula and von Sonntag, 2003)) and moderately with

protonated phenol (referred as phenol below) ( $k(\text{phenol}) = 1.3 \times 10^4 \text{ M}^{-1} \text{ s}^{-1}$  (Mvula and von Sonntag, 2003)), which results in a reaction with phenolate at a normal pH for drinking water treatment ( $\sim 7.5$ ). The aim of this study was to demonstrate for the first time as a proof of concept the correlation of ozone reaction kinetics with the extent of observed isotope fractionation. To that end, we systematically investigate the ozonation of phenol and phenols with electron-withdrawing and electron-donating substituents (4-chlorophenol (CPh), 4-methylphenol (MePh) and 4-methoxyphenol (MxPh)) by isotopic fractionation at different pH-values. Furthermore, the results of the phenols were compared with other electron-rich moieties (double bond (3-buten-2-ol) and triple bond (3-butyn-2-ol)).

## 5.2 Material and methods

### 5.2.1 Chemicals

All chemicals and solvents were used as received from the according supplier. A complete list of all chemicals used can be found in the Table 5.1.

### 5.2.2 Sample preparation for batch experiments

All samples were prepared in a similar procedure. The reaction solution consisted of the investigated compound (Table 5.3), phosphate buffer ( $1.0 \times 10^{-2} \text{ M}$ ; adjusted for different pH values) and, in the case of phenols, *tert.*-butanol (*tert.*-BuOH), which were placed in a 20-mL headspace vial at room temperature. The initial concentrations of the compounds are shown in Table 5.4. *Tert.*-BuOH was added in all experiments to scavenge  $\geq 95\%$  of the OH radicals, which may be formed in the reaction of the phenols with  $\text{O}_3$  since in this study, the focus is on the direct reaction of  $\text{O}_3$  with phenols. The concentration of *tert.*-BuOH is shown in Table 5.5 and was calculated by Equation 5.5 in Chapter 5.5. Only the experiments for 3-buten-2-ol and 3-butyn-2-ol were performed in the absence of the radical scavenger at  $\text{pH } 2.00 \pm 0.05$ . At this pH, the reaction of  $\text{O}_3$  with  $\text{H}_2\text{O}_2$ , which can be formed in the reaction of  $\text{O}_3$  with olefins and is the precursor for OH radicals, is slow ( $k_{\text{obs}}(\text{H}_2\text{O}_2 + \text{O}_3) = 1.09 \times 10^{-2} \text{ M}^{-1} \text{ s}^{-1}$ ) and can thus not interfere (von Sonntag and von Gunten, 2012). The reaction of phenol with  $\text{O}_3$  is pH-dependent. Phenolate ( $k(\text{O}_3 + \text{phenolate}) = 1.4 \times 10^9 \text{ M}^{-1} \text{ s}^{-1}$ ) reacts six orders of magnitude faster with  $\text{O}_3$  than phenol ( $k(\text{O}_3 + \text{phenol}) = 1.3 \times 10^3 \text{ M}^{-1} \text{ s}^{-1}$ ) (the fractions of species are shown in Figure 5.5) (von Gunten, 2003b). For that reason, the experiments for phenol were performed at pH 2.3, 3.2, 4.1, 4.9, 6.0, 7.2 and 10.2. The fraction of  $\text{O}_3$ , which reacts with the phenols, depends on the  $\text{p}K_{\text{a}}$  values and the species-specific reaction rate constants. These values for the

substituted phenols are shown in Figure 5.6., Figure 5.7 and Figure 5.8. Consequently, the investigated pH values for the substituted phenols were different. CPh was investigated at pH 2.0, 3.2, 7.0 and 11.0, MePh at pH 2.2, 5.3 7.0 and 12.0 and MxPh at pH 2.0 and 7.0. As all unsubstituted phenol samples were measured from the headspace, the sample volume of all samples was kept constant. O<sub>3</sub> is generated by BMT 802X from BMT Messtechnik (Berlin, Germany). For details, see Chapter 5.5.2. The reaction solutions were treated with six different dosages of O<sub>3</sub> (from  $2.0 \times 10^{-6}$  M to  $1.5 \times 10^{-3}$  M; O<sub>3</sub> concentrations of all individual samples are shown in Table 5.6). All samples were analyzed > 12 h after the experiment was performed. After this reaction time, O<sub>3</sub> was consumed entirely. Experiments were performed in triplicates at each dose. Before and after the experiments the pH values were controlled to make sure they were constant. If the change of pH was higher than 0.5 units, the samples were not considered for measurements and experiments were repeated. The calibration of each investigated compound was integrated into each measurement sequence. The isotopic fractionation of phenol, 3-buten-2-ol and 3-butyn-2-ol was measured by gas chromatography – isotope ratio mass spectrometer (see chapter 5.2.4.1). The isotope fractionation of CPh, MePh and MxPh was measured by liquid chromatography-IRMS (see chapter 5.2.4.2).

### 5.2.3 Determination of the second-order reaction rate constant of phenol-<sup>13</sup>C<sub>6</sub> with ozone

Competition kinetics was used to determine the reaction rate constant of phenol-<sup>13</sup>C<sub>6</sub> (all six carbon atoms are <sup>13</sup>C atoms) with O<sub>3</sub> according to “Method IV” of the SI of Dodd et al. (2006). In brief, a compound (competitor), which has a similar reaction rate constant as the compound under study, is added to the sample to yield approximately the same concentration as the compound under study. After the reaction with a substoichiometric concentration of O<sub>3</sub>, the concentration ratio of the two compounds is determined. This ratio is multiplied by the known reaction rate constant of the competitor. MePh (experiment A) and unlabeled phenol (phenol-<sup>12</sup>C) (experiment B) were used as competitors (two different experiments).

Experiment A: The reaction solution consisted of  $1 \times 10^{-5}$  M phenol-<sup>13</sup>C<sub>6</sub>,  $1 \times 10^{-5}$  M MePh,  $3 \times 10^{-2}$  M *tert.*-BuOH and  $1 \times 10^{-2}$  M phosphate buffer. The pH was adjusted to  $7.0 \pm 0.1$  and different concentrations of O<sub>3</sub> were added to the reaction system (Table 5.6). The concentrations of phenol-<sup>13</sup>C<sub>6</sub> and MePh were measured by high-pressure liquid chromatography coupled with UV detection (See chapter 5.2.4.4).

Experiment B: The reaction solution consisted of  $1 \times 10^{-4}$  M phenol-<sup>13</sup>C<sub>6</sub>,  $1 \times 10^{-4}$  M phenol-<sup>12</sup>C,  $3 \times 10^{-1}$  M *tert.*-BuOH and  $1 \times 10^{-2}$  M phosphate buffer. The pH was adjusted to  $2.3 \pm 0.1$

and  $7.0 \pm 0.1$  and different concentrations of  $O_3$  were added to the reaction system (Table S6 in SI). The concentrations of phenol- $^{13}C_6$  and phenol- $^{12}C$  were measured by gas chromatography coupled with a mass spectrometer (GC-MS, see chapter 5.2.4.3).

## 5.2.4 Analytical instrumentation and methods

### 5.2.4.1 Gas chromatography-isotope ratio mass spectrometry (GC-IRMS)

The GC-IRMS set-up is consist of Trace GC Ultra (Thermo Fisher Scientific, Oberhausen, Germany), HTC PAL autosampler (CTC analytics, Berlin, Germany) and Finnigan MAT 253 (Thermo Fisher Scientific). The GC and the IRMS is coupled with a GC-C/TC III interface (Thermo Fisher Scientific). To increase the signal in the chromatogram, a magnetic stirring bar and 2.5 g NaCl were added to each sample directly before the analysis. The salt enhances the transfer of the analytes to the headspace. Additionally, a solid-phase microextraction arrow (SPME arrow) was used to enrich the model compounds from the headspace (fiber phase: polyacrylate,  $df = 100 \mu m$ , needle size = 1.1 mm, CTC analytics). After an incubation time of 10 min ( $50 \text{ }^\circ C$ ), the compounds were extracted from the headspace for 10 min at  $50 \text{ }^\circ C$  and desorbed in the injector over 3 min at  $250 \text{ }^\circ C$ . Injection was carried out in splitless mode for 3 min. All analytes were separated on a Stabilwax-DA  $60 m \times 0.32 mm \times 1 \mu m$  column (Restek, Bellfonte, USA) with different GC temperature programs (Figure 5.9 - Figure 5.11) and a helium flow of  $2.4 mL \text{ min}^{-1}$ . After chromatographic separation, the column effluent was transformed into  $CO_2$  using a GC-C/TC III combustion interface. The operating temperatures of the oxidation reactors were  $940 \text{ }^\circ C$ . The  $CO_2$  was analyzed with a Finnigan MAT 253 IRMS, scanning for the masses 44, 45 and 46 with two reference peaks at the beginning of the run (with open split).  $\delta^{13}C$  values of reactants were normalized to the international VPDB scale using a two point normalization relative to the international reference standards IAEA- $CH_6$  (Sucrose,  $\delta^{13}C = -10.45 \text{ } \text{‰}$ ) and IAEA-600 (Caffeine,  $\delta^{13}C = -27.77 \text{ } \text{‰}$ ) (both IAEA, Vienna, Austria) with certified  $\delta^{13}C$  values by EA-IRMS measurements.

### 5.2.4.2 Liquid chromatography-isotope ratio mass spectrometry (LC-IRMS)

The separation of the substituted phenols from *tert.*-BuOH was performed with ultrapure water, which was acidified by  $H_2SO_4$  to a pH of 4.4, on a Zirchrom  $5 \mu m$  PBD column ( $150 \times 3.0 mm$ ) (Thermo Fisher Scientific, Oberhausen, Germany) at  $30 \text{ }^\circ C$ . The flow rate of the eluent was  $0.3 mL \text{ min}^{-1}$  for CPh and MxPh and  $0.15 mL \text{ min}^{-1}$  for MePh (Dionex Ultimate 300 HPLC System, Thermo Fisher Scientific). After chromatographic separation, the column effluent was mixed in LC IsoLink interface (Thermo Fisher Scientific) with  $30 \mu L \text{ min}^{-1}$  of 1.5 M *ortho*-phosphoric

acid and 30  $\mu\text{L min}^{-1}$  of 0.84 M sodium peroxodisulfate in the oxidation reactor at 99.9  $^{\circ}\text{C}$ . After passing the gas separation unit, the generated  $\text{CO}_2$  was transferred by a helium stream at a flow rate of 1.2  $\text{mL min}^{-1}$  to the open split of the Delta-V Advantage IRMS (Thermo Fisher Scientific). At the start of the measurement, the split remained closed for 500 seconds, to cut out *tert.*-BuOH to extend filament lifetime. Three reference peaks were applied at the beginning of the run (with open split) and three peaks at the end (with closed split). The  $\delta^{13}\text{C}$  values were normalized to the international VPDB scale using a two point normalization relative to the international reference standards IAEA-CH<sub>6</sub> (Sucrose,  $\delta^{13}\text{C} = -10.45 \text{ ‰}$ ) and IAEA-600 (Caffeine,  $\delta^{13}\text{C} = -27.77 \text{ ‰}$ ) (both IAEA, Vienna, Austria) with certified  $\delta^{13}\text{C}$  values.

#### 5.2.4.3 Gas chromatography-mass spectrometry (GC-MS)

The sample preparation and GC temperature program was the same as for GC-IRMS (Figure 5.11) excepted the carrier gas was hydrogen and the flow was 1.5  $\text{mL min}^{-1}$ . After separation, phenols (phenol- $^{13}\text{C}_6$  and phenol- $^{12}\text{C}$ ) were detected with a Finnigan PolarisQ – ion trap mass spectrometer (Thermo Fisher Scientific). MS scan modes were: full scan (24 ms) in the mass range 50 - 110  $\text{g mol}^{-1}$ ; selected ion monitoring (SIM) (38 ms) in the mass range  $94 \pm 2 \text{ g mol}^{-1}$  and SIM (38 ms) in the mass range  $100 \pm 2 \text{ g mol}^{-1}$ .

#### 5.2.4.4 High-pressure liquid chromatography-UV (HPLC-UV)

Phenol and MePh were separated with a Kinetex C18 column (150 x 30 mm, particle size 5  $\mu\text{m}$ ) (Phenomenex, Aschaffenburg, Germany) with an isocratic eluent flow of 0.5  $\text{mL min}^{-1}$  of an eluent composed of 75% water pH 2 (acidified with hydrochloric acid) and 25% acetonitrile. The injection volume was 50  $\mu\text{L}$  and the absorption at 270 nm was determined.

#### 5.2.5 Calculation of the enrichment factor

The IRMS determined the ratio of the heavy isotopes to lighter isotopes (R). R of the compounds was compared to the R of the international reference material, VPDB, and resulted in the delta value ( $\delta^{13}\text{C}$ , Equation 5.2). (Schmidt and Jochmann, 2012)

$$\delta^{13}\text{C} = \left( \frac{R_{phenol} - R_{VPDB}}{R_{VPDB}} \right) \quad (\text{Equation 5.2})$$

Using the Rayleigh equation (Equation 5.3), the enrichment factor ( $\epsilon$ ) is calculated (Schmidt and Jochmann, 2012).

$$\ln \left( \frac{1 + \delta^{13}\text{C}}{1 + \delta^{13}\text{C}_0} \right) = \epsilon \cdot \ln \left( \frac{c}{c_0} \right) \quad (\text{Equation 5.3})$$



with  $\delta^{13}\text{C}_0$  as the delta value of phenols without adding  $\text{O}_3$  and  $c$  as the concentration of phenols ( $c_0 =$  without  $\text{O}_3$  dosage). Here  $\varepsilon$  is determined as the slope of a Rayleigh plot and as usual expressed in permil (Figure 5.12 - Figure 5.15). The uncertainty of  $\varepsilon$  is the 95% confidence interval of the slope. In this study, the enrichment factor is used and not the apparent kinetic isotope effect (AKIE). For the AKIE the point of attack and the number of similar reactive positions were necessary (Willach et al., 2020). This information is not clear for the reaction of ozone with phenols.

### 5.3 Results and discussion

The reported reaction mechanism of  $\text{O}_3$  with phenol by Mvula and von Sonntag (2003) shows that  $\text{O}_3$  reacts with carbon atoms of the aromatic ring, preferring the addition reaction at the *para*- or *ortho*-position. Therefore, a significant isotopic effect of carbon was expected. To determine this isotopic effect for phenol, three different approaches were investigated. Two of them used an established method based on a comparison of isotope-labeled phenol with unlabeled phenol. The natural isotope abundance of  $^{13}\text{C}$  is  $\sim 1.1\%$ , so the enrichment effect of  $^{13}\text{C}$  is in a very small range. Therefore, a completely labeled phenol was used to ensure that the heavy  $^{13}\text{C}$  is present at the reaction site, which increases the measured effect. Isotope labelling approaches are commonly used for the investigation of reaction mechanisms and pathways, which need standard analytical equipment (GC-MS and LC-UV). For example, it has been used successfully for the investigation of persulfate-based oxidation of cyclohexane. In the third approach, the natural isotope abundance was determined by CSIA which requires the use of an IRMS.

The first approach was the determination of the reaction rate constant of phenol- $^{13}\text{C}_6$  and unlabeled phenol by competition kinetics. As a competitor, MePh was used because of having a comparable reaction rate constant ( $k_{\text{obs}}(\text{MePh} + \text{O}_3) = 1.6 \times 10^6 \text{ M}^{-1} \text{ s}^{-1}$  at pH 7 (Tentscher et al., 2018)). The determined reaction rate constants are shown in Figure 5.1A. However, the difference between the mean values of triplicates was not significant. The deviation of triplicates of the determined reaction rate constants ranged from 0.22% to 12%. Consequently, with this approach the determination of isotopic fractionation is not possible.

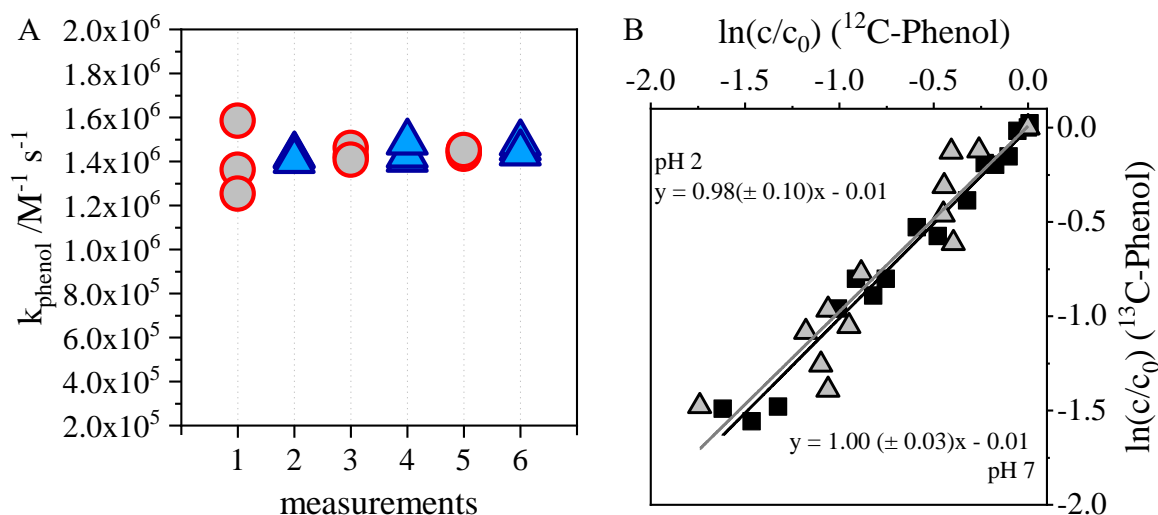


**Figure 5.1:** A) Reaction rate constants of phenol with ozone in the presence of *tert.*-BuOH at pH 7. Determined by competition kinetics method with 4-methylphenol as a competitor (red circles: unlabeled phenol, blue triangles: fully  $^{13}\text{C}$ -labeled phenol ( $c_0(\text{phenol}) = 10 \mu\text{M}$ ,  $c_0(4\text{-methylphenol}) = 10 \mu\text{M}$ ,  $c(\text{O}_3) = 0 - 60 \mu\text{M}$ ,  $c(\text{phosphate buffer}) = 10 \text{mM}$ ,  $c(\text{tert.}-\text{BuOH}) = 30 \text{mM}$ ; the concentrations of phenol and 4-methylphenol were determined by HPLC-UV). B) Comparison of  $^{13}\text{C}_6$ -labeled phenol with unlabeled phenol at pH 2 (grey) and at pH 7 (black) ( $c_0(^{13}\text{C}\text{-phenol}) = 100 \mu\text{M}$ ,  $c_0(^{12}\text{C}\text{-phenol}) = 100 \mu\text{M}$ ,  $c(\text{O}_3) = 0 - 600 \mu\text{M}$ ;  $c(\text{phosphate buffer}) = 10 \text{mM}$ ;  $c(\text{tert.}-\text{BuOH}) = 300 \text{mM}$ ; concentrations of both phenols were determined by GC-MS).

Second, a direct comparison of unlabeled phenol with phenol- $^{13}\text{C}_6$  was done, where both compounds were degraded with  $\text{O}_3$  in the same sample. It was expected that the lighter phenol (unlabeled phenol) would be faster degraded than the heavier phenol (phenol  $^{13}\text{C}_6$ ). However, the difference again was not significant (Figure 5.1B, black squares, pH 7). Hence, both phenols reacted at the same nominal rate with  $\text{O}_3$  (slope of  $1.00 \pm 0.03$ ). This can be explained by the high reaction rate of the phenolate species, which is close to the diffusion-controlled limit. The reaction rate constant of phenol is slower than the phenolate, and it is conceivable that an isotope effect may be more pronounced. Therefore, the same approach was performed at a pH of  $2.0 \pm 0.1$ . At this pH, only phenol reacted with  $\text{O}_3$ . However, the slope was  $0.98 \pm 0.10$  (Figure 5.1B, grey triangles, pH 2), so the isotope fractionation could not be discerned by this approach, too. In conclusion, with standard analytical equipment and methods, the determination of the isotopic fractionation of the ozonation of phenols was not possible.

The third approach used CSIA to determine the change of the isotopic ratio. To this end, all further experiments were analyzed by GC-IRMS (phenol and olefins) or LC-IRMS (substituted phenols). In Figure 5.2A the change of  $\delta^{13}\text{C}$  at different  $\text{O}_3$  dosages at a range of pH values for unsubstituted phenol is shown. For pH 7.2 and 10.3, no significant change of  $\delta^{13}\text{C}$  of phenol

with  $O_3$  was detectable ( $\Delta\delta^{13}C \leq 0.5\text{‰}$ ) (turnover of phenol was  $> 60\%$ , which shows that the degradation happened (Figure 5.16)). With decreasing pH, the change of  $\delta^{13}C$  becomes more pronounced (pH 2.3:  $\Delta\delta^{13}C = 6.7\text{‰}$ , normal isotope effect).

The calculated  $\epsilon$  values for all pH values are shown in Figure 5.2B. With decreasing pH, the absolute value of  $\epsilon$  increases. These results suggest that ozonation of the two phenol species involves different isotopic enrichment and therefore, different rate-limiting steps in their reaction mechanism could be possible. I.e., phenol has an  $\epsilon$  of about  $-5.2 \pm 0.3\text{‰}$  while phenolate has no significant  $\epsilon$ . This difference can be explained by the different reaction kinetics of the two species. Phenol reacts with a reaction rate of about  $1.3 \times 10^4 \text{ M}^{-1} \text{ s}^{-1}$ , while phenolate has a rate close to the diffusion limit ( $10^9 \text{ M}^{-1} \text{ s}^{-1}$ ) (Mvula and von Sonntag, 2003). Hence, in the case of phenolate, any kinetic discrimination of heavy isotope bearing molecules becomes insignificant.

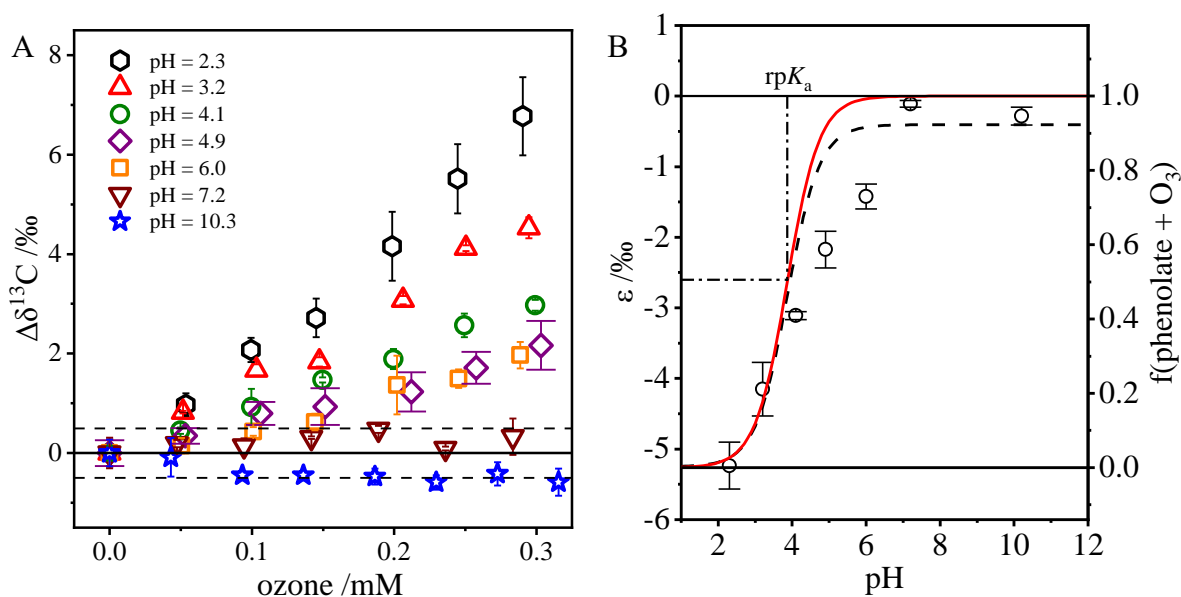


**Figure 5.2:** A) Change of the  $\delta^{13}C$ -value during the reaction of phenol with ozone in the presence of *tert.*-butanol plotted vs the ozone concentration at different pH values (the measured value of the sample without ozone was set to zero; Rayleigh plots are shown in SI) B) Enrichment factor ( $\epsilon$ ) at different pH values for the reaction of phenol with ozone in the presence of *tert.*-butanol. The dashed line represents the  $\epsilon$  calculated with Equation 5.4 and has a deviation of 3‰ to the determined values. The red line represents the fraction of ozone that reacts with phenolate.  $rpK_a$  marked the reactivity  $pK_a$  of the reaction of phenol with  $O_3$  ( $c_0(\text{phenol}) = 0.15 \text{ mM}$ ,  $c_0(\text{tert.-BuOH}) = 125 \text{ mM}$ ,  $c(\text{ozone}) = 0.05 - 0.30 \text{ mM}$  and  $c(\text{phosphate buffer}) = 10 \text{ mM}$ . The isotope ratio of phenol was measured by GC-IRMS, mean values of the triplicates are presented).

A similar effect was reported by Joe-Wong and Maher (2020). They showed that a faster redox reaction (i.e., electron transfer) induces less kinetic isotope fractionation. (Joe-Wong and Maher, 2020) However, in the case of phenol,  $\epsilon$  was significant since  $k$  is way below the diffusion-controlled reaction rate. The lower the pH, the higher the fraction of phenol that is involved in  $O_3$  reactions. At pH 7.2, more than 99% of  $O_3$  react with phenolate ( $f_{O_3, \text{phenolate}} > 0.99$ ) but at pH 2.3, 97% of  $O_3$  react with phenol ( $f_{O_3, \text{phenolate}} = 0.03$ ). At the reactivity  $pK_a$  (3.87),  $f_{O_3, \text{phenolate}}$  is 0.50, and indeed the  $\epsilon$  is the average of the two species ( $\epsilon \sim 2.6\text{‰}$ ).

With this approach, a model calculation is possible, and  $\epsilon$  for each pH could be calculated ( $\epsilon_{\text{obs}}$ ) (Equation 5.4).

$$\epsilon_{\text{obs}} = \frac{1}{1 + \frac{10^{-rpK_a}}{10^{-pH}}} \cdot \epsilon_{AH} + 1 - \frac{1}{1 + \frac{10^{-rpK_a}}{10^{-pH}}} \cdot \epsilon_{A-} \quad (\text{Equation 5.4})$$

with  $\epsilon_{AH}$  as the  $\epsilon$  of the protonated species and  $\epsilon_{A-}$  as the  $\epsilon$  of the deprotonated species. Additionally,  $rpK_a$  represents the reactivity  $pK_a$  of the substance with  $O_3$ .

The dashed curve in Figure 5.2B was calculated by applying Equation 5.4 for phenol and is very similar to the red curve indicating the fraction of  $O_3$  reacting with phenolate. These results suggest that the faster a reaction of ozone becomes, the less pronounced is the isotopic fractionation. Additionally, substituents on the aromatic ring of phenol change the electron density of the ring. Electron-withdrawing substituents (e.g., Cl) decrease the electron density of the ring and result in a lower reaction rate constant with  $O_3$  (von Sonntag and von Gunten, 2012). On the contrary, electron-donating substituents (e.g.,  $-CH_3$  or  $-OCH_3$ ) increase the electron density and activate the ring resulting in a higher reaction rate constant with  $O_3$  (Hoigné and Bader, 1983a). Consequently, the reaction rate constants of the protonated species with  $O_3$  increase in the order CPh, phenol, MePh and MxPh ( $k(\text{CPh} + O_3) = 6 \times 10^2 \text{ M}^{-1} \text{ s}^{-1}$ ;  $k(\text{phenol} + O_3) = 1.3 \times 10^3 \text{ M}^{-1} \text{ s}^{-1}$ ;  $k(\text{MePh} + O_3) = 3 \times 10^4 \text{ M}^{-1} \text{ s}^{-1}$ ;  $k(\text{MxPh} + O_3) = 4.7 \times 10^5 \text{ M}^{-1} \text{ s}^{-1*}$ ) (Tentscher et al., 2018). The deprotonated species of the four compounds react all very fast with  $O_3$ , and the difference among the four compounds becomes much smaller than for the protonated species ( $k(\text{CPh} + O_3) = 6 \times 10^8 \text{ M}^{-1} \text{ s}^{-1}$ ;  $k(\text{phenolate} + O_3) = 1.4 \times 10^9 \text{ M}^{-1} \text{ s}^{-1}$ ;  $k(\text{MePh} + O_3) = 3.2 \times 10^9 \text{ M}^{-1} \text{ s}^{-1*}$ ;  $k(\text{MxPh} + O_3) = 1.1 \times 10^{10} \text{ M}^{-1} \text{ s}^{-1*}$ ) (Tentscher et al., 2018). Note that some of the listed values are experimental data taken from literature. Others were estimated with quantum chemical calculations. The latter are marked with an asterisk above.

All determined  $^{13}\text{C}$  enrichment factors plotted vs the observed reaction rate constants ( $k_{\text{obs}}$ ) for the investigated phenols and further data from other studies (Maier et al., 2016, Willach et al., 2017, Willach et al., 2020) on ozonation of aromatic rings are collectively shown in Figure 5.3. In Figure 5.3, reaction rate constants can be organized in three groups, which are highlighted with the colors green, orange, and red. The green color marks a group of reaction rate constants, which hardly show a correlation of reaction kinetics vs enrichment factor. This zone comprises compounds with reaction rate constants lower than  $10^3 \text{ M}^{-1} \text{ s}^{-1}$ , which also exhibit the highest isotope enrichment amongst the investigated compounds. Divergent is only anisole and phenol at  $\text{pH} < 2.3$ . With reaction kinetics in the range of  $10^3$  to  $10^5 \text{ M}^{-1} \text{ s}^{-1}$  (orange group), the isotope fractionation decreases with increasing reaction rate constant. Reactions of aromatic compounds with ozone with reaction rate constants faster than  $10^5 \text{ M}^{-1} \text{ s}^{-1}$  do not display a significant enrichment of  $^{13}\text{C}$  in the remaining compound anymore (red group).

The concept developed above correlating  $\epsilon$  and reaction kinetics in ozone reactions is well supported by the compiled data from literature shown in Figure 5.3. Benzene and its derivatives have reaction rate constants lower than  $10^3 \text{ M}^{-1} \text{ s}^{-1}$  and a similar enrichment factor ( $-4.6$  -  $-3.7\%$ ) (Willach et al., 2020). SMX reacts faster with  $\text{O}_3$  ( $4.8 \times 10^4 \text{ M}^{-1} \text{ s}^{-1}$  at  $\text{pH} 3$ ) and shows a smaller enrichment of  $^{13}\text{C}$  ( $-2.2 \pm 0.1\%$ ) (Willach et al., 2017). In the case of diclofenac, no significant  $^{13}\text{C}$ -enrichment was determined because the reaction rate constant with  $\text{O}_3$  is higher than  $10^5 \text{ M}^{-1} \text{ s}^{-1}$  ( $6.8 \times 10^5 \text{ M}^{-1} \text{ s}^{-1}$ ), which explains the finding in the study of Maier et al. (2016).

The reaction centers of 3-buten-2-ol and 3-butyn-2-ol (C-C double and triple bond) react in the same order of magnitude with  $\text{O}_3$  ( $10^4 \text{ M}^{-1} \text{ s}^{-1}$ ) and also have the same enrichment factor ( $\epsilon(3\text{-buten-2-ol}) = -5.9 \pm 0.5\%$ ;  $\epsilon(3\text{-butyn-2-ol}) = -5.9 \pm 0.4\%$ ). These values do not fit into the concept shown above. Although the reaction rate constant is higher than  $10^3 \text{ M}^{-1} \text{ s}^{-1}$ , the enrichment factor is more negative than for the protonated phenol ( $-5.2 \pm 0.3\%$ ). These results show that there is a difference in the reaction of aromatic compounds and olefinic compounds that could be explained by a change in reaction mechanism to electron transfer for the aromatics. However, this point surely needs a more thorough investigation. On the other hand, the same enrichment factor for 3-buten-2-ol and 3-butyn-2-ol implies the same rate-limiting step in the reaction with  $\text{O}_3$ . For 3-buten-2-ol monodentate addition of  $\text{O}_3$  to the double bond has been shown (Dowideit and von Sonntag, 1998). For 3-butyn-2-ol no experimental evidence is yet available but a quantum mechanical calculation suggested the same reaction mechanism (Cremer et al., 2001). This is consistent with the here presented data on isotope enrichment in the rate-limiting step.

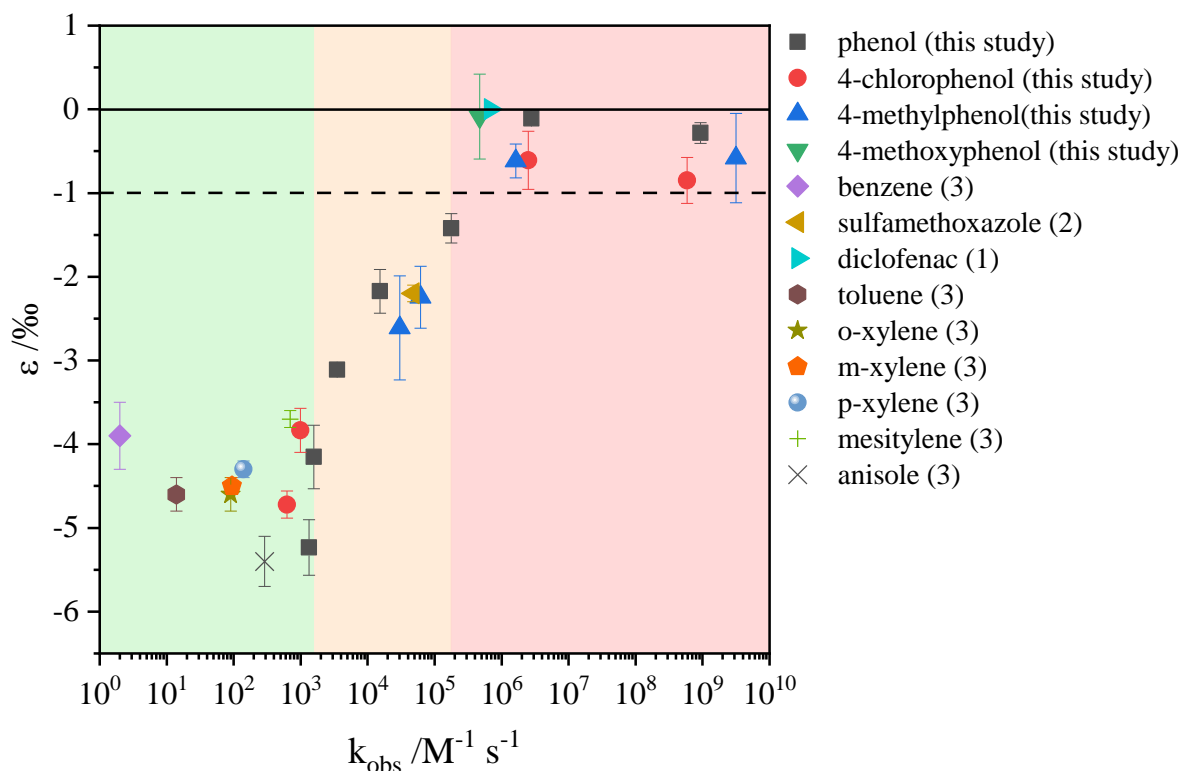


**Figure 5.3:** Enrichment factors plotted against observed reaction rate constants of all compounds under study with ozone in presence of *tert*-BuOH in comparison to literature data ((1)Maier et al. (2016), (2)Willach et al. (2020) (3)Willach et al. (2017)). Experimental conditions for phenol:  $c_0(\text{phenol}) = 0.15 \text{ mM}$ ,  $c_0(\text{tert.-BuOH}) = 125 \text{ mM}$ ,  $c(\text{ozone}) = 0.05 - 0.30 \text{ mM}$  and  $c(\text{phosphate buffer}) = 10 \text{ mM}$ . For 4-chlorophenol:  $c_0(4\text{-chlorophenol}) = 0.50 \text{ mM}$ ,  $c_0(\text{tert.-BuOH}) = 125 \text{ mM}$ ,  $c(\text{ozone}) = 0.15 - 0.90 \text{ mM}$ ,  $c(\text{phosphate buffer}) = 10 \text{ mM}$ . For 4-methylphenol:  $c_0(4\text{-methylphenol}) = 0.50 \text{ mM}$ ,  $c_0(\text{tert.-BuOH}) = 195 \text{ mM}$ ,  $c(\text{ozone}) = 0.15 - 0.90 \text{ mM}$ ,  $c(\text{phosphate buffer}) = 10 \text{ mM}$ . For 4-methoxyphenol:  $c_0(4\text{-methoxyphenol}) = 0.50 \text{ mM}$ ,  $c_0(\text{tert.-BuOH}) = 195 \text{ mM}$ ,  $c(\text{ozone}) = 0.15 - 0.90 \text{ mM}$ ,  $c(\text{phosphate buffer}) = 10 \text{ mM}$ . The isotope ratios of phenol were measured by GC-IRMS and of 4-chlorophenol, 4-methylphenol and 4-methoxyphenol were measured by LC-IRMS.

## 5.4 Conclusions

The enrichment factor of the reaction of phenols with  $\text{O}_3$  depends on the pH value and, therefore, on their speciation. This result underlines the importance of pH for oxidative transformation of TrOCs. At the current point, it is impossible to disentangle with the shown data if with the shifting speciation a change in reaction mechanism occurs. The enrichment factor can be correlated with the ratio of reaction rate constants for the two species (e.g., phenolate reacts six orders of magnitude faster than phenol). The faster a reaction of  $\text{O}_3$  is, the less pronounced the isotopic fractionation becomes. In this study, a limit of reaction rate constant for determination of isotopic fractionation of aromatic compound was observed at

about  $10^5 \text{ M}^{-1} \text{ s}^{-1}$ . Above this limit, the difference between the reaction of  $\text{O}_3$  with the heavy isotope and the light isotope cannot be measured by the presented approach. At rate constants below  $10^3 \text{ M}^{-1} \text{ s}^{-1}$  a distinct but rather constant isotope enrichment factor was observed. Overall, this information could be used to test experimentally determined rate constants for plausibility. Furthermore, following the work of Willach et al. (2020), stable isotope analysis may also be used to test for the relevance of direct ozonation vs. OH-radical based reactions since the latter do not show a measureable isotope fractionation in the reaction with aromatic compounds. (Willach et al., 2020) This is of the utmost importance in the investigation and use of oxidative processes commonly used in water treatment. However, to reinforce the introduced concept, further studies of the reaction of  $\text{O}_3$  with a larger set of aromatic model compounds are necessary. These studies should also include stable isotope analysis of other elements than carbon in a dual-isotope approach that may allow further mechanistic insights into this important reaction in water treatment.

## 5.5 Supporting Information

### 5.5.1 Reaction pathways of phenol with ozone

The reaction of phenol with  $\text{O}_3$  was investigated in many studies (Tentscher et al., 2018, Mvula and von Sonntag, 2003, Ramseier and von Gunten, 2009). The focus of the studies was the determination of the formation of TPs (e.g. p-benzoquinone, hydroquinone and catechol) and stoichiometry. However, the mass balance of this reaction was not closed. The reaction mechanism is postulated by Mvula and von Sonntag (2003).  $\text{O}_3$  react fast with the deprotonated phenol ( $k(\text{phenolate}) = 1.4 \times 10^9 \text{ M}^{-1} \text{ s}^{-1}$ ) and moderate with the phenol ( $k(\text{phenol}) = 1.3 \times 10^4 \text{ M}^{-1} \text{ s}^{-1}$ ). At normal pH for the drinking water treatment ( $\sim 7.5$ ),  $\text{O}_3$  reacts with phenolate. The monodentate attack of ozone at the aromatic ring leading to adduct formation (Figure 5.4). This attack can happen at the *para*- and *ortho*-position (1. reaction and 2. reaction in Figure 5.4). Additionally, an electron transfer reaction can take place with the formation of an ozonide radical and phenoxy radical (3. reaction in Figure 5.4). All intermediates (adduct and radicals) react further to the stable products such p-benzoquinone, hydroquinone, catechol or *cis,cis*-muconic. For the degradation of one mol phenol, two to three mol of ozone are necessary.

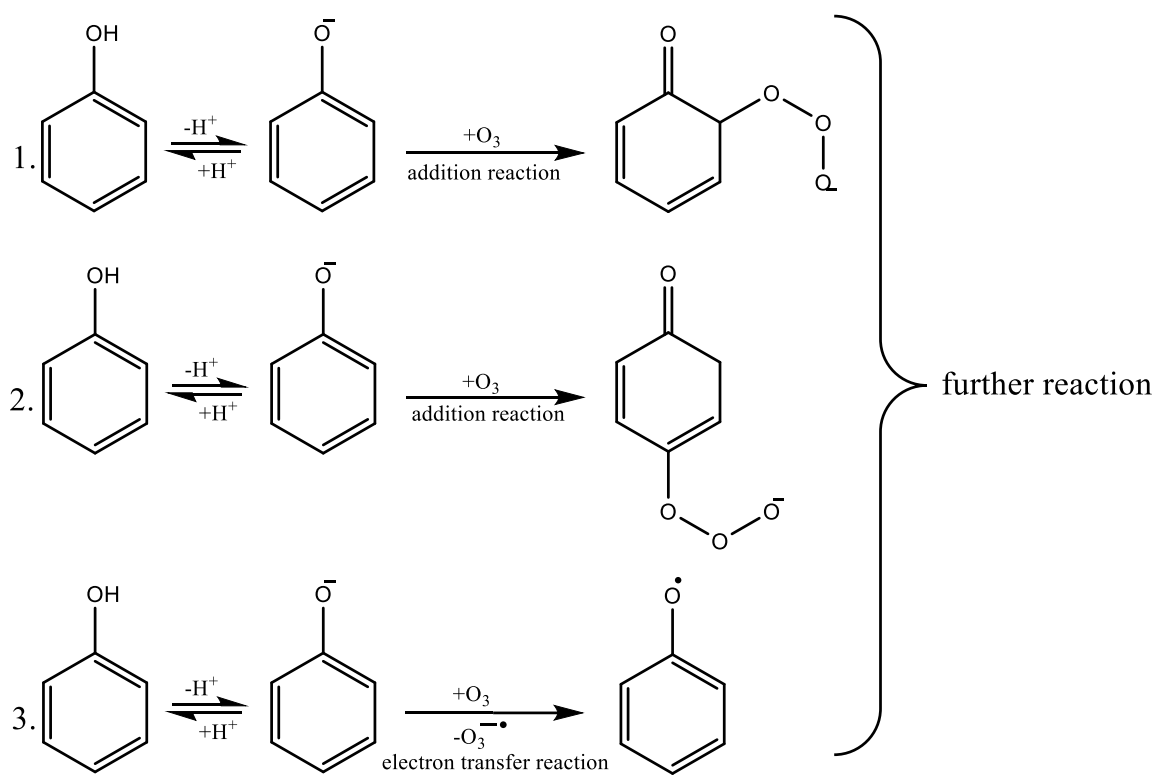


**Figure 5.4:** Reaction pathways of phenol with ozone (modified from Mvula and von Sonntag (2003)).



5. Chapter: Reaction rate dependent carbon isotope fractionation during ozonation of phenols

**Table 5.1: Chemicals used in Chapter 5.**

Substance	Structural formula	Purity	Manufacturer
phenol ( $pK_a = 9.98$ )	$C_6H_5OH$	99 %	Merck (Darmstadt, Germany)
phenol- $^{13}C_6$ ( $pK_a = 9.98$ )	$^{13}C_6H_5OH$	99%	Merck
4-methylphenol ( $pK_a = 10.3$ )	$C_6H_4OHCH_3$	$\geq 99\%$	Merck
4-chlorphenol ( $pK_a = 9.38$ )	$C_6H_4OHCl$	$\geq 99\%$	Merck
4-methoxyphenol ( $pK_a = 10.21$ )	$C_6H_4OHCH_3$	$\geq 98.5\%$	Merck
3-buten-2-ol	$C_4H_7OH$	97 %	Alfa Aesar (Kandel, Germany)
3-butyn-2-ol	$C_4H_5OH$	98 %	Alfa Aesar
sodium chloride	$NaCl$	99.5 %	Bernd Kraft (Duisburg, Germany)
sodium hydroxide	$NaOH$	99 %	VWR Chemicals (Langenfeld, Germany)
dipotassium hydrogen phosphate	$K_2HPO_4$	$\geq 99\%$	AppliChem (Steinheim, Germany)
sodium dihydrogen phosphate	$NaH_2PO_4$	$\geq 99\%$	AppliChem
<i>ortho</i> -phosphoric acid	$H_3PO_4$	85 % p. a.	AppliChem
<i>tert.</i> -butanol	$C_4H_9OH$	$\geq 99.5\%$	Merck
helium gas	He	1.0	Air Liquide (Düsseldorf, Germany)
carbon dioxide	$CO_2$	N45	Air Liquide
oxygen gas	$O_2$	1.0	Air Liquide

**Table 5.2: Used equipment**

Name	Components	Description	Manufacturer
HPLC/UV	Pump	LC-20AT	Shimadzu  (Duisburg, Germany)
	UV/VIS-detector	SPD-20A	Shimadzu
	Autosampler	SIL-20A	Shimadzu
	Software	LabSolutions  (Version 1.25 SP4)	Shimadzu
	Column oven	CTO-10AS	Shimadzu
	Column	Kinetex C18 column (150 x 30 mm, particle size 5 µm)	Phenomenex  (Aschaffenburg, Germany)
	Communication element	CBM-20A	Shimadzu
	Degasser	DGU-20A <sub>5</sub>	Shimadzu
SPME-arrow-GC-IRMS	Autosampler	HTC PAL autosampler	CTC analytics  (Berlin, Germany)
	Software	Cycle Composer Version 1.6.0	CTC analytics
	Fiber	SPME Arrow 1.1 mm  Polyacrylate 100 µm	CTC analytics
	GC	Trace GC Ultra	Thermo Fisher Scientific  (Oberhausen, Germany)

5. Chapter: Reaction rate dependent carbon isotope fractionation during ozonation of phenols

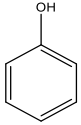
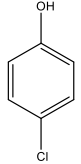
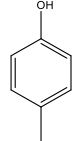
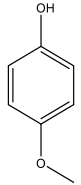
	Column	Stabilwax-DA 60 m × 0.32 mm × 1 μm	Restek  (Bellfonte, USA)
	Interface	GC-C/TC III	Thermo Fisher Scientific
	IRMS	Finnigan MAT 253	Thermo Fisher Scientific
	Software	Isodat 3.0	Thermo Fisher Scientific
SPME-arrow-GC-MS	Autosampler	HTC PAL autosampler	CTC analytics
	PAL-Software	Cycle Composer Version 1.6.0	CTC analytics
	Fiber	SPME Arrow 1.1 mm Polyacrylate 100 μm	CTC analytics
	GC	Trace GC Ultra	Thermo Fisher Scientific
	Column	Stabilwax-DA 60 m × 0.32 mm × 1 μm	Restek
	MS	Finnigan Polaris Q	Thermo Fisher Scientific
	GC-Software	Xcalibur	Thermo Fisher Scientific
LC-IRMS	HPLC System	Dionex Ultimate 3000	Thermo Fisher Scientific
	Software	Isodate 3.0	Thermo Fisher Scientific
	Column oven	HT HPLC 200	Thermo Fisher Scientific
	Column	Zirchrom 5 μm PBD 150×3.0 mm	Thermo Fisher Scientific
	Interface	LC IsoLink	Thermo Fisher Scientific
	Detector	DELTA-V Advantage IRMS	Thermo Fisher Scientific

## 5. Chapter: Reaction rate dependent carbon isotope fractionation during ozonation of phenols

---

Balance			Sartorius
pH meter	827 pH		Metrohm
O <sub>3</sub> generator	BMT 802X		BMT Messtechnik (Berlin, Germany)
ultrapure water generator	Purelab ultra		ELGA (Celle, Germany)

**Table 5.3: Structure, reaction rate constants and p*K*<sub>a</sub> values of the compounds under study (Values from Tentscher et al. (2018)).**

Name		<i>k</i> (neutral species with ozone) / M <sup>-1</sup> s <sup>-1</sup>	<i>k</i> (anionic species with ozone) / M <sup>-1</sup> s <sup>-1</sup>	p <i>K</i> <sub>a</sub>	rp <i>K</i> <sub>a</sub>
phenol		1.3 × 10 <sup>3</sup>	1.4 × 10 <sup>9</sup>	9.98	3.9
4-chlorophenol		6.0 × 10 <sup>2</sup>	6.0 × 10 <sup>8</sup>	9.38	3.2
4-methylphenol		3.0 × 10 <sup>4</sup>	3.2 × 10 <sup>9</sup>	10.3	5.3
4-methoxyphenol		4.7 × 10 <sup>5</sup>	1.1 × 10 <sup>10</sup>	10.21	5.8

**Table 5.4: Start concentration of the compounds at the different experiments (GC-IRMS and LC-IRMS: Isotopic fractionation; GC-MS: Competitions kinetic for labelled phenol; LC-UV: Competition kinetic for 4-methylphenol; 4-chlorophenol (CPh), 4-methylphenol (MePh); 4-methoxyphenol (MxPh)).**

Instrument	Phenol [mM]	3-buten-2-ol [mM]	3-butyn-2-ol [mM]	CPh [mM]	MePh [mM]	MxPh [mM]
GC-IRMS	0.15	1.00	1.00	----	----	----
LC-IRMS	----	----	----	0.50	0.50	0.50
GC-MS	0.10	----	----	----	----	----
LC-UV	0.01	----	----	----	----	----

**Table 5.5: Concentration of *tert.*-BuOH in the different experiments (GC-IRMS and LC-IRMS: Isotopic fractionation; GC-MS: Competitions kinetic for labelled phenol; LC-UV: Competition kinetic for 4-methylphenol; CPh = 4-chlorophenol; MePh = 4-methylphenol; MxPh = 4-methoxyphenol).**

Instrument	Phenol [mM]	3-buten-2-ol [mM]	3-butyn-2-ol [mM]	CPh [mM]	MePh [mM]	MxPh [mM]
GC-IRMS	0.125	----	----	----	----	----
LC-IRMS	----	----	----	0.125	0.195	0.195
GC-MS	0.300	----	----	----	----	----
LC-UV	0.030	----	----	----	----	----

$$[tert - BuOH]_{min} = \frac{f_{tert-BuOH+OH} \times k_{phenol+OH} \times [Phenol] + f_{tert-BuOH+OH} \times k_{O_3+OH} \times [ozone]}{k_{tert-BuOH+OH} \times (1 - f_{tert-BuOH+OH})} \quad (\text{Equation 5.5})$$

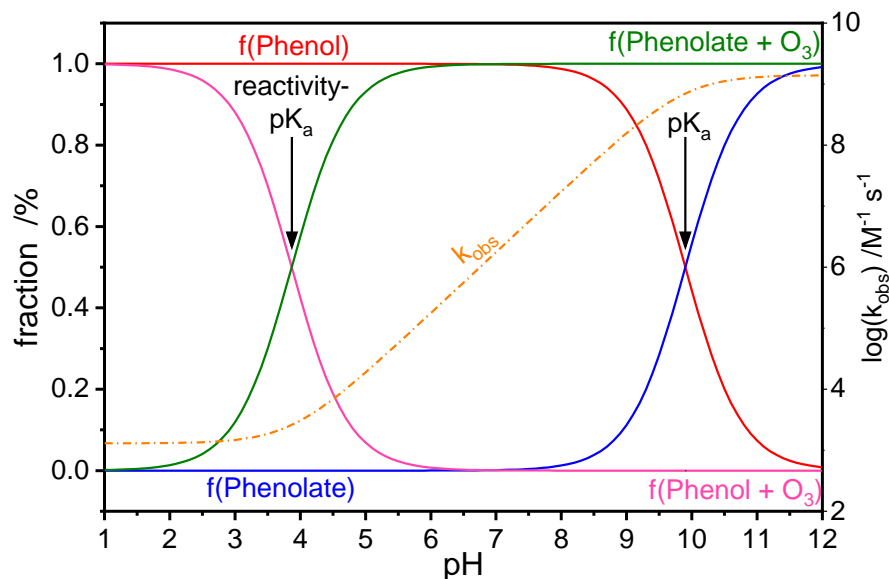


**Figure 5.5:** Fraction of phenol (red line) and the fraction of phenolate (blue line) at different pH values. Additionally, the reacting fraction of  $\text{O}_3$  with phenol (pink line) and phenolate (green line) is shown. The crossing point of the fractions shows the  $\text{pK}_a$  value and the crossing point of the reacting fraction are called the reactivity- $\text{pK}_a$ . The  $k_{\text{obs}}$  are plotted on a logarithmic scale against the pH values (orange line).

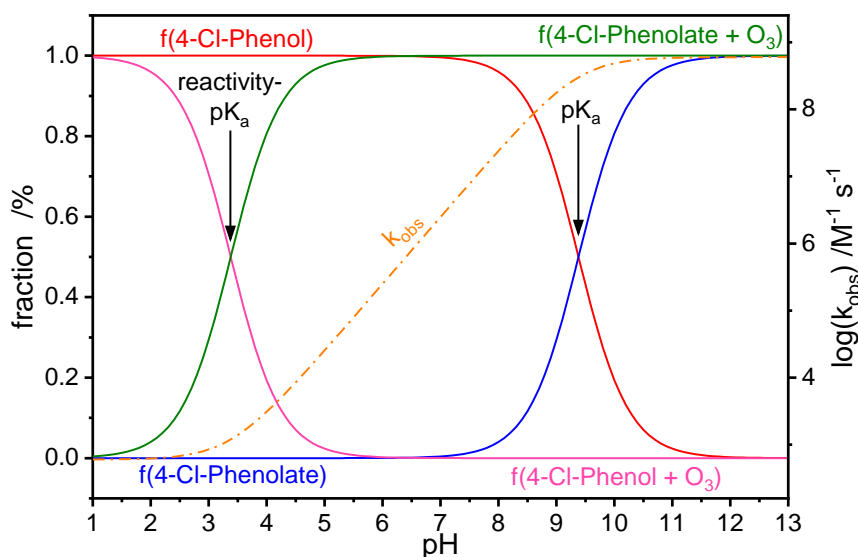


**Figure 5.6:** Fraction of 4-chlorophenol (red line) and the fraction of 4-chlorophenolate (blue line) at different pH values. Additionally, the reacting fraction of ozone with neutral species (pink line) and anionic species (green line) is shown. The crossing point of the fractions shows the  $\text{pK}_a$  value and the crossing point of the reacting fraction are called the reactivity- $\text{pK}_a$ . The  $k_{\text{obs}}$  are plotted on a logarithmic scale against the pH values (orange line).

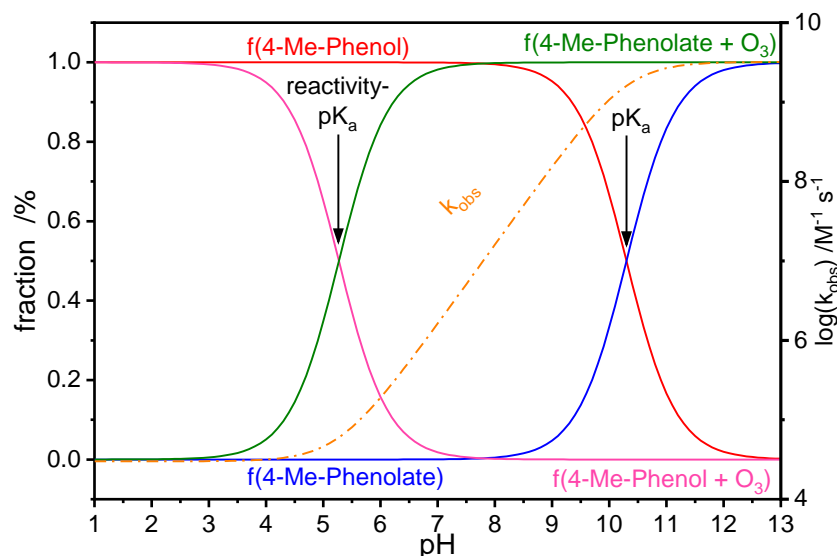


**Figure 5.7:** Fraction of 4-methylphenol (red line) and the fraction of 4-methylphenolate (blue line) at different pH values. Additionally, the reacting fraction of ozone with neutral species (pink line) and anionic species (green line) is shown. The crossing point of the fractions shows the  $pK_a$  value and the crossing point of the reacting fraction are called the reactivity- $pK_a$ . The  $k_{obs}$  are plotted on a logarithmic scale against the pH values (orange line).

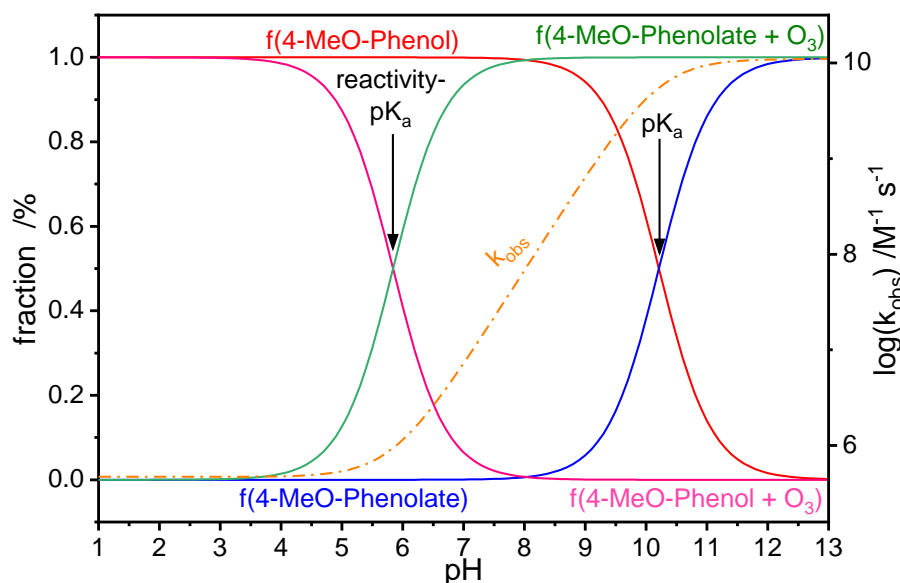


**Figure 5.8:** Fraction of 4-methoxyphenol (red line) and the fraction of 4-methoxyphenolate (blue line) at different pH values. Additionally, the reacting fraction of ozone with neutral species (pink line) and anionic species (green line) is shown. The crossing point of the fractions shows the  $pK_a$  value and the crossing point of the reacting fraction are called the reactivity- $pK_a$ . The  $k_{obs}$  are plotted on a logarithmic scale against the pH values (orange line).



### 5.5.2 Generation of ozone stock solutions

Ozone stock solutions were prepared by bubbling ozone-containing gas, produced with an ozone generator (Table 5.2), through ice cooled ultrapure water. After an enrichment phase of approximated 45 minutes, the O<sub>3</sub> concentration was determined by UV absorption of 1:3 diluted O<sub>3</sub> stock solution at 258 nm;  $\epsilon(\text{O}_3) = 3200 \text{ M}^{-1}\text{cm}^{-1}$  (Tentscher et al., 2018). The O<sub>3</sub> concentration in the stock solution ranged between  $1.6 \times 10^{-3} - 1.8 \times 10^{-3} \text{ M}$ . Continuous purging of the stock solution with gaseous O<sub>3</sub> was required to keep the O<sub>3</sub> concentration constant.

**Table 5.6: Final O<sub>3</sub> concentration in the different experiments (GC-IRMS and LC-IRMS: Isotopic fractionation; GC-MS: Competitions kinetic for labelled phenol; LC-UV: Competition kinetic for 4-methylphenol; CPh = 4-chlorphenol; MePh = 4-methylphenol; MxPh = 4-methoxyphenol).**

Instrument	Phenol [mM]	3-buten-2-ol [mM]	3-butyn-2-ol [mM]	CPh [mM]	MePh [mM]	MxPh [mM]
GC-IRMS	0.05 – 0.30	----	----	----	----	----
LC-IRMS	----	----	----	0.15 – 0.90	0.15 – 0.90	0.15 – 0.90
GC-MS	0.10 – 0.60	----	----	----	----	----
LC-UV	0.01 – 0.06	----	----	----	----	----

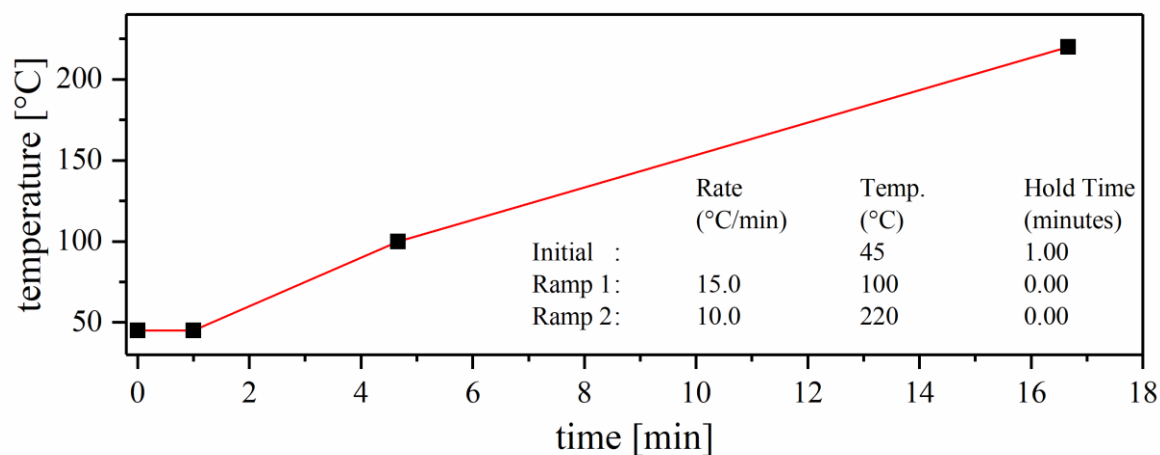


**Figure 5.9:** GC oven parameter of the 3-buten-2-ol measurements (Inlet: temperature = 250 °C; Split flow = 20 mL min<sup>-1</sup>; splitless time = 0.5 min; Purge: constant septum purge; Mode = splitless; constant carrier flow = 2.4 mL min<sup>-1</sup>).

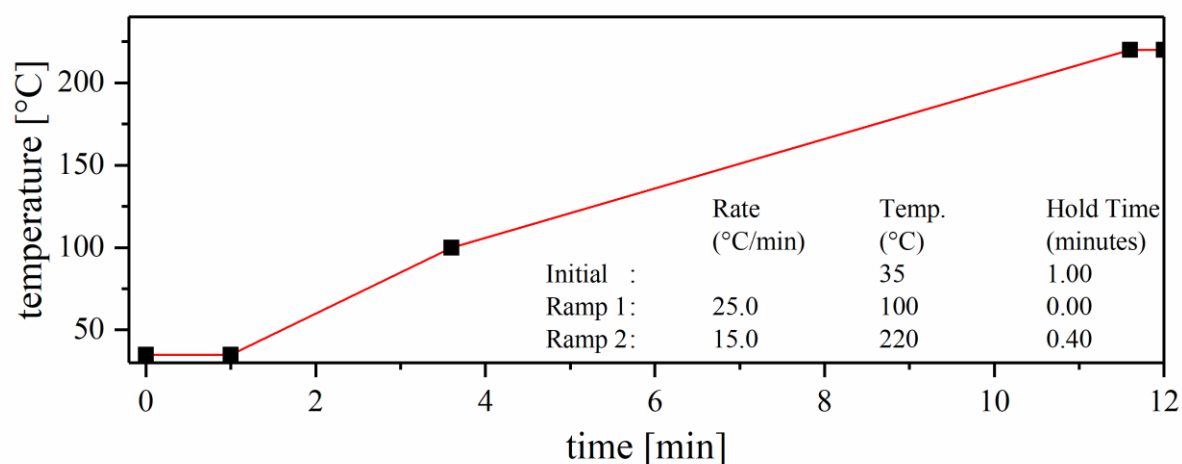


**Figure 5.10:** GC oven parameter of the 3-butyne-2-ol measurements (Inlet: temperature = 250 °C; Split flow = 20 mL min<sup>-1</sup>; splitless time = 0.5 min; Purge: constant septum purge; Mode = splitless; constant carrier flow = 2.4 mL min<sup>-1</sup>).

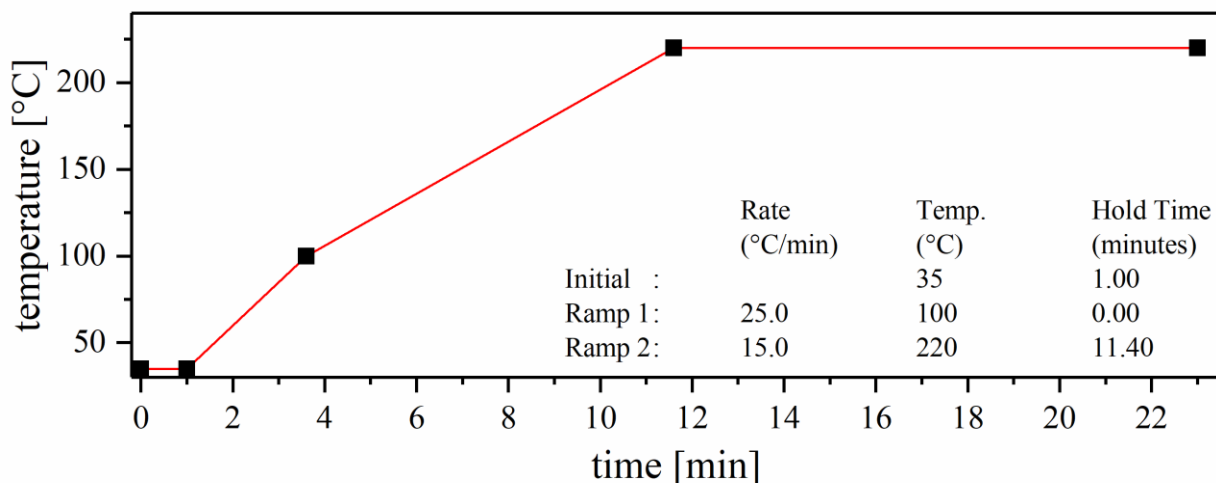


**Figure 5.11: GC oven parameter of the phenol measurements (Inlet: temperature = 250 °C; Split flow = 20 mL min<sup>-1</sup>; splitless time = 0.5 min; Purge: constant septum purge; Mode = splitless; constant carrier flow = 2.4 mL min<sup>-1</sup>).**

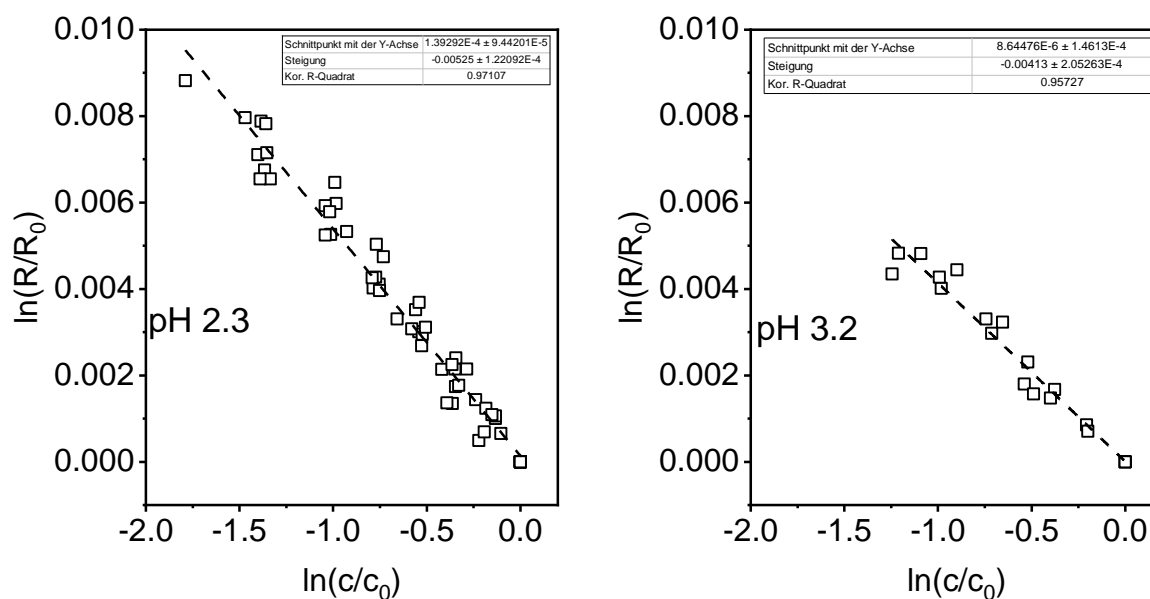


**Figure 5.12: Rayleigh plot of the degradation of phenol with ozone with different ozone concentration at pH 2.3 (right) and 3.2 (left). ( $c_0(\text{phenol}) = 0.15 \text{ mM}$ ,  $c_0(\text{tert.-BuOH}) = 125 \text{ mM}$ ,  $c(\text{ozone}) = 0.05 - 0.30 \text{ mM}$  and  $c(\text{phosphate buffer}) = 10 \text{ mM}$ . The isotope ratio of phenol was measured by GC-IRMS). The error of the slope is the 95% confidence interval.**

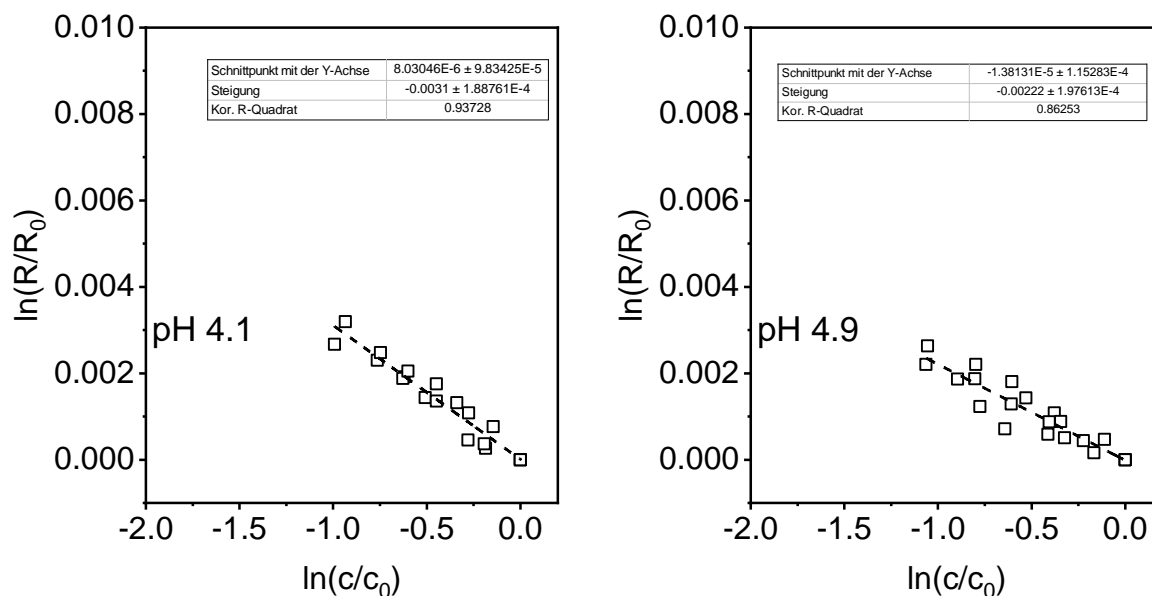


**Figure 5.13:** Rayleigh plot of the degradation of phenol with ozone with different ozone concentration at pH 4.1 (right) and 4.9 (left). ( $c_0(\text{phenol}) = 0.15 \text{ mM}$ ,  $c_0(\text{tert.-BuOH}) = 125 \text{ mM}$ ,  $c(\text{ozone}) = 0.05 - 0.30 \text{ mM}$  and  $c(\text{phosphate buffer}) = 10 \text{ mM}$ . The isotope ratio of phenol was measured by GC-IRMS). The error of the slope is the 95% confidence interval.

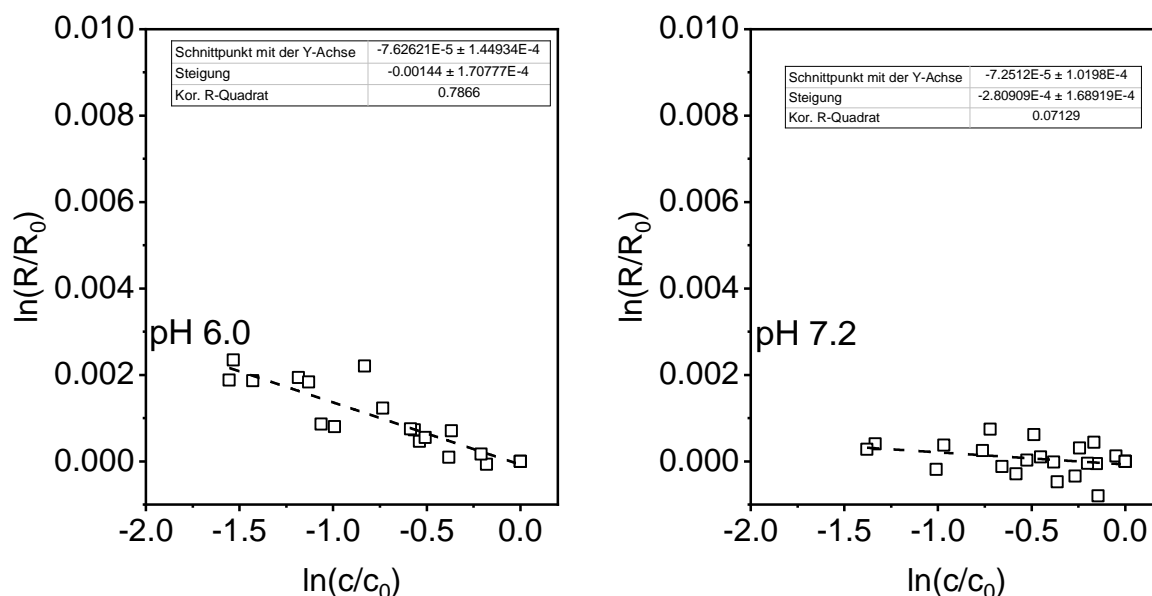


**Figure 5.14:** Rayleigh plot of the degradation of phenol with ozone with different ozone concentration at pH 6.0 (right) and 7.2 (left). ( $c_0(\text{phenol}) = 0.15 \text{ mM}$ ,  $c_0(\text{tert.-BuOH}) = 125 \text{ mM}$ ,  $c(\text{ozone}) = 0.05 - 0.30 \text{ mM}$  and  $c(\text{phosphate buffer}) = 10 \text{ mM}$ . The isotope ratio of phenol was measured by GC-IRMS). The error of the slope is the 95% confidence interval.

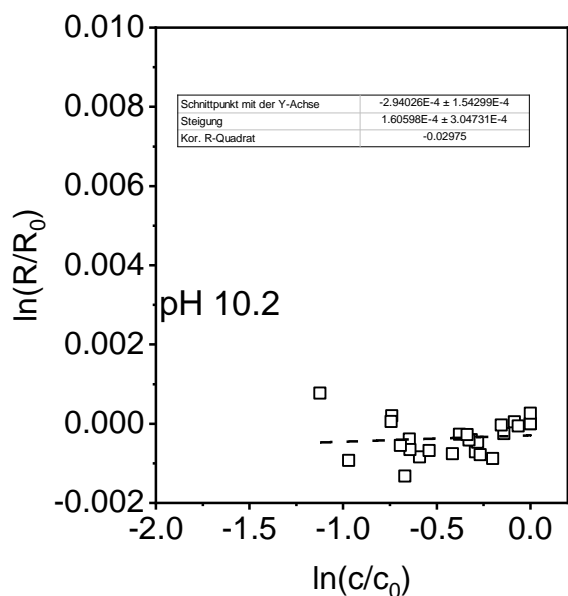


**Figure 5.15:** Rayleigh plot of the degradation of phenol with ozone with different ozone concentration at pH 10.2. ( $c_0(\text{phenol}) = 0.15 \text{ mM}$ ,  $c_0(\text{tert.-BuOH}) = 125 \text{ mM}$ ,  $c(\text{ozone}) = 0.05 - 0.30 \text{ mM}$  and  $c(\text{phosphate buffer}) = 10 \text{ mM}$ . The isotope ratio of phenol was measured by GC-IRMS). The error of the slope is the 95% confidence interval.

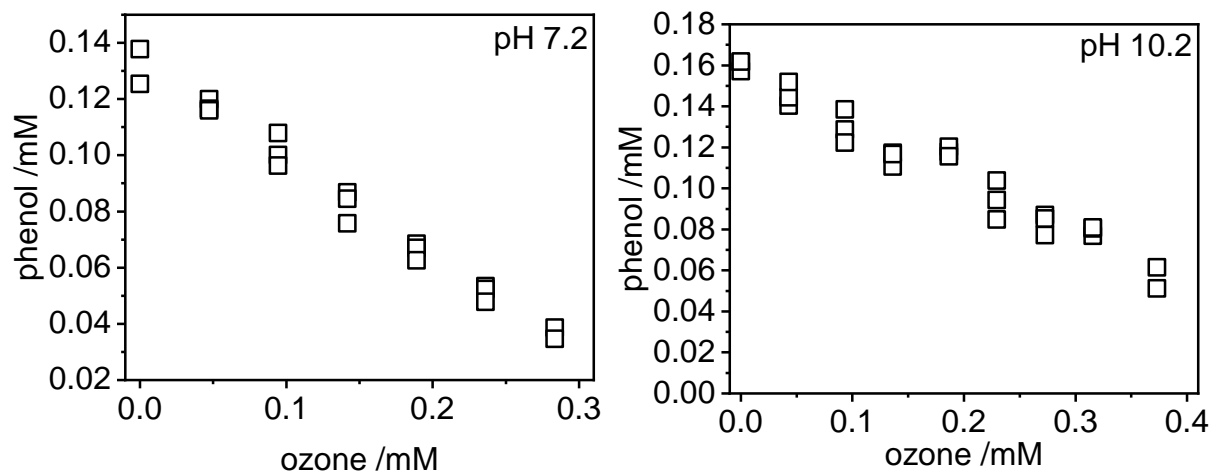


**Figure 5.16:** Degradation of phenol with difference ozone concentration at pH 7.2 (left) and pH 10.2 (right). ( $c_0(\text{phenol}) = 0.15 \text{ mM}$ ,  $c_0(\text{tert.-BuOH}) = 125 \text{ mM}$ ,  $c(\text{ozone}) = 0.05 - 0.30 \text{ mM}$  and  $c(\text{phosphate buffer}) = 10 \text{ mM}$ . The isotope ratio of phenol was measured by GC-IRMS).

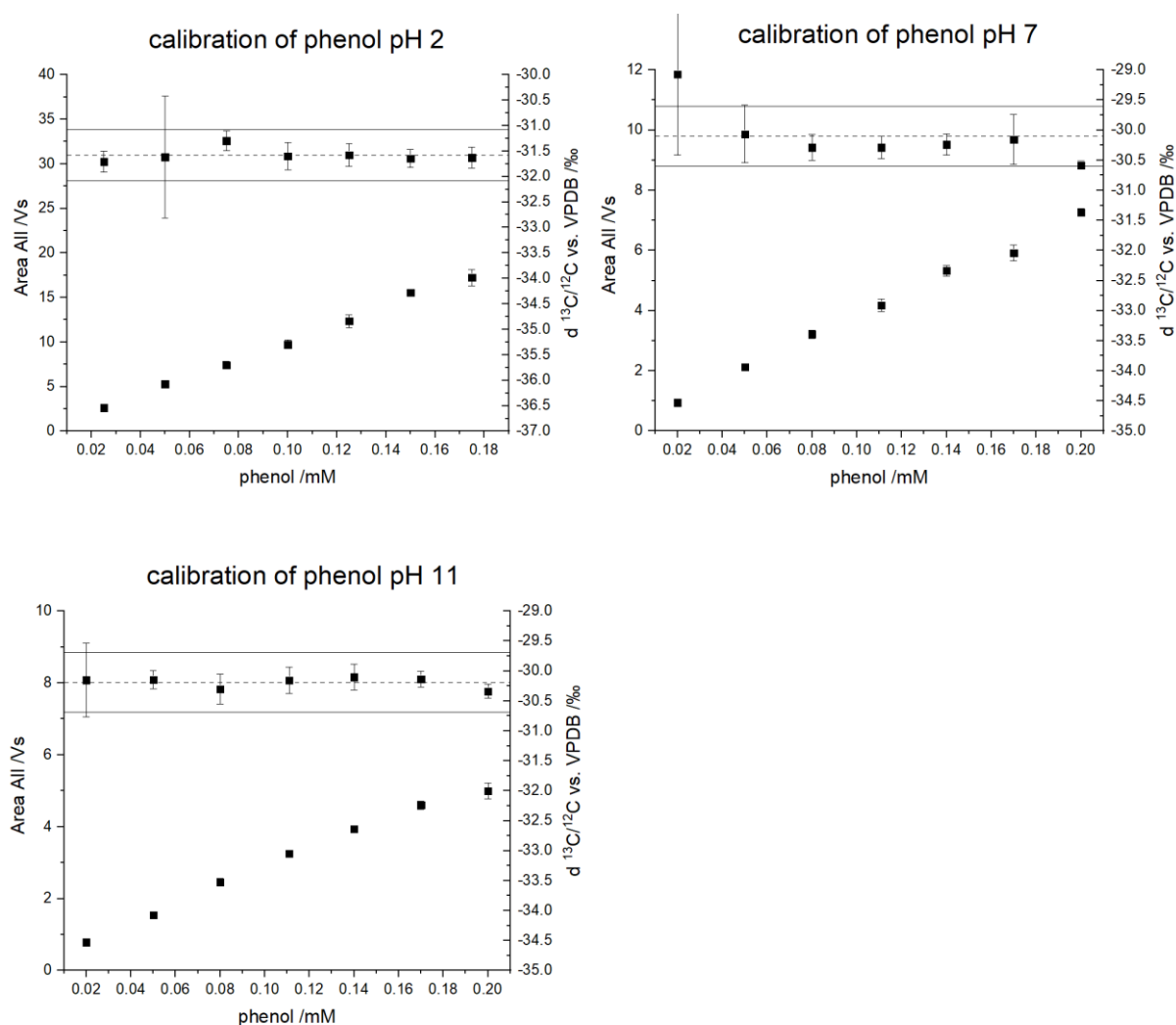


**Figure 5.17: Calibration of phenol with GC-IRMS at pH 2.3, pH 7.2 and pH 10.2. Left y-axis shows the peak area and the right y-axis shows the delta value. The dash line represents the mean value of the delta values for all ozone concentration and the lines shows the  $\pm 0.5\text{‰}$  of the mean value. In Jochmann and Schmidt (2012) is the method detection limit the last concentration which delta value is in the range of  $0.5\text{‰}$ . After this method the MDL at pH 2 is 0.025 mM, at pH 7 0.05 mM and at pH 11 0.02 mM.**

# **6. Chapter: General conclusions & Outlook**

In this thesis, the reaction of phenol with ozone ( $O_3$ ) and chlorine dioxide ( $ClO_2$ ) was investigated. The relevance of fundamental aspects such as the formation of secondary oxidants and the influence of pH was shown. Additionally, new concepts for the further investigation of reaction mechanisms were developed. Further, this work reveals open questions for often-investigated compounds, like phenol. Many results are taken for granted, such as stoichiometric ratio or the formation of secondary oxidants, but the reason for the high stoichiometric ratio and the impact of the secondary oxidants on the use of oxidative processes has not been shown, yet.

The proof of HOCl formation in the  $ClO_2$  application brings new opportunities and challenges in transformation reactions of TrOCs. The formed HOCl increases the number of transformable TrOCs in the  $ClO_2$  application. The studies of Hey et al. (2012) and Lee and von Gunten (2010) show the degradation of compounds in  $ClO_2$  applications reacting slowly with  $ClO_2$  and fast with HOCl. During the reaction of  $ClO_2$  with TrOCs, HOCl is formed. However, the knowledge of the formation of HOCl as well as its influence on the transformation process is still in its infancy. Therefore, additional investigations with more TrOCs as reaction partners for  $ClO_2$  are necessary. Additionally, with new developed methods for the determination of free chlorine (HOCl) (Abdighahroudi et al., 2020), this gap can be closed and the  $ClO_2$  application could be better rated for use in water treatment. Hupperich et al. (2020) started with the investigation of model compounds such as vanillin, dimedone and hydroquinone with  $ClO_2$ . To increase the use of  $ClO_2$  for pollutant control in water treatment, other functional groups such as amines or thiolates must be investigated for the formation of inorganic products (e.g. HOCl or  $ClO_2^-$ ). Additionally, important further investigations address the formation of disinfection by-products by  $ClO_2$ . Chlorination has a bad reputation due to the formation of trihalomethanes (THMs) (Henry, 2013). Hua and Reckhow (2007) reported that the application of  $ClO_2$  barely formed THMs, however, other halogenated by-products can be formed (Han et al., 2017). The investigation of these by-products is important for the development of  $ClO_2$  applications in water treatment.

The results of the reversed order dosage concept show the influence of oxidant dosage on the stoichiometric ratio of the oxidant and the product yield (Schreiber and Mitch, 2005). The dosages are differentiated in the excess of the reaction partners at the reaction interface. In the determination concept of the HOCl yield, the influence of the dosage order was high. In contrast, for the suppression of the reaction between  $O_3$  and the formed products, the influence was low. Therefore, further experiments with the investigation of different excesses (10 times, 100 times, etc.) and different reaction rate constants on the product yield will be interesting to



find experimental limit values. Limit values will help in planning experiments to choose the right order of dosing.

Additionally, all chapters represent the difficulty of the investigation of only primary oxidant reactions. The secondary oxidants (e.g. HOCl, OH radicals) must be directly scavenged. However, all secondary oxidants must be known and possible to scavenge. For example, the formed superoxide in the reaction of O<sub>3</sub> with phenol has an impact on the O<sub>3</sub> stoichiometric ratio with phenol. Superoxide reacts very fast with O<sub>3</sub> (Sehested et al., 1983) and interferes with the compound under study, e.g. phenol, during the reaction with O<sub>3</sub>. Therefore, detailed investigations with the dosage of superoxide by, e.g., KO<sub>2</sub> or scavenging of superoxide by, e.g., tetranitromethane in the reaction of O<sub>3</sub> with phenol would be helpful to show the real impact of superoxide.

In all three main chapters, the pH value has a key role in the transformation of phenol. The reactivity of HOCl (Chapter 3) (Deborde and von Gunten, 2008) and the speciation of phenol are controlled by the pH (Chapter 4) (Mvula and von Sonntag, 2003). Additionally, the pH value influences indirectly the isotopic fractionation with the change in reactive species of phenol (Chapter 5). The fundamental impact of the adjustment of pH on the oxidative reaction experiments should always be kept in mind. The buffering and the control of the pH value during the reaction are decisive for the success of an experiment. Therefore, the selection of suitable buffer conditions for the reaction is a fundamental part of any process study. Before starting the experiment, a suitable buffer substance (e.g. phosphate buffer or borate buffer) and the optimal concentration must be found. Additionally, the control of the pH must be a part of each oxidative experiment. Pre-experiments for the investigation of the pH value could be necessary to track the change of pH during the experiment. The best case is the determination of the pH value in real-time without influencing the reaction under study.

In the last main chapter, compounds-specific stable isotope analysis (CSIA) was used for the investigation of the reaction of O<sub>3</sub> with phenol. CSIA is not yet often used for the characterization of oxidative transformation reactions. Maier et al. (2016), Willach et al. (2017) and Willach et al. (2020) investigated different compounds with CSIA and found hints for the reaction mechanism. In this work, a relation of the reaction kinetics with the isotope enrichment factor for aromatic compounds was demonstrated. The correlation shows a reaction rate constant limit of 10<sup>5</sup> M<sup>-1</sup>s<sup>-1</sup> for the determination of isotopic fractionation. For reactions of aromatic compounds with a reaction rate constant > 10<sup>5</sup> M<sup>-1</sup> s<sup>-1</sup>, the determination of isotopic

fractionation is no longer possible. To corroborate this limit, more compounds with a reaction rate constant between  $10^3 \text{ M}^{-1} \text{ s}^{-1}$  and  $10^5 \text{ M}^{-1} \text{ s}^{-1}$  must be investigated with CSIA. For example, the degradation of aniline with  $\text{O}_3$  investigated by CSIA could be a conceivable helpful study.  $\text{O}_3$  attacks the aromatic ring or the amine of the aniline (Tekle-Röttering et al., 2016b). The determination of the enrichment factor of carbon and nitrogen for aniline will be interesting. The dependence on the pH value must be the main part of this study. Additionally, the investigation of different other functional groups such as double bonds, triple bonds or amines with CSIA would be interesting. In Chapter 5, first investigations with two compounds (2-buten-1-ol, 2-butyl-1ol) are shown. However, for the comparison of the olefins with the aromatic compounds, additional compounds with only double bonds or triple bonds as the point of attack and with the same number of carbon atoms as phenol, e.g., 3-hexenol or 2-hexenol would be helpful. This thesis only investigated the reaction with  $\text{O}_3$  by CSIA. Investigation of additional oxidants like  $\text{ClO}_2$  or OH radicals by CSIA and with the dependence of pH value may show different limit values for the isotopic fractionation. With these approaches, a database of enrichment factors for the reaction of oxidants with functional groups could be created and support the investigation of reaction mechanisms.

In general, the understanding of reaction mechanisms of TrOCs transformations with oxidants is of utmost importance for the use of chemical oxidation processes in water treatment. Fundamental parameters such as stoichiometric ratio and reaction kinetics and new methods such as CSIA should be combined in future investigations of transformation processes, which supports securing the high quality of drinking water.

## **7. Chapter: References**

- ABDIGHAHROUDI, M. S., JÜTTE, M., HUPPERICH, K., MUTKE, X. A. M., SCHMIDT, T. C. & LUTZE, H. V. 2021. Chapter Three - Mechanisms and byproduct formation in the application of chlorine dioxide. *In: MANASFI, T. & BOUDENNE, J.-L. (eds.) Comprehensive Analytical Chemistry*. Elsevier.
- ABDIGHAHROUDI, M. S., SCHMIDT, T. C. & LUTZE, H. V. 2020. Determination of free chlorine based on ion chromatography—application of glycine as a selective scavenger. *Analytical and Bioanalytical Chemistry*, 412, 7713-7722.
- ACERO, J. L., PIRIOU, P. & VON GUNTEN, U. 2005. Kinetics and mechanisms of formation of bromophenols during drinking water chlorination: Assessment of taste and odor development. *Water Research*, 39, 2979-2993.
- AIETA, E. M. & BERG, J. D. 1986. A review of chlorine dioxide in drinking water treatment. *Journal AWWA*, 78, 62-72.
- ALEXANDER, N. M. 1962. A spectrophotometric assay for iodide oxidation by thyroid peroxidase. *Analytical Biochemistry*, 4, 341-345.
- BAKKOUR, R., BOLOTIN, J., SELLERGREN, B. & HOFSTETTER, T. B. 2018. Molecularly imprinted polymers for compound-specific isotope analysis of polar organic micropollutants in aquatic environments. *Analytical Chemistry*, 90, 7292-7301.
- BERG, M., BOLOTIN, J. & HOFSTETTER, T. B. 2007. Compound-specific nitrogen and carbon isotope analysis of nitroaromatic compounds in aqueous samples using solid-phase microextraction coupled to GC/IRMS. *Analytical Chemistry*, 79, 2386-2393.
- BIELSKI, B. H. J., CABELLI, D. E., ARUDI, R. L. & ROSS, A. B. 1985. Reactivity of HO<sub>2</sub>/O<sub>2</sub><sup>-</sup> radicals in aqueous solution. *Journal of Physical and Chemical Reference Data*, 14, 1041-1100.
- BUXTON, G. V., GREENSTOCK, C. L., HELMAN, W. P. & ROSS, A. B. 1988. Critical review of rate constants for reactions of hydrated electrons, hydrogen atoms and hydroxyl radicals (<sup>-</sup>OH/<sup>-</sup>O<sup>-</sup>) in aqueous solution. *Journal of Physical and Chemical Reference Data*, 17, 513-886.
- CREMER, D., KRAKA, E., CREHUET, R., ANGLADA, J. & GRÄFENSTEIN, J. 2001. The ozone–acetylene reaction: concerted or non-concerted reaction mechanism? A quantum chemical investigation. *Chemical Physics Letters*, 347, 268-276.
- CRICQUET, J., RODRIGUEZ, E. M., ALLARD, S., WELLAUER, S., SALHI, E., JOLL, C. A. & VON GUNTEN, U. 2015. Reaction of bromine and chlorine with phenolic compounds and natural organic matter extracts – Electrophilic aromatic substitution and oxidation. *Water Research*, 85, 476-486.
- DEBORDE, M. & VON GUNTEN, U. 2008. Reactions of chlorine with inorganic and organic compounds during water treatment—Kinetics and mechanisms: A critical review. *Water Research*, 42, 13-51.
- DEEB, A. A., STEPHAN, S., SCHMITZ, O. J. & SCHMIDT, T. C. 2017. Suspect screening of micropollutants and their transformation products in advanced wastewater treatment. *Science of the Total Environment*, 601-602, 1247-1253.
- DODD, M. C., BUFFLE, M.-O. & VON GUNTEN, U. 2006. Oxidation of antibacterial molecules by aqueous ozone: moiety-specific reaction kinetics and application to ozone-based wastewater treatment. *Environmental Science & Technology*, 40, 1969-1977.
- DOWIDEIT, P. & VON SONNTAG, C. 1998. Reaction of ozone with ethene and its methyl- and chlorine-substituted derivatives in aqueous solution. *Environmental Science & Technology*, 32, 1112-1119.

- EBERT, I., AMATO, R., HEIN, A. & KONRADI, S. 2014. Arzneimittel in der Umwelt- vermeiden, reduzieren, überwachen. *Umweltbundesamt 04/2014*.
- ELIASSON, B., HIRTH, M. & KOGELSCHATZ, U. 1987. Ozone synthesis from oxygen in dielectric barrier discharges. *Journal of Physics D: Applied Physics*, 20, 1421-1437.
- ELLIOT, A. J. & MCCRACKEN, D. R. 1989. Effect of temperature on O•- reactions and equilibria: A pulse radiolysis study. *International Journal of Radiation Applications and Instrumentation. Part C. Radiation Physics and Chemistry*, 33, 69-74.
- ELSNER, M. 2010. Stable isotope fractionation to investigate natural transformation mechanisms of organic contaminants: principles, prospects and limitations. *Journal of Environmental Monitoring*, 12, 2005-2031.
- ELSNER, M., JOCHMANN, M. A., HOFSTETTER, T. B., HUNKELER, D., BERNSTEIN, A., SCHMIDT, T. C. & SCHIMMELMANN, A. 2012. Current challenges in compound-specific stable isotope analysis of environmental organic contaminants. *Analytical and Bioanalytical Chemistry*, 403, 2471-2491.
- ELSNER, M., ZWANK, L., HUNKELER, D. & SCHWARZENBACH, R. P. 2005. A new concept linking observable stable isotope fractionation to transformation pathways of organic pollutants. *Environmental Science & Technology*, 39, 6896-6916.
- FISCHBACHER, A., LÖPPENBERG, K., VON SONNTAG, C. & SCHMIDT, T. C. 2015. A new reaction pathway for bromite to bromate in the ozonation of bromide. *Environmental Science & Technology*, 49, 11714-11720.
- FISCHBACHER, A., VON SONNTAG, J., VON SONNTAG, C. & SCHMIDT, T. C. 2013. The •OH radical yield in the H<sub>2</sub>O<sub>2</sub> + O<sub>3</sub> (peroxone) reaction. *Environmental Science & Technology*, 47, 9959-9964.
- FUNKE, J., PRASSE, C. & TERNES, T. A. 2016. Identification of transformation products of antiviral drugs formed during biological wastewater treatment and their occurrence in the urban water cycle. *Water Research*, 98, 75-83.
- FURMAN, C. S. & MARGERUM, D. W. 1998. Mechanism of chlorine dioxide and chlorate ion formation from the reaction of hypobromous acid and chlorite ion. *Inorganic Chemistry*, 37, 4321-4327.
- GAO, S., ZHAO, Z., XU, Y., TIAN, J., QI, H., LIN, W. & CUI, F. 2014. Oxidation of sulfamethoxazole (SMX) by chlorine, ozone and permanganate—A comparative study. *Journal of Hazardous Materials*, 274, 258-269.
- GARCÍA-GALÁN, M. J., SILVIA DÍAZ-CRUZ, M. & BARCELÓ, D. 2008. Identification and determination of metabolites and degradation products of sulfonamide antibiotics. *TrAC Trends in Analytical Chemistry*, 27, 1008-1022.
- GATES, D. J. 1998. *The chlorine dioxide handbook*, Denver, American water works Association.
- GATES, D. Z., G.; OZEKIN, K. 2009. *State of the science of chlorine dioxide in drinking water*, Water Research Foundation and Fondazione AMGA.
- GLAZE, W. H., KANG, J.-W. & CHAPIN, D. H. 1987. The chemistry of water treatment processes involving ozone, hydrogen peroxide and ultraviolet radiation. *Ozone: Science & Engineering*, 9, 335-352.
- GÖTZ, C. W., STAMM, C., FENNER, K., SINGER, H., SCHÄRER, M. & HOLLENDER, J. 2010. Targeting aquatic microcontaminants for monitoring: exposure categorization and application to the Swiss situation. *Environmental Science and Pollution Research*, 17, 341-354.

- 
- GUROL, M. D. & NEKOUINAINI, S. 1984. Kinetic behavior of ozone in aqueous solutions of substituted phenols. *Industrial & Engineering Chemistry Fundamentals*, 23, 54-60.
- HAN, J., ZHANG, X., LIU, J., ZHU, X. & GONG, T. 2017. Characterization of halogenated DBPs and identification of new DBPs trihalomethanols in chlorine dioxide treated drinking water with multiple extractions. *Journal of Environmental Sciences*, 58, 83-92.
- HARTENBACH, A. E., HOFSTETTER, T. B., TENTSCHER, P. R., CANONICA, S., BERG, M. & SCHWARZENBACH, R. P. 2008. Carbon, hydrogen, and nitrogen isotope fractionation during light-induced transformations of atrazine. *Environmental Science & Technology*, 42, 7751-7756.
- HENRY, H. 2013. EPA's stage 2 disinfection byproducts rules (DBPR) and northern kentucky water: An economic and scientific review. *Dose-Response*, 11, 532-557.
- HEY, G., GRABIC, R., LEDIN, A., LA COUR JANSEN, J. & ANDERSEN, H. R. 2012. Oxidation of pharmaceuticals by chlorine dioxide in biologically treated wastewater. *Chemical Engineering Journal*, 185–186, 236-242.
- HOFSTETTER, T. B. & BERG, M. 2011. Assessing transformation processes of organic contaminants by compound-specific stable isotope analysis. *TrAC - Trends in Analytical Chemistry*, 30, 618-627.
- HOFSTETTER, T. B., BOLOTIN, J., PATI, S. G., SKARPELI-LIATI, M., SPAHR, S. & WIJKER, R. S. 2014. Isotope effects as new proxies for organic pollutant transformation. *CHIMIA International Journal for Chemistry*, 68, 788-792.
- HOFSTETTER, T. B., SCHWARZENBACH, R. P. & BERNASCONI, S. M. 2008. Assessing transformation processes of organic compounds using stable isotope fractionation. *Environmental Science and Technology*, 42, 7737-7743.
- HOIGNÉ, J. & BADER, H. 1980. Bestimmung von Ozon und Chlordioxid in Wasser mit der Indigo-Methode. *Vom Wasser*, 55, 261-280.
- HOIGNÉ, J. & BADER, H. 1983a. Rate constants of reactions of ozone with organic and inorganic compounds in water—I. *Water Research*, 17, 173-183.
- HOIGNÉ, J. & BADER, H. 1983b. Rate constants of reactions of ozone with organic and inorganic compounds in water—II. *Water Research*, 17, 185-194.
- HOIGNÉ, J. & BADER, H. 1994. Kinetics of reactions of chlorine dioxide (OCIO) in water—I. Rate constants for inorganic and organic compounds. *Water Research*, 28, 45-55.
- HUA, G. & RECKHOW, D. A. 2007. Comparison of disinfection byproduct formation from chlorine and alternative disinfectants. *Water Research*, 41, 1667-1678.
- HUBER, M. M., CANONICA, S., PARK, G.-Y. & VON GUNTEN, U. 2003. Oxidation of pharmaceuticals during ozonation and advanced oxidation processes. *Environmental Science & Technology*, 37, 1016-1024.
- HUBER, M. M., KORHONEN, S., TERNES, T. A. & VON GUNTEN, U. 2005. Oxidation of pharmaceuticals during water treatment with chlorine dioxide. *Water Research*, 39, 3607-3617.
- HÜBNER, U., VON GUNTEN, U. & JEKEL, M. 2015. Evaluation of the persistence of transformation products from ozonation of trace organic compounds – A critical review. *Water Research*, 68, 150-170.
- HULL, L. A., DAVIS, G. T., ROSENBLATT, D. H., WILLIAMS, H. K. R. & WEGLEIN, R. C. 1967. Oxidations of amines. III. Duality of mechanism in the reaction of amines with chlorine dioxide. *Journal of the American Chemical Society*, 89, 1163-1170.

- HUNKELER, D., MECKENSTOCK, R. U., SHERWOOD LOLLAR, B., SCHMIDT, T. C. & WILSON, J. T. 2008. A guide for assessing biodegradation and source identification of organic ground water contaminants using compound specific isotope analysis (CSIA).
- HUPPERICH, K., MUTKE, X. A. M., ABDIGHAHOUDI, M. S., JÜTTE, M., SCHMIDT, T. C. & LUTZE, H. V. 2020. Reaction of chlorine dioxide with organic matter – formation of inorganic products. *Environmental Science: Water Research & Technology*, 6, 2597-2606.
- ISON, A., ODEH, I. N. & MARGERUM, D. W. 2006. Kinetics and mechanisms of chlorine dioxide and chlorite oxidations of cysteine and glutathione. *Inorganic Chemistry*, 45, 8768-8775.
- JIANG, J., ZHANG, X., ZHU, X. & LI, Y. 2017. Removal of intermediate aromatic halogenated DBPs by activated carbon adsorption: A new approach to controlling halogenated DBPs in chlorinated drinking water. *Environmental Science & Technology*, 51, 3435-3444.
- JOCHMANN, M. A., BLESSING, M., HADERLEIN, S. B. & SCHMIDT, T. C. 2006. A new approach to determine method detection limits for compound-specific isotope analysis of volatile organic compounds. *Rapid Communications in Mass Spectrometry*, 20, 3639-3648.
- JOCHMANN, M. A. & SCHMIDT, T. C. 2012. *Compound-specific stable isotope analysis*, RSC publishing.
- JOE-WONG, C. & MAHER, K. 2020. A model for kinetic isotope fractionation during redox reactions. *Geochimica et Cosmochimica Acta*, 269, 661-677.
- JOSS, A., SIEGRIST, H. & TERNES, T. A. 2008. Are we about to upgrade wastewater treatment for removing organic micropollutants? *Water Science and Technology*.
- KNOCKE, W. R., VAN BENSCHOTEN, J. E., KEARNEY, M. J., SOBORSKI, A. W. & RECKHOW, D. A. 1991. Kinetics of manganese and iron oxidation by potassium permanganate and chlorine dioxide. *Journal AWWA*, 83, 80-87.
- KNOOP, O., ITZEL, F., TUERK, J., LUTZE, H. V. & SCHMIDT, T. C. 2018. Endocrine effects after ozonation of tamoxifen. *Science of the Total Environment*, 622-623, 71-78.
- KONSTANTINOVA, M. L., RAZUMOVSKII, S. D. & ZAIKOV, G. E. 1991. Kinetics and mechanism of the reaction of ozone with phenol in alkaline media. *Bulletin of the Academy of Sciences of the USSR, Division of chemical science*, 40, 266-270.
- KORSHIN, G. V. 2011. Chlorine based oxidants for water purification and disinfection. *Aquatic Redox Chemistry*. American Chemical Society.
- KRAUSS, M., SINGER, H. & HOLLENDER, J. 2010. LC–high resolution MS in environmental analysis: from target screening to the identification of unknowns. *Analytical and Bioanalytical Chemistry*, 397, 943-951.
- KUJAWINSKI, D. M., STEPHAN, M., JOCHMANN, M. A., KRAJENKE, K., HAAS, J. & SCHMIDT, T. C. 2010. Stable carbon and hydrogen isotope analysis of methyl tert-butyl ether and tert-amyl methyl ether by purge and trap-gas chromatography-isotope ratio mass spectrometry: Method evaluation and application. *Journal of Environmental Monitoring*, 12, 347-354.
- KUJAWINSKI, D. M., ZHANG, L., SCHMIDT, T. C. & JOCHMANN, M. A. 2012. When other separation techniques fail: Compound-specific carbon isotope ratio analysis of sulfonamide containing pharmaceuticals by high-temperature-liquid

- chromatography-isotope ratio mass spectrometry. *Analytical Chemistry*, 84, 7656-7663.
- KUMAR, K. & MARGERUM, D. W. 1987. Kinetics and mechanism of general-acid-assisted oxidation of bromide by hypochlorite and hypochlorous acid. *Inorganic Chemistry*, 26, 2706-2711.
- LEE, Y. & VON GUNTEN, U. 2010. Oxidative transformation of micropollutants during municipal wastewater treatment: Comparison of kinetic aspects of selective (chlorine, chlorine dioxide, ferrate<sup>VI</sup>, and ozone) and non-selective oxidants (hydroxyl radical). *Water Research*, 44, 555-566.
- LENGYEL, I., LI, J., KUSTIN, K. & EPSTEIN, I. R. 1996. Rate constants for reactions between iodine- and chlorine-containing species: A detailed mechanism of the chlorine dioxide/chlorite-iodide reaction. *Journal of the American Chemical Society*, 118, 3708-3719.
- LI, Z., KASERZON, S. L., PLASSMANN, M. M., SOBEK, A., GÓMEZ RAMOS, M. J. & RADKE, M. 2017. A strategic screening approach to identify transformation products of organic micropollutants formed in natural waters. *Environmental Science: Processes & Impacts*, 19, 488-498.
- LIU, J. & ZHANG, X. 2014. Comparative toxicity of new halophenolic DBPs in chlorinated saline wastewater effluents against a marine alga: Halophenolic DBPs are generally more toxic than haloaliphatic ones. *Water Research*, 65, 64-72.
- LUTZE, H. V., KERLIN, N. & SCHMIDT, T. C. 2015. Sulfate radical-based water treatment in presence of chloride: Formation of chlorate, inter-conversion of sulfate radicals into hydroxyl radicals and influence of bicarbonate. *Water Research*, 72, 349-360.
- MAIER, M. P., DE CORTE, S., NITSCHKE, S., SPAETT, T., BOON, N. & ELSNER, M. 2014. C & N isotope analysis of diclofenac to distinguish oxidative and reductive transformation and to track commercial products. *Environmental Science and Technology*, 48, 2312-2320.
- MAIER, M. P., PRASSE, C., PATI, S. G., NITSCHKE, S., LI, Z., RADKE, M., MEYER, A., HOFSTETTER, T. B., TERNES, T. A. & ELSNER, M. 2016. Exploring trends of C and N isotope fractionation to trace transformation reactions of diclofenac in natural and engineered systems. *Environmental Science & Technology*, 50, 10933-10942.
- MCKENZIE, K. S., SARR, A. B., MAYURA, K., BAILEY, R. H., MILLER, D. R., ROGERS, T. D., NORRED, W. P., VOSS, K. A., PLATTNER, R. D., KUBENA, L. F. & PHILLIPS, T. D. 1997. Oxidative degradation and detoxification of mycotoxins using a novel source of ozone. *Food and Chemical Toxicology*, 35, 807-820.
- MELSBACH, A., PONSIN, V., TORRENTÓ, C., LIHL, C., HOFSTETTER, T. B., HUNKELER, D. & ELSNER, M. 2019. <sup>13</sup>C- and <sup>15</sup>N-isotope analysis of desphenylchloridazon by liquid chromatography–isotope-ratio mass spectrometry and derivatization gas chromatography–isotope-ratio mass spectrometry. *Analytical Chemistry*, 91, 3412-3420.
- MERÉNYI, G., LIND, J., NAUMOV, S. & SONNTAG, C. V. 2010a. Reaction of ozone with hydrogen peroxide (peroxone process): A revision of current mechanistic concepts based on thermokinetic and quantum-chemical considerations. *Environmental Science & Technology*, 44, 3505-3507.
- MERÉNYI, G., LIND, J., NAUMOV, S. & VON SONNTAG, C. 2010b. The reaction of ozone with the hydroxide ion: mechanistic considerations based on



- thermokinetic and quantum chemical calculations and the role of HO<sub>4</sub><sup>-</sup> in superoxide dismutation. *Chemistry – A European Journal*, 16, 1372-1377.
- MORTIMER, C. E. & MÜLLER, U. 2010. *Chemie : das Basiswissen der Chemie*, Stuttgart [u.a.], Thieme.
- MVULA, E. & VON SONNTAG, C. 2003. Ozonolysis of phenols in aqueous solution. *Organic & Biomolecular Chemistry*, 1, 1749-1756.
- NAPOLITANO, M. J., GREEN, B. J., NICOSON, J. S. & MARGERUM, D. W. 2005. Chlorine dioxide oxidations of tyrosine, N-acetyltyrosine, and dopa. *Chemical Research in Toxicology*, 18, 501-508.
- NAPOLITANO, M. J., STEWART, D. J. & MARGERUM, D. W. 2006. Chlorine dioxide oxidation of guanosine 5'-monophosphate. *Chemical Research in Toxicology*, 19, 1451-1458.
- NETA, P., HUIE, R. E. & ROSS, A. B. 1988. Rate constants for reactions of inorganic radicals in aqueous solution. *Journal of Physical and Chemical Reference Data*, 17, 1027-1284.
- NIKA, M. C., BLETSSOU, A. A., KOUMAKI, E., NOUTSOPOULOS, C., MAMAI, D., STASINAKIS, A. S. & THOMAIDIS, N. S. 2017. Chlorination of benzothiazoles and benzotriazoles and transformation products identification by LC-HR-MS/MS. *Journal of Hazardous Materials*, 323, 400-413.
- NÖTHER, T., FAHLENKAMP, H. & VON SONNTAG, C. 2009. Ozonation of wastewater: rate of ozone consumption and hydroxyl radical yield. *Environmental Science & Technology*, 43, 5990-5995.
- OKAZAKI, S., SUGIMITSU, H., NIWA, H., KOGOMA, M., MORIWAKI, T. & INOMATA, T. 1988. Ozone formation from the reaction of O<sub>2</sub>-activated N<sub>2</sub> molecules and a new type of ozone generator with fine wire electrode. *Ozone: Science & Engineering*, 10, 137-151.
- PAN, Y. & ZHANG, X. 2013. Four groups of new aromatic halogenated disinfection byproducts: effect of bromide concentration on their formation and speciation in chlorinated drinking water. *Environmental Science & Technology*, 47, 1265-1273.
- PATTISON, D. I. & DAVIES, M. J. 2001. Absolute rate constants for the reaction of hypochlorous acid with protein side chains and peptide bonds. *Chemical Research in Toxicology*, 14, 1453-1464.
- PEINTLER, G., NAGYPAL, I. & EPSTEIN, I. R. 1990. Systematic design of chemical oscillators. 60. Kinetics and mechanism of the reaction between chlorite ion and hypochlorous acid. *The Journal of Physical Chemistry*, 94, 2954-2958.
- PENNING, H., SØRENSEN, S. R., MEYER, A. H., AAMAND, J. & ELSNER, M. 2010. C, N, and H isotope fractionation of the herbicide Isoproturon reflects different microbial transformation pathways. *Environmental Science & Technology*, 44, 2372-2378.
- PETROVIC, M., PETROVIC, M. & BARCELÓ, D. 2007. LC-MS for identifying photodegradation products of pharmaceuticals in the environment. *TrAC Trends in Analytical Chemistry*, 26, 486-493.
- PINKERNELL, U. & VON GUNTEN, U. 2001. Bromate minimization during ozonation: Mechanistic considerations. *Environmental Science & Technology*, 35, 2525-2531.
- PRASSE, C. & TERNES, T. A. 2016. Chapter 9 - Application of orbitrap mass spectrometry for the identification of transformation products of trace organic contaminants formed in the environment. In: PÉREZ, S., EICHHORN, P. & BARCELÓ, D. (eds.) *Comprehensive Analytical Chemistry*. Elsevier.

- 
- PURSCHKE, K., ZOELL, C., LEONHARDT, J., WEBER, M. & SCHMIDT, T. C. 2020. Identification of unknowns in industrial wastewater using offline 2D chromatography and non-target screening. *Science of The Total Environment*, 706, 135835.
- RAMSEIER, M. K., PETER, A., TRABER, J. & VON GUNTEN, U. 2011. Formation of assimilable organic carbon during oxidation of natural waters with ozone, chlorine dioxide, chlorine, permanganate, and ferrate. *Water Research*, 45, 2002-2010.
- RAMSEIER, M. K. & VON GUNTEN, U. 2009. Mechanisms of phenol ozonation—kinetics of formation of primary and secondary reaction products. *Ozone: Science & Engineering*, 31, 201-215.
- RATTI, M., CANONICA, S., MCNEILL, K., BOLOTIN, J. & HOFSTETTER, T. B. 2015a. Isotope fractionation associated with the photochemical dechlorination of chloroanilines. *Environmental Science and Technology*, 49, 9797-9806.
- RATTI, M., CANONICA, S., MCNEILL, K., ERICKSON, P. R., BOLOTIN, J. & HOFSTETTER, T. B. 2015b. Isotope fractionation associated with the direct photolysis of 4-chloroaniline. *Environmental Science and Technology*, 49, 4263-4273.
- RAV-ACHA, C. 1984. The reactions of chlorine dioxide with aquatic organic materials and their health effects. *Water Research*, 18, 1329-1341.
- RAV-ACHA, C. H. & BLITS, R. 1985. The different reaction mechanisms by which chlorine and chlorine dioxide react with polycyclic aromatic hydrocarbons (PAH) in water. *Water Research*, 19, 1273-1281.
- REINNICKE, S., BERNSTEIN, A. & ELSNER, M. 2010. Small and reproducible isotope effects during methylation with trimethylsulfonium hydroxide (TMSH): A convenient derivatization method for isotope analysis of negatively charged molecules. *Analytical Chemistry*, 82, 2013-2019.
- REISZ, E., FISCHBACHER, A., NAUMOV, S., VON SONNTAG, C. & SCHMIDT, T. C. 2014. Hydride transfer: A dominating reaction of ozone with tertiary butanol and formate ion in aqueous solution. *Ozone: Science and Engineering*, 36, 532-539.
- REUNGOAT, J., ESCHER, B. I., MACOVA, M., ARGAUD, F. X., GERNJAK, W. & KELLER, J. 2012. Ozonation and biological activated carbon filtration of wastewater treatment plant effluents. *Water Research*, 46, 863-872.
- REUNGOAT, J., MACOVA, M., ESCHER, B. I., CARSWELL, S., MUELLER, J. F. & KELLER, J. 2010. Removal of micropollutants and reduction of biological activity in a full scale reclamation plant using ozonation and activated carbon filtration. *Water Research*, 44, 625-637.
- RICHARDSON, S. D. & KIMURA, S. Y. 2016. Water Analysis: Emerging contaminants and current issues. *Analytical Chemistry*, 88, 546-582.
- ROOK, J. J. 1977. Chlorination reactions of fulvic acids in natural waters. *Environmental Science & Technology*, 11, 478-482.
- ROSENBLATT, D. H., HULL, L. A., DE LUCA, D. C., DAVIS, G. T., WEGLEIN, R. C. & WILLIAMS, H. K. R. 1967. Oxidations of amines. II. Substituent effects in chlorine dioxide oxidations. *Journal of the American Chemical Society*, 89, 1158-1163.
- SCHLÜSENER, M. P., KUNKEL, U. & TERNES, T. A. 2015. Quaternary triphenylphosphonium compounds: A new class of environmental pollutants. *Environmental Science & Technology*, 49, 14282-14291.

- SCHMIDT, T. C. & JOCHMANN, M. A. 2012. Origin and fate of organic compounds in water: characterization by compound-specific stable isotope analysis. *Annual Review of Analytical Chemistry*, 5, 133-155.
- SCHREGLMANN, K., HOECHE, M., STEINBEISS, S., REINNICKE, S. & ELSNER, M. 2013. Carbon and nitrogen isotope analysis of atrazine and desethylatrazine at sub-microgram per liter concentrations in groundwater. *Analytical and Bioanalytical Chemistry*, 405, 2857-2867.
- SCHREIBER, I. M. & MITCH, W. A. 2005. Influence of the order of reagent addition on NDMA formation during chloramination. *Environmental Science & Technology*, 39, 3811-3818.
- SCHWARZENBACH, R. P., ESCHER, B. I., FENNER, K., HOFSTETTER, T. B., JOHNSON, C. A., VON GUNTEN, U. & WEHRLI, B. 2006. The challenge of micropollutants in aquatic systems. *Science*, 313, 1072-1077.
- SCHYMANSKI, E. L., SINGER, H. P., SLOBODNIK, J., IPOLYI, I. M., OSWALD, P., KRAUSS, M., SCHULZE, T., HAGLUND, P., LETZEL, T., GROSSE, S., THOMAIDIS, N. S., BLETSOU, A., ZWIENER, C., IBÁÑEZ, M., PORTOLÉS, T., DE BOER, R., REID, M. J., ONGHENA, M., KUNKEL, U., SCHULZ, W., GUILLON, A., NOYON, N., LEROY, G., BADOS, P., BOGIALLI, S., STIPANIČEV, D., ROSTKOWSKI, P. & HOLLENDER, J. 2015. Non-target screening with high-resolution mass spectrometry: critical review using a collaborative trial on water analysis. *Analytical and Bioanalytical Chemistry*, 407, 6237-6255.
- SEHESTED, K. & HOLCMAN, J. 1996. A pulse radiolysis study of the OH radical induced autoxidation of methanesulfinic acid. *Radiation Physics and Chemistry*, 47, 357-360.
- SEHESTED, K., HOLCMAN, J., BJERGBAKKE, E. & HART, E. J. 1984. A pulse radiolytic study of the reaction hydroxyl+ ozone in aqueous medium. *The Journal of Physical Chemistry*, 88, 4144-4147.
- SEHESTED, K., HOLCMAN, J. & HART, E. J. 1983. Rate constants and products of the reactions of e-aq, dioxide(1-) (O<sub>2</sub><sup>-</sup>) and proton with ozone in aqueous solutions. *The Journal of Physical Chemistry*, 87, 1951-1954.
- SHAH, A. D., LIU, Z.-Q., SALHI, E., HÖFER, T. & VON GUNTEN, U. 2015. Peracetic acid oxidation of saline waters in the absence and presence of H<sub>2</sub>O<sub>2</sub>: Secondary oxidant and disinfection byproduct formation. *Environmental Science & Technology*, 49, 1698-1705.
- SHEN, X., LIND, J. & MERENYI, G. 1987. One-electron oxidation of indoles and acid-base properties of the indolyl radicals. *The Journal of Physical Chemistry*, 91, 4403-4406.
- SINGER, P. C. & GUROL, M. D. 1983. Dynamics of the ozonation of phenol—I. Experimental observations. *Water Research*, 17, 1163-1171.
- SKARPELI-LIATI, M., JISKRA, M., TURGEON, A., GARR, A. N., ARNOLD, W. A., CRAMER, C. J., SCHWARZENBACH, R. P. & HOFSTETTER, T. B. 2011. Using nitrogen isotope fractionation to assess the oxidation of substituted anilines by manganese oxide. *Environmental Science & Technology*, 45, 5596-5604.
- SPAHR, S., CIRPKA, O. A., VON GUNTEN, U. & HOFSTETTER, T. B. 2017a. Formation of N-nitrosodimethylamine during chloramination of secondary and tertiary amines: Role of molecular oxygen and radical intermediates. *Environmental Science & Technology*, 51, 280-290.

- SPAHR, S., VON GUNTEN, U. & HOFSTETTER, T. B. 2017b. Carbon, hydrogen, and nitrogen isotope fractionation trends in N-nitrosodimethylamine reflect the formation pathway during chloramination of tertiary amines. *Environmental Science and Technology*, 51, 13170-13179.
- STAEHELIN, J. & HOIGNE, J. 1982. Decomposition of ozone in water: rate of initiation by hydroxide ions and hydrogen peroxide. *Environmental Science & Technology*, 16, 676-681.
- STEINER, M. G. & BABBS, C. F. 1990. Quantitation of the hydroxyl radical by reaction with dimethyl sulfoxide. *Archives of Biochemistry and Biophysics*, 278, 478-481.
- STEVENSON, I. L. & SCHNITZER, M. 1982. Transmission electron microscopy of extracted fulvic and humic acids. *Soil Science*, 133, 179-185.
- STEWART, D. J., NAPOLITANO, M. J., BAKHMUTOVA-ALBERT, E. V. & MARGERUM, D. W. 2008. Kinetics and mechanisms of chlorine dioxide oxidation of tryptophan. *Inorganic Chemistry*, 47, 1639-1647.
- TEE, O. S., PAVENTI, M. & BENNETT, J. M. 1989. Kinetics and mechanism of the bromination of phenols and phenoxide ions in aqueous solution. Diffusion-controlled rates. *Journal of the American Chemical Society*, 111, 2233-2240.
- TEKLE-RÖTTERING, A., JEWELL, K. S., REISZ, E., LUTZE, H. V., TERNES, T. A., SCHMIDT, W. & SCHMIDT, T. C. 2016a. Ozonation of piperidine, piperazine and morpholine: Kinetics, stoichiometry, product formation and mechanistic considerations. *Water Research*, 88, 960-971.
- TEKLE-RÖTTERING, A., VON SONNTAG, C., REISZ, E., EYSER, C. V., LUTZE, H. V., TÜRK, J., NAUMOV, S., SCHMIDT, W. & SCHMIDT, T. C. 2016b. Ozonation of anilines: Kinetics, stoichiometry, product identification and elucidation of pathways. *Water Research*, 98, 147-159.
- TENTSCHER, P. R., BOURGIN, M. & VON GUNTEN, U. 2018. Ozonation of para-substituted phenolic compounds yields p-benzoquinones, other cyclic  $\alpha,\beta$ -unsaturated ketones, and substituted catechols. *Environmental Science & Technology*, 52, 4763-4773.
- TORRENTÓ, C., BAKKOUR, R., GLAUSER, G., MELSBACH, A., PONSIN, V., HOFSTETTER, T. B., ELSNER, M. & HUNKELER, D. 2019. Solid-phase extraction method for stable isotope analysis of pesticides from large volume environmental water samples. *Analyst*, 144, 2898-2908.
- TRATNYEK, P. G. & HOIGNÉ, J. 1994. Kinetics of reactions of chlorine dioxide (OCIO) in water—II. Quantitative structure-activity relationships for phenolic compounds. *Water Research*, 28, 57-66.
- UHLMANN, H. 2012. *Verfahren zur Herstellung einer wässrigen stabilen Chlordioxidlösung*.
- USEPA 1999. Alternative disinfections and oxidants guidance manual. *US Environmental Protection Agency - Office of water*, EPA 815-R-99-014.
- VELTWISCH, D., JANATA, E. & ASMUS, K. D. 1980. Primary processes in the reaction of OH $\cdot$ -radicals with sulphoxides. *Journal of the Chemical Society, Perkin Transactions 2*, 146-153.
- VON GUNTEN, U. 2003a. Ozonation of drinking water: Part I. Oxidation kinetics and product formation. *Water Research*, 37, 1443-1467.
- VON GUNTEN, U. 2003b. Ozonation of drinking water: Part II. Disinfection and by-product formation in presence of bromide, iodide or chlorine. *Water Research*, 37, 1469-1487.
- VON GUNTEN, U. 2018. Oxidation processes in water treatment: Are we on track? *Environmental Science & Technology*, 52, 5062-5075.

- VON SONNTAG, C., DOWIDEIT, P., FANG, X., MERTENS, R., PAN, X., SCHUCHMANN, M. N. & SCHUCHMANN, H. P. 1997a. The fate of peroxy radicals in aqueous solution. *Water Science and Technology*.
- VON SONNTAG, C., DOWIDEIT, P., XINGWANG, F., MERTENS, R., XIANMING, P., SCHUCHMANN, M. N. & SCHUCHMANN, H.-P. 1997b. The fate of peroxy radicals in aqueous solution. *Water Science and Technology*, 35, 9-15.
- VON SONNTAG, C. & VON GUNTEN, U. 2012. *Chemistry of ozone in water and wastewater treatment*, IWA publishing.
- WAJON, J. E., ROSENBLATT, D. H. & BURROWS, E. P. 1982. Oxidation of phenol and hydroquinone by chlorine dioxide. *Environmental Science & Technology*, 16, 396-402.
- WANG, P., HE, Y.-L. & HUANG, C.-H. 2010. Oxidation of fluoroquinolone antibiotics and structurally related amines by chlorine dioxide: Reaction kinetics, product and pathway evaluation. *Water Research*, 44, 5989-5998.
- WENK, J., AESCHBACHER, M., SALHI, E., CANONICA, S., VON GUNTEN, U. & SANDER, M. 2013. Chemical oxidation of dissolved organic matter by chlorine dioxide, chlorine, and ozone: Effects on its optical and antioxidant properties. *Environmental Science & Technology*, 47, 11147-11156.
- WHO 2017. Guidelines for drinking-water quality: fourth edition incorporating the first addendum. Licence: CC BY-NC-SA 3.0 IGO.
- WIJKER, R. S., KURT, Z., SPAIN, J. C., BOLOTIN, J., ZEYER, J. & HOFSTETTER, T. B. 2013. Isotope fractionation associated with the biodegradation of 2- and 4-nitrophenols via monooxygenation pathways. *Environmental Science & Technology*, 47, 14185-14193.
- WILLACH, S., LUTZE, H. V., ECKEY, K., LÖPPENBERG, K., LÜLING, M., TERHALLE, J., WOLBERT, J.-B., JOCHMANN, M. A., KARST, U. & SCHMIDT, T. C. 2017. Degradation of sulfamethoxazole using ozone and chlorine dioxide - Compound-specific stable isotope analysis, transformation product analysis and mechanistic aspects. *Water Research*, 122, 280-289.
- WILLACH, S., LUTZE, H. V., SOMNITZ, H., TERHALLE, J., STOJANOVIC, N., LÜLING, M., JOCHMANN, M. A., HOFSTETTER, T. B. & SCHMIDT, T. C. 2020. Carbon isotope fractionation of substituted benzene analogs during oxidation with ozone and hydroxyl radicals: How should experimental data be interpreted? *Environmental Science and Technology*, 54, 6713-6722.
- WILLE, A., PROOST, R. & STEINBACH, A. 2010. Spurenbestimmung von Bromat in Wasser. *Österreichische Wasser- und Abfallwirtschaft*, 62, a27-a30.
- YANG, X., GUO, W. & LEE, W. 2013. Formation of disinfection byproducts upon chlorine dioxide preoxidation followed by chlorination or chloramination of natural organic matter. *Chemosphere*, 91, 1477-1485.
- ZWANK, L., BERG, M., SCHMIDT, T. C. & HADERLEIN, S. B. 2003. Compound-specific carbon isotope analysis of volatile organic compounds in the low-microgram per liter range. *Analytical Chemistry*, 75, 5575-5583.

## **8. Chapter: Appendix**

## 8.1 List of Figures

Figure 1.1: Relative contribution of the various water solutes to the consumption of oxidants. Micropollutants is another word for TrOCs (von Gunten, 2018). .....	3
Figure 1.2: Hypothetic structure of a part of dissolved organic matter (Stevenson and Schnitzer, 1982).....	4
Figure 1.3: Example plot of the determination of reaction rate constant $k$ of the reaction of $\text{ClO}_2$ with phenol ( $\text{pH} = 1.03$ ; $c(\text{phenol}) = 3 \times 10^{-2} \text{ M}$ ; $c_0(\text{ClO}_2) = 3 \times 10^{-4} \text{ M}$ ; $c(\text{sulfur acid buffer}) = 1 \times 10^{-1} \text{ M}$ ; $T = 25^\circ\text{C}$ ). .....	10
Figure 2.1: Graphical overview of the major content of this work. ....	17
Figure 3.1: Yield of bromophenols per HOCl consumed. A: $60 \mu\text{M}$ HOCl was added to the solution of phenol ( $1.0 \times 10^{-3} \text{ M}$ ) and bromide ( $1.0 \times 10^{-2} \text{ M}$ ). B: the solution of phenol ( $1.0 \times 10^{-3} \text{ M}$ ) and bromide ( $1.0 \times 10^{-2} \text{ M}$ ) was added to the solution of HOCl with a concentration of $60 \mu\text{M}$ . C: The solution of phenol ( $6.0 \times 10^{-3} \text{ M}$ ) and bromide ( $6.0 \times 10^{-2} \text{ M}$ ) was added to the solution of HOCl with a concentration of $60 \mu\text{M}$ ( $\text{pH} = 4.00 \pm 0.05$ ). .....	26
Figure 3.2: a) Yield of chlorite and hypochlorous acid and b) yield of chlorite and chloride in the reaction of phenol with $\text{ClO}_2$ in presence of bromide at $\text{pH} 4.00$ ( $[\text{phenol}] = 1 \times 10^{-3} \text{ M}$ , $[\text{bromide}] = 1 \times 10^{-2} \text{ M}$ , $[\text{phosphate buffer}] = 5 \times 10^{-3} \text{ M}$ , different $\text{ClO}_2$ dosages, $T = 25^\circ\text{C}$ , in ultrapure water). The horizontal lines mark the 100 % yield and the error bars are the standard deviation of the triplicates. ....	28
Figure 3.3: Transformation of atenolol by $\text{ClO}_2$ in absence (circles) and presence (triangles) of glycine. The predicted value was calculated with equation 1 and the exposure of $\text{ClO}_2$ (star) (dashed line: linear regression forced through $x/y = 0/1$ , $[\text{atenolol}]_0 = 1 \times 10^{-6} \text{ M}$ , $[\text{glycine}] = 5 \times 10^{-4} \text{ M}$ , $\text{DOC} = 8.11 \pm 0.12 \text{ mg L}^{-1}$ ; $[\text{NH}_3] < 0.1 \text{ mg L}^{-1}$ ; $\text{pH} = 7.90 \pm 0.05$ , $T = 22^\circ\text{C}$ , error bars are the standard deviation of the triplicates, recovery = $99 \pm 5 \%$ , reaction time $> 24 \text{ h}$ ). ....	31
Figure 3.4: a) Transformation of micropollutants in wastewater after different $\text{ClO}_2$ dosage and formation of chlorite (absence of glycine). b) Transformation of micropollutants in wastewater after different $\text{O}_3$ dosages and formation of bromate ( $[\text{micropollutant}]_0 = 1 \times 10^{-6} \text{ M}$ , $\text{DOC} = 8.3 \pm 1 \text{ mg L}^{-1}$ , $\text{pH} = 7.80 \pm 0.05$ , $T = 20^\circ\text{C}$ , $[\text{Br}^-]_0 = 225.5 \pm 2.7 \mu\text{g L}^{-1}$ $[\text{NH}_3] < 0.1 \text{ mg L}^{-1}$ , error bars are the standard deviation of the triplicates; recovery rate = 82 – 102 %). Filled squares show the concentration of formed chlorite (4a) and bromate (4b).....	34
Figure 3.5: Reaction mechanism of the reaction between phenol and chlorine dioxide (modified from Wajon et al. (1982)).....	36

Figure 3.6: Apparatus for ClO <sub>2</sub> production (bottle No.3: 50 mL 0.885 M NaClO <sub>2</sub> + 50 mL Na <sub>2</sub> S <sub>2</sub> O <sub>8</sub> ; bottle No. 4: 100 mL 0.111 M NaClO <sub>2</sub> ).....	40
Figure 3.7: Structure of the organic compounds under study. ....	41
Figure 3.8: Formation of bromophenols in reaction of ClO <sub>2</sub> with phenol in the presence of bromide.....	42
Figure 3.9: Reaction of indigo trisulfonate with chlorine dioxide and ozone.....	46
Figure 3.10: Experimental approach for the depletion experiment of ClO <sub>2</sub> . ....	47
Figure 3.11: Calibration of indigo trisulfonate method for ClO <sub>2</sub> determination (grey area = 95 % confidence interval). ....	47
Figure 3.12: Formation of the bromophenols by the reaction of phenol + bromide + ClO <sub>2</sub> at pH 7.00 ([phenol] = 1 × 10 <sup>-3</sup> M; [bromide] = 1 × 10 <sup>-2</sup> M; [phosphate-buffer] = 5 × 10 <sup>-3</sup> M; different ClO <sub>2</sub> dose) .....	49
Figure 3.13: Formation of the bromophenols by the reaction of phenol + bromide + ClO <sub>2</sub> at pH 4.00 ([phenol] = 1 × 10 <sup>-3</sup> M; [bromide] = 1 × 10 <sup>-2</sup> M; [phosphate-buffer] = 5 × 10 <sup>-3</sup> M; different ClO <sub>2</sub> dose) .....	49
Figure 3.14: Yield of the bromophenols in the reaction of phenol with HOCl in presence of bromide at pH 4.00 without addition of glycine ([phenol] = 1 × 10 <sup>-3</sup> M, [bromide] = 1 × 10 <sup>-2</sup> M; [phosphate buffer] = 1 × 10 <sup>-3</sup> M, pH = 4, T = 20 °C). The horizontal line marks the 100 % yield, 2-bromophenols were found but the values are below the limit of quantification = 10.89 μM. ....	50
Figure 3.15: Yield of bromophenols at the dosage of phenol and bromide to HOCl dilutions (final concentrations [phenol] = 1.0 × 10 <sup>-3</sup> M and [bromide] = 1.0 × 10 <sup>-2</sup> M; HOCl concentration ranged between 2.0 × 10 <sup>-5</sup> – 1.2 × 10 <sup>-4</sup> M; pH = 4,00).....	50
Figure 3.16: Yield of bromophenols at the dosage of phenol and bromide to HOCl dilutions (final concentrations [phenol] = 6.0 × 10 <sup>-3</sup> M and [bromide] = 6.0 × 10 <sup>-2</sup> M; HOCl concentration ranged between 2.0 × 10 <sup>-5</sup> – 1.2 × 10 <sup>-4</sup> M; pH = 4,00).....	51
Figure 3.17: Depletion curve of a) 5 × 10 <sup>-5</sup> M ClO <sub>2</sub> and b) 1 × 10 <sup>-4</sup> M O <sub>3</sub> in wastewater. Oxidant concentration was determined with the indigo method. The marked area below the depletion curve represents the exposure of ClO <sub>2</sub> (3.2 × 10 <sup>-2</sup> M × s) and O <sub>3</sub> (2.0 × 10 <sup>-3</sup> M × s) (pH = 7.90 ± 0.05, DOC = 8.11 ± 0.12 mg L <sup>-1</sup> , T = 22°C). ....	52
Figure 3.18: Depletion curves of three initial chlorine dioxide concentrations in the present wastewater. Chlorine dioxide concentration was determined by indigo method (pH = 7.90 ± 0.05; T = 22°C).....	52



Figure 3.19: Depletion curve of three initial ozone concentration in the present wastewater. Ozone concentration was determined by indigo method (pH = 7.90 ± 0.05; T = 22°C). .....	53
Figure 3.20: Ratio of the micropollutant transformation related to reactions with HOCl and to reactions with ClO <sub>2</sub> (ATL= atenolol; MET = metoprolol; CIP = ciprofloxacin; SMX = sulfamethoxazole). .....	53
Figure 3.21: Transformation of metoprolol with ClO <sub>2</sub> in absence (circles) and in presence of glycine (triangles). The calculated values were calculated with equation 1 (main text) (star), dashed line: linear regression forced through x/y = 0/1 ([metoprolol] <sub>0</sub> = 1 × 10 <sup>-6</sup> M, pH = 7.90 ± 0.05, T = 22°C, recovery = 92 ± 8 %). .....	54
Figure 3.22: Transformation of sulfamethoxazole with ClO <sub>2</sub> in absence (circles) and in presence of glycine (triangles). The predicted degradation was calculated with equation 1 (main text) (star), dashed line: linear regression forced through x/y = 0/1 ([SMX] <sub>0</sub> = 1 × 10 <sup>-6</sup> M, DOC = 8.11 ± 0.12 mg L <sup>-1</sup> , pH = 7.90 ± 0.05, T = 22°C, recovery = 99 ± 1 %). .....	54
Figure 3.23: Transformation of 5,6-dimethyl-1- <i>H</i> -benzotriazol with ClO <sub>2</sub> in absence (circles) and in presence of glycine (triangles). The predicted degradation was calculated with equation 1 (main text) (star), dashed line: linear regression forced through x/y = 0/1 ([DMBT] <sub>0</sub> = 1 × 10 <sup>-6</sup> M, DOC = 8.11 ± 0.12 mg L <sup>-1</sup> , pH = 7.90 ± 0.05, T = 22°C; recovery = 98 ± 5 %). .....	55
Figure 4.1: Reaction steps of ozone with phenol at <i>para</i> -position; Further reaction to adduct formation (2), superoxide formation (3), singlet oxygen formation (4) and electron transfer reaction (5 and 6) (modified from Mvula and von Sonntag (2003)). .....	58
Figure 4.2: Ozone-consuming chain reaction due to reformation of phenolate per reaction of the phenoxyl radical with the hydroquinone anion (modified from Mvula and von Sonntag (2003)) .....	59
Figure 4.3: Fraction of phenol (red line) and phenolate (blue line) at different pH values. Additionally, the reacting fraction of O <sub>3</sub> with phenol (pink line) and phenolate (green line) is shown. The crossing point of the fractions shows the p <i>K</i> <sub>a</sub> value, and the crossing point of the reacting fraction is called the reactivity-p <i>K</i> <sub>a</sub> . The <i>k</i> <sub>obs</sub> is plotted on a logarithmic scale against the pH values (orange line). .....	62
Figure 4.4: The O <sub>3</sub> consumption in the reaction with phenol at different pH values, different OH radicals scavengers, and different dosages. Normal dosage is the addition of O <sub>3</sub> to the reaction solution of phenol, phosphate buffer, and <i>tert.</i> -BuOH. Reverse order dosage: Adding the reaction solution of phenol, phosphate buffer, and <i>tert.</i> -BuOH to a mixture of O <sub>3</sub> , phosphate buffer, and <i>tert.</i> -BuOH. Superoxide test: Using methanol instead of <i>tert.</i> -BuOH as OH radical scavenger. ....	66

- Figure 4.5: O<sub>3</sub> consumption during the reaction of O<sub>3</sub> with phenol (stars), 4-chlorophenol (triangle), 4-methylphenol (square), and 4-methoxyphenol (circle) at different pH values. A: in the presence of *tert.*-BuOH and B: In the absence of *tert.*-BuOH. .... 68
- Figure 4.6: Observed reaction rate constant ( $k_{\text{obs}}$ ) of phenol and catechol vs. pH. Red lines present the pH values under study..... 70
- Figure 4.7: Fraction of 4-chlorophenol (red line) and the fraction of 4-chlorophenolate (blue line) at different pH values. Additionally, the reacting fraction of ozone with neutral species (pink line) and anionic species (green line) is shown. The crossing point of the fractions shows the  $pK_a$  value and the crossing point of the reacting fraction are called the reactivity- $pK_a$ . The  $k_{\text{obs}}$  is plotted on a logarithmic scale against the pH values (orange line). .... 76
- Figure 4.8: Fraction of 4-methylphenol (red line) and the fraction of 4-methylphenolate (blue line) at different pH values. Additionally, the reacting fraction of ozone with neutral species (pink line) and anionic species (green line) is shown. The crossing point of the fractions shows the  $pK_a$  value and the crossing point of the reacting fraction are called the reactivity- $pK_a$ . The  $k_{\text{obs}}$  is plotted on a logarithmic scale against the pH values (orange line). .... 76
- Figure 4.9: Fraction of 4-methoxyphenol (red line) and the fraction of 4-methoxyphenolate (blue line) at different pH values. Additionally, the reacting fraction of ozone with neutral species (pink line) and anionic species (green line) is shown. The crossing point of the fractions shows the  $pK_a$  value and the crossing point of the reacting fraction are called the reactivity- $pK_a$ . The  $k_{\text{obs}}$  is plotted on a logarithmic scale against the pH values (orange line). .... 77
- Figure 4.10: Concentration of OH radicals plotted against ozone concentration at pH 2. OH radicals were determined by DMSO-method (see above). .... 77
- Figure 4.11: Concentration of OH radicals plotted against ozone concentration at pH 7. OH radicals were determined by DMSO-method (see above). .... 78
- Figure 4.12: Concentration of OH radicals plotted against ozone concentration at pH 11. OH radicals were determined by DMSO-method (see above). .... 78
- Figure 5.1: A) Reaction rate constants of phenol with ozone in the presence of *tert.*-BuOH at pH 7. Determined by competition kinetics method with 4-methylphenol as a competitor (red circles: unlabeled phenol, blue triangles: fully <sup>13</sup>C-labeled phenol ( $c_0(\text{phenol}) = 10 \mu\text{M}$ ,  $c_0(4\text{-methylphenol}) = 10 \mu\text{M}$ ,  $c(\text{O}_3) = 0 - 60 \mu\text{M}$ ,  $c(\text{phosphate buffer}) = 10 \text{mM}$ ,  $c(\text{tert.}-\text{BuOH}) = 30 \text{mM}$ ; the concentrations of phenol and 4-methylphenol were determined by HPLC-UV). B) Comparison of <sup>13</sup>C<sub>6</sub>-labeled phenol with unlabeled phenol at pH 2 (grey) and at pH 7 (black) ( $c_0(^{13}\text{C-phenol}) = 100 \mu\text{M}$ ,  $c_0(^{12}\text{C-phenol}) = 100 \mu\text{M}$ ,  $c(\text{O}_3) = 0 - 600 \mu\text{M}$ ;  $c(\text{phosphate buffer})$ )

= 10 mM; $c(\text{tert.}-\text{BuOH}) = 300 \text{ mM}$ ; concentrations of both phenols were determined by GC-MS).....	88
Figure 5.2: A) Change of the $\delta^{13}\text{C}$ -value during the reaction of phenol with ozone in the presence of <i>tert.</i> -butanol plotted vs the ozone concentration at different pH values (the measured value of the sample without ozone was set to zero; Rayleigh plots are shown in SI) B) Enrichment factor ( $\epsilon$ ) at different pH values for the reaction of phenol with ozone in the presence of <i>tert.</i> -butanol. The dashed line represents the $\epsilon$ calculated with Equation 5.4 and has a deviation of 3% to the determined values. The red line represents the fraction of ozone that reacts with phenolate. $\text{rp}K_a$ marked the reactivity $\text{p}K_a$ of the reaction of phenol with $\text{O}_3$ ( $c_0(\text{phenol}) = 0.15 \text{ mM}$ , $c_0(\text{tert.}-\text{BuOH}) = 125 \text{ mM}$ , $c(\text{ozone}) = 0.05 - 0.30 \text{ mM}$ and $c(\text{phosphate buffer}) = 10 \text{ mM}$ . The isotope ratio of phenol was measured by GC-IRMS, mean values of the triplicates are presented).....	89
Figure 5.3: Enrichment factors plotted against observed reaction rate constants of all compounds under study with ozone in presence of <i>tert.</i> -BuOH in comparison to literature data ((1)Maier et al. (2016), (2)Willach et al. (2020) (3)Willach et al. (2017)). Experimental conditions for phenol: $c_0(\text{phenol}) = 0.15 \text{ mM}$ , $c_0(\text{tert.}-\text{BuOH}) = 125 \text{ mM}$ , $c(\text{ozone}) = 0.05 - 0.30 \text{ mM}$ and $c(\text{phosphate buffer}) = 10 \text{ mM}$ . For 4-chlorophenol: $c_0(4\text{-chlorophenol}) = 0.50 \text{ mM}$ , $c_0(\text{tert.}-\text{BuOH}) = 125 \text{ mM}$ , $c(\text{ozone}) = 0.15 - 0.90 \text{ mM}$ , $c(\text{phosphate buffer}) = 10 \text{ mM}$ . For 4-methylphenol: $c_0(4\text{-methylphenol}) = 0.50 \text{ mM}$ , $c_0(\text{tert.}-\text{BuOH}) = 195 \text{ mM}$ , $c(\text{ozone}) = 0.15 - 0.90 \text{ mM}$ , $c(\text{phosphate buffer}) = 10 \text{ mM}$ . For 4-methoxyphenol: $c_0(4\text{-methoxyphenol}) = 0.50 \text{ mM}$ , $c_0(\text{tert.}-\text{BuOH}) = 195 \text{ mM}$ , $c(\text{ozone}) = 0.15 - 0.90 \text{ mM}$ , $c(\text{phosphate buffer}) = 10 \text{ mM}$ . The isotope ratios of phenol were measured by GC-IRMS and of 4-chlorophenol, 4-methylphenol and 4-methoxyphenol were measured by LC-IRMS.....	92
Figure 5.4: Reaction pathways of phenol with ozone (modified from Mvula and von Sonntag (2003)).....	94
Figure 5.5: Fraction of phenol (red line) and the fraction of phenolate (blue line) at different pH values. Additionally, the reacting fraction of $\text{O}_3$ with phenol (pink line) and phenolate (green line) is shown. The crossing point of the fractions shows the $\text{p}K_a$ value and the crossing point of the reacting fraction are called the reactivity- $\text{p}K_a$ . The $k_{\text{obs}}$ are plotted on a logarithmic scale against the pH values (orange line). .....	101
Figure 5.6: Fraction of 4-chlorophenol (red line) and the fraction of 4-chlorophenolate (blue line) at different pH values. Additionally, the reacting fraction of ozone with neutral species (pink line) and anionic species (green line) is shown. The crossing point of the fractions shows	

---

the $pK_a$ value and the crossing point of the reacting fraction are called the reactivity- $pK_a$ . The $k_{obs}$ are plotted on a logarithmic scale against the pH values (orange line). .....	101
Figure 5.7: Fraction of 4-methylphenol (red line) and the fraction of 4-methylphenolate (blue line) at different pH values. Additionally, the reacting fraction of ozone with neutral species (pink line) and anionic species (green line) is shown. The crossing point of the fractions shows the $pK_a$ value and the crossing point of the reacting fraction are called the reactivity- $pK_a$ . The $k_{obs}$ are plotted on a logarithmic scale against the pH values (orange line). .....	102
Figure 5.8: Fraction of 4-methoxyphenol (red line) and the fraction of 4-methoxyphenolate (blue line) at different pH values. Additionally, the reacting fraction of ozone with neutral species (pink line) and anionic species (green line) is shown. The crossing point of the fractions shows the $pK_a$ value and the crossing point of the reacting fraction are called the reactivity- $pK_a$ . The $k_{obs}$ are plotted on a logarithmic scale against the pH values (orange line). .....	102
Figure 5.9: GC oven parameter of the 3-buten-2-ol measurements (Inlet: temperature = 250 °C; Split flow = 20 mL min <sup>-1</sup> ; splitless time = 0.5 min; Purge: constant septum purge; Mode = splitless; constant carrier flow = 2.4 mL min <sup>-1</sup> ). .....	104
Figure 5.10: GC oven parameter of the 3-butyn-2-ol measurements (Inlet: temperature = 250 °C; Split flow = 20 mL min <sup>-1</sup> ; splitless time = 0.5 min; Purge: constant septum purge; Mode = splitless; constant carrier flow = 2.4 mL min <sup>-1</sup> ). .....	104
Figure 5.11: GC oven parameter of the phenol measurements (Inlet: temperature = 250 °C; Split flow = 20 mL min <sup>-1</sup> ; splitless time = 0.5 min; Purge: constant septum purge; Mode = splitless; constant carrier flow = 2.4 mL min <sup>-1</sup> ). .....	105
Figure 5.12: Rayleigh plot of the degradation of phenol with ozone with different ozone concentration at pH 2.3 (right) and 3.2 (left). ( $c_0(\text{phenol}) = 0.15$ mM, $c_0(\text{tert.-BuOH}) = 125$ mM, $c(\text{ozone}) = 0.05 - 0.30$ mM and $c(\text{phosphate buffer}) = 10$ mM. The isotope ratio of phenol was measured by GC-IRMS). The error of the slope is the 95% confidence interval. ....	105
Figure 5.13: Rayleigh plot of the degradation of phenol with ozone with different ozone concentration at pH 4.1 (right) and 4.9 (left). ( $c_0(\text{phenol}) = 0.15$ mM, $c_0(\text{tert.-BuOH}) = 125$ mM, $c(\text{ozone}) = 0.05 - 0.30$ mM and $c(\text{phosphate buffer}) = 10$ mM. The isotope ratio of phenol was measured by GC-IRMS). The error of the slope is the 95% confidence interval. ....	106
Figure 5.14: Rayleigh plot of the degradation of phenol with ozone with different ozone concentration at pH 6.0 (right) and 7.2 (left). ( $c_0(\text{phenol}) = 0.15$ mM, $c_0(\text{tert.-BuOH}) = 125$ mM, $c(\text{ozone}) = 0.05 - 0.30$ mM and $c(\text{phosphate buffer}) = 10$ mM. The isotope ratio of phenol was measured by GC-IRMS). The error of the slope is the 95% confidence interval. ....	106

- 
- Figure 5.15: Rayleigh plot of the degradation of phenol with ozone with different ozone concentration at pH 10.2. ( $c_0(\text{phenol}) = 0.15 \text{ mM}$ ,  $c_0(\text{tert.-BuOH}) = 125 \text{ mM}$ ,  $c(\text{ozone}) = 0.05 - 0.30 \text{ mM}$  and  $c(\text{phosphate buffer}) = 10 \text{ mM}$ . The isotope ratio of phenol was measured by GC-IRMS). The error of the slope is the 95% confidence interval..... 107
- Figure 5.16: Degradation of phenol with difference ozone concentration at pH 7.2 (left) and pH 10.2 (right). ( $c_0(\text{phenol}) = 0.15 \text{ mM}$ ,  $c_0(\text{tert.-BuOH}) = 125 \text{ mM}$ ,  $c(\text{ozone}) = 0.05 - 0.30 \text{ mM}$  and  $c(\text{phosphate buffer}) = 10 \text{ mM}$ . The isotope ratio of phenol was measured by GC-IRMS). ..... 107
- Figure 5.17: Calibration of phenol with GC-IRMS at pH 2.3, pH 7.2 and pH 10.2. Left y-axis shows the peak area and the right y-axis shows the delta value. The dash line represents the mean value of the delta values for all ozone concentration and the lines shows the  $\pm 0.5\%$  of the mean value. In Jochmann and Schmidt (2012) is the method detection limit the last concentration which delta value is in the range of  $0.5\%$ . After this method the MDL at pH 2 is  $0.025 \text{ mM}$ , at pH 7  $0.05 \text{ mM}$  and at pH 11  $0.02 \text{ mM}$ ..... 108

## 8.2 List of Tables

Table 3.1: Second order rate constants of the compounds under study at pH 8, exception DMBT pH 7* .....	29
Table 3.2: Chemicals and wastewater used in the present study .....	37
Table 3.3: Used equipment.....	38
Table 3.4: HPLC-UV methods.....	43
Table 3.5: IC- methods with the post-column reaction system (CD = Conductivity detector, n. a. = not applicable).....	45
Table 4.1: Moles of O <sub>3</sub> per mole degraded phenol at three different pH values. Right column: ratio of O <sub>3</sub> concentration to phenol concentration. ....	66
Table 4.2: Reaction rate constants of the compounds under study with O <sub>3</sub> at different pH values (upper part), the reaction rate constants of phenol products (organic and inorganic) with O <sub>3</sub> (middle part), and yield of the main products of the substances under study with O <sub>3</sub> at pH 7 (lower part); note that the reactivity pK <sub>a</sub> values of hydroquinone, catechol and cis,cis-muconic acid are > 10, hence k <sub>app</sub> hardly changes at the below given pH range (2-12).....	69
Table 4.3: Chemicals used in the present study .....	71
Table 4.4: Used equipment.....	72
Table 4.5: Structure, reaction rate constants and pK <sub>a</sub> values of the compounds under study..	74
Table 5.1: Chemicals used in the present study .....	95
Table 5.2: Used equipment.....	96
Table 5.3: Structure, reaction rate constants and pK <sub>a</sub> values of the compounds under study (Values from Tentscher et al. (2018)). ....	99
Table 5.4: Start concentration of the compounds at the different experiments (GC-IRMS and LC-IRMS: Isotopic fractionation; GC-MS: Competitions kinetic for labelled phenol; LC-UV: Competition kinetic for 4-methylphenol; 4-chlorophenol (CPh), 4-methylphenol (MePh); 4-methoxyphenol (MxPh)). ....	100
Table 5.5: Concentration of <i>tert.</i> -BuOH in the different experiments (GC-IRMS and LC-IRMS: Isotopic fractionation; GC-MS: Competitions kinetic for labelled phenol; LC-UV: Competition kinetic for 4-methylphenol; CPh = 4-chlorophenol; MePh = 4-methylphenol; MxPh = 4-methoxyphenol).....	100
Table 5.6: Final O <sub>3</sub> concentration in the different experiments (GC-IRMS and LC-IRMS: Isotopic fractionation; GC-MS: Competitions kinetic for labelled phenol; LC-UV: Competition	

kinetic for 4-methylphenol; CPh = 4-chlorphenol; MePh = 4-methylphenol; MxPh = 4-methoxyphenol)..... 103

---

### 8.3 List of Abbreviations

AC	activated carbon
AKIE	apparent kinetic isotope effect
AOP	advanced oxidative processes
ATL	atenolol
BDOC	biodegradable dissolved organic carbon
Br <sup>-</sup>	bromide
BrO <sub>3</sub> <sup>-</sup>	bromate
CIP	ciprofloxacin
Cl <sup>-</sup>	chloride
Cl <sub>2</sub>	chlorine
ClO <sub>2</sub>	chlorine dioxide
ClO <sub>2</sub> <sup>-</sup>	chlorite
ClO <sub>3</sub> <sup>-</sup>	chlorate
ClPh	4-chlorphenol
CO <sub>2</sub>	carbon dioxide
CSIA	compound specific stable isotope analysis
DBPs	disinfection by-products
DMBT	5,6-dimethyl-1-H-benzotriazol
DMSO	dimethyl sulfoxide
DOC	dissolved organic carbon
DOM	dissolved organic matter
GC	gas chromatography



---

H <sub>2</sub> O	water
H <sub>2</sub> O <sub>2</sub>	hydrogen peroxide
HCl	hydrochloric acid
HO <sub>2</sub> <sup>•</sup>	perhydroxyl radical
HOBr	hypobromous acid
HOCl	hypochlorous acid
HRMS	high-resolution mass spectrometry
I <sup>-</sup>	iodide
I <sub>3</sub> <sup>-</sup>	triiodide
IC	ion chromatography
IRMS	isotope ratio mass spectrometry
KIE	kinetic isotope effect
LC	liquid chromatography
LOQ	limit of quantification
M <sup>-</sup>	deprotonated species of M
MCL	maximum containment level
MeOH	methanol
MePh	4-methylphenol
MET	metoprolol
MH	protonated species of M
MSIA	methanesulfinic acid
MSOA	methanesulonic acid
MxPh	4-methoxyphenol

---

Na <sub>2</sub> S <sub>2</sub> O <sub>8</sub>	sodium persulfate
NaClO <sub>2</sub>	sodium chlorite
NaOCl	sodium hypochlorite
NDMA	N-Nitrosodimethylamine
NMR	nuclear magnetic resonance spectrometry
NPOC	non-purgeable organic carbon
O <sub>2</sub>	oxygen
O <sub>2</sub> <sup>•-</sup>	superoxide
O <sub>3</sub>	ozone
O <sub>3</sub> <sup>•-</sup>	ozonide radical anion
OCl <sup>-</sup>	hypochlorite anion
OH radicals	hydroxyl radicals
OH <sup>-</sup>	hydroxyl ion
ROD	reversed order dosage
rp <i>K</i> <sub>a</sub>	reactivity p <i>K</i> <sub>a</sub>
SIM	selected ion monitoring
SMX	sulfamethoxazole
SOT	superoxide test
SPME	solid-phase microextraction
t	time
<i>Tert.</i> -BuOH	<i>tertiary</i> butanol
THM	trihalomethanes
TOC	total organic carbon

TOX	total organic halides
TPs	Transformation products
TrOCs	trace organic compounds
US-EPA	United states environmental protection agency
UV	ultra violet
VPDB	Vienna
$\alpha$	degree of dissociation

## 8.4 List of Publications

### 8.4.1 Publications in peer-reviewed journals

Willach, S., Lutze, H.V., Eckey, K., Löppenberg, K., Lüling, M., Terhalle, J., Wolbert, J.-B., Jochmann, M.A., Karst, U., Schmidt, T.C., **2017**. *Degradation of sulfamethoxazole using ozone and chlorine dioxide - Compound-specific stable isotope analysis, transformation product analysis and mechanistic aspects*. Water Research 122, 280-289.

Terhalle, J., Kaiser, P., Jütte, M., Buss, J., Yasar, S., Marks, R., Uhlmann, H., Schmidt, T.C., Lutze, H.V., **2018**. *Chlorine dioxide—Pollutant transformation and formation of hypochlorous acid as a secondary oxidant*. Environ. Sci. Technol. 52, 9964-9971.

Willach, S., Lutze, H.V., Somnitz, H., Terhalle, J., Stojanovic, N., Lüling, M., Jochmann, M.A., Hofstetter, T.B., Schmidt, T.C., **2020**. *Carbon isotope fractionation of substituted benzene analogs during oxidation with ozone and hydroxyl radicals: How should experimental data be interpreted?* Environ. Sci. Technol. 54, 6713-6722.

Terhalle, J., Nikutta, S.E., Krzeczesa, D.L., Lutze, H.V., Jochmann, M.A., Schmidt, T.C., **2022**. *Linking reaction rate constants and isotope fractionation of ozonation reactions using phenols as probes*. Water Research 210, 117931.

Terhalle, J., Tintrop, L.K., Nikutta, S.E., Krzeczesa, D.L., Lutze, H.V., Schmidt, T.C., **2022**. *Ozone consumption in the reaction with phenolic compounds: Effects of pH, radical scavenger and products*. Chemosphere, submitted

### 8.4.2 Oral presentations

Terhalle, J., Krzeczesa, D., Lutz, H. V., Jochmann, M. A., Schmidt, T. C., *Isotopic effect of ozonation of specific reaction sites*. 22<sup>th</sup> September – 25<sup>th</sup> September 2019, 8<sup>th</sup> Late Summer Workshop Lake of Haltern, Lake of Haltern, Germany

### 8.4.3 Poster presentations

Terhalle, J., Lutze, H. V., Kaiser, P., Jütte, M.; Buss, J., Marks, R., Grübel, A., Uhlmann, H., Schmidt, T. C., *Formation of HOCl in the chlorine dioxide based oxidation process*. 07<sup>th</sup>–09<sup>th</sup> May 2018, Wasser, Papenburg, Germany

Terhalle, J., Trintrop, L., Lutze, H. V., Schmidt, T. C., *Reaktion von Phenol mit Ozon*. 27<sup>th</sup>–29<sup>th</sup> May 2019, Wasser, Erfurt, Germany

Terhalle, J., Lutze, H. V., Kaiser, P., Jütte, M.; Buss, J., Yasar, S., Marks, R., Uhlmann, H., Schmidt, T. C., *Mixing effects on product formation during oxidation*. 16<sup>th</sup>–20<sup>th</sup> June 2019, International conference on chemistry and the environment, Thessaloniki, Greece

Terhalle, J., Nikutta, S. E., Krzeczesa, D., Lutze, H. V., Jochmann, M. A., Schmidt, T. C., *Isotopic effect of ozonation of specific reaction sites*. 07<sup>th</sup>–12<sup>th</sup> July 2019, Isotopes, Raitenhaslach, Germany

Terhalle, J., Nikutta, S. E., Krzeczesa, D., Lutze, H. V., Jochmann, M. A., Schmidt, T. C., *Isotopic effect of ozonation of specific reaction sites*. 18<sup>th</sup>–20<sup>th</sup> May 2020, Wasser, Potsdam, Germany

### 8.5 Declaration of scientific contributions

This thesis includes work that has been conducted and published together with co-authors. The single contributions are declared in the following:

Chapter 3: Terhalle, J., Kaiser, P., Jütte, M., Buss, J., Yasar, S., Marks, R., Uhlmann, H., Schmidt, T.C., Lutze, H.V., **2018**. *Chlorine dioxide—Pollutant transformation and formation of hypochlorous acid as a secondary oxidant*. Environ. Sci. Technol. 52, 9964-9971.

Declaration of own contributions: Planning and evaluation of the oxidation experiments were done by JT. Experiments were conducted by JT with support of SY, PK, JB, MJ. HPLC-UV measurements were performed by JT with support of RM. The manuscript draft was written and corrected by JT. Revisions of the manuscript were done before submission by HU, HVL and TCS.

Chapter 4: Terhalle, J., Tintrop, L.K., Nikutta, S.E., Krzeczieska D.L., Schmidt, T.C. and Lutze, H.V., **2022**. *Ozone consumption in the reaction with phenolic compounds: Effects of pH, radical scavengers and products*. Chemosphere, submitted

Declaration of own contributions: Planning and evaluation of the oxidation experiments were done by JT. Experiments were conducted by JT with support of SEN, DLK and LKT. GC-MS and HPLC-UV measurements were performed by JT with support of SEN and DLK. The manuscript draft was written and corrected by JT. Revisions of the manuscript were done before submission by LKT, HVL and TCS

Chapter 5: Terhalle, J., Nikutta, S.E., Krzeczieska, D.L., Lutze, H.V., Jochmann, M.A., Schmidt, T.C., **2022**. *Linking reaction rate constants and isotope fractionation of ozonation reactions using phenols as probes*. Water Research 210, 117931.

Declaration of own contributions: Planning and evaluation of the oxidation experiments were done by JT. Experiments were conducted by JT with support of SEN, DLK,. GC-IRMS measurements were performed by JT with support of SEN. The manuscript draft was written and corrected by JT. Revisions of the manuscript were done before submission by MAJ, HVL and TCS

## **8.6 Curriculum Vitae**

Der Lebenslauf ist in der Online-Version aus Gründen des Datenschutzes nicht enthalten.

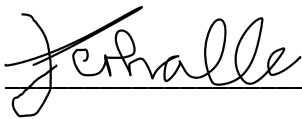
## 8.7 Erklärung

Hiermit versichere ich, dass ich die vorliegende Arbeit mit dem Titel:

**“Investigation of transformation reactions of phenolic compounds by oxidative processes in aqueous systems”**

selbständig verfasst habe, zur Abfassung der Dissertation nur die angegebenen Hilfsmittel benutzt wurden und ich alle wörtlich oder inhaltlich übernommenen Stellen als solche gekennzeichnet habe. Ich habe nie ein anderes Promotionsverfahren begonnen und bin daher in keinem vorausgegangenen Promotionsverfahren endgültig gescheitert. Die vorliegende Dissertation wurde nur in diesem Promotionsverfahren eingereicht.

Essen, im Februar 2022



---

Jens Terhalle



## 8.8 Danksagung

Mein besonderer Dank gilt Herrn Prof. Dr. Torsten C. Schmidt für die Möglichkeit meine Arbeit in seiner Arbeitsgruppe anzufertigen und die hervorragende Betreuung. Er gab mir die Möglichkeit meine eigenen Ideen umzusetzen und stand mir als verlässlicher Ansprechpartner bei Bedarf und Problemen immer mit Rat und Tat zur Seite.

Des Weiteren möchte ich mich herzlichst bei Herrn Prof. Dr. Holger V. Lutze für die unzähligen und sehr hilfreichen Diskussionen, Anregungen und die Übernahme des Zweitgutachtens dieser Arbeit bedanken. Ohne sein Feedback und seine stets konstruktive Kritik wäre meine wissenschaftliche Karriere nicht so erfolgreich verlaufen.

Dank gebührt ebenfalls Simon E. Nikutta und Lucie K. Tintrop, die im Rahmen ihrer Abschlussarbeiten wertvolle Vorarbeiten für die Kapitel dieser Arbeit geleistet haben. Außerdem gilt mein Dank Michelle Lüling und Pascal Kaiser für ihre ausdauernde Unterstützung im Labor.

Bei allen derzeitigen und ehemaligen Mitarbeitern der Arbeitsgruppe Instrumentellen Analytischen Chemie möchte ich mich für die angenehme Arbeitsatmosphäre, die gute Zusammenarbeit, für die guten Gespräche und die schöne gemeinsame Zeit bedanken. Insbesondere möchte ich Dr. Laura Wiegand, Dr. Sarah Willach, Robert Marks, Dr. Alexandra Fischbacher, Dr. Wiebke Kaziur-Cegla, Dr. Vanessa Wirzberger, Dr. Uschi Telgheder, Dr. Klaus Kerpen und Katharina Klein für den hilfreichen, fachlichen Austausch, das angenehme Miteinander im Büro und die vielen besonderen Ausflüge danken.

Abschließend möchte ich ganz besonders meiner Familie und Freunden, die mich über den gesamten Zeitraum unterstützt, ermutigt und mir diese Ausbildung ermöglicht haben, danken. Einen großen Dank richte ich an Kirsten, die immer an mich geglaubt und mich in den letzten Jahren motiviert hat.